PERFORMANCE OF A NOVEL IN-SITU HCL FOR CARBONATE AND SANDSTONE RESERVOIRS

A Thesis

by

EMRE ARSLAN

Submitted to the Office of Graduate and Professional Studies of
Texas A&M University
in partial fulfillment of the requirements for the degree of

MASTER OF SCIENCE

Chair of Committee,	Hisham Nasr-El-Din
Committee Members,	Jerome Schubert
	Mahmoud El-Halwagi
Head of Department,	A. Daniel Hill

August 2017

Major Subject: Petroleum Engineering

Copyright 2017 Emre Arslan

ABSTRACT

The oil industry has been utilizing different acid systems, both organic and inorganic, to stimulate sandstone and carbonate reservoirs. Among these, hydrochloric acid (HCl) is the most commonly used acid because it is cheap and efficient. In carbonate reservoirs, HCl is used by itself to decrease skin damage by creating conductive wormholes; whereas in sandstone reservoirs, HCl is mixed generally with hydrofluoric acid for stimulation of the reservoir.

Although HCl is widely used to increase hydrocarbon recovery from reservoirs, it has some drawbacks like high reaction and corrosion rates, especially in high pressure, high temperature environments. Therefore, an alternative acid system, which eliminates these problems while maintaining the advantages of HCl, is needed.

In a previous study, a new in-situ generated acid system was introduced for this purpose as an alternative to HCl at high temperatures, and its effectiveness was investigated. The objective of this study is to optimize the performance of this new acid system in Grey Berea Sandstone, Bandera Sandstone, Silurian Dolomite and Indiana Limestone. Elemental analysis of precipitates obtained at the end of aging cell tests will be investigated first. Coreflood experiments will be modified (flow rate, injected PV of acid, different additives etc.) accordingly, and results of elemental analysis of effluent samples and X-ray computed tomography (CT) of cores will be discussed. Finally, reaction type between the new acid system and carbonate (diffusion or reaction controlled) will be determined according to results of rotating disk apparatus (RDA) tests.

DEDICATION

I dedicate this thesis to my family for their infinite support and belief in me.

ACKNOWLEDGEMENTS

I would like to thank my advisor, Prof. Hisham Nasr-El-Din, for providing the opportunity to work on this project and for his continuous support. I would also like to thank my committee members, Dr. Jerome Schubert and Dr. Mahmoud El-Halwagi, for reviewing this work. Moreover, I would like to thank Turkish Petroleum for providing the financial support during my research at Texas A&M University. Furthermore, I would like to thank my colleagues, Khatere Sokhanvarian and Thanakrich Pummarapanthu, for their collaboration during this study. Finally, I would like to thank the Lubrizol Company for providing the chemicals and giving the permission to publish this work.

CONTRIBUTORS AND FUNDING SOURCES

Contributors

This study was supervised by thesis committee consisting of Professor Hisham Nasr-El-Din and Jerome Schubert of the Harold Vance Department of Petroleum Engineering and Professor Mahmoud El-Halwagi of the Artie McFerrin Department of Chemical Engineering.

All work for the coreflood studies part of the thesis was completed by the student, in collaboration with Khatere Sokhanvarian and Thanakrich Pummarapanthu. All work for the part of the thesis on rotating disk apparatus studies was completed independently by the student.

Funding Sources

This work was made possible with the scholarship provided by Turkish Petroleum.

NOMENCLATURE

ACS	American Chemical Society
BT	breakthrough
C_b	bulk concentration of acid, gmole/cm^3
CT	computed tomography
C_s	surface concentration of acid, gmole/cm^3
D	diffusion coefficient, cm^2/s
D_0	pre-exponential factor in units of D
DI	deionized
E_a	activation energy, kJ/gmole
gpt	gallons per thousand gallons
ICP-OES	Inductively Coupled Plasma-Optical Emission Spectroscopy
J_{mt}	rate of mass transfer of reactant to rotating disk, gmole/s.cm^2
K	specific reaction rate, (gmole/s.cm^2) (gmole/cm^3)$^{-n}$
k_0	pre-exponential factor in units of k
k_i	initial permeability, milidarcy
k_f	final permeability, milidarcy
n	reaction order, dimensionless
psi	pound per square inch
PV	pore volume
R	gas constant, 8.314 kJ/gmole.K

RDA	rotating disk apparatus
$-r_{HCl}$	rate of consumption, gmole/s.cm^2
rpm	revolution per minute
Sc	Schmidt number=υ/D, dimensionless
T	absolute temperature, ^oK
υ	kinematic viscosity, cm^2/s
ω	disk rotational speed, rad/s

TABLE OF CONTENTS

LIST OF FIGURES

LIST OF TABLES

CHAPTER I

INTRODUCTION AND LITERATURE REVIEW

The use of acids to stimulate oil wells dates back to 1896, when Standard Oil patented the use of hydrochloric acid (HCl) to increase production from oil and gas wells (Crowe et al. 1992). However, because of excessive corrosion caused by HCl to metal equipment such as casings, the acidizing technique was abandoned until the use of arsenic inhibitors by Pure Oil and Dow Chemical to treat limestone reservoirs in 1932 (Coulter Jr. et al. 1987). Since HCl does not react with silicate, the stimulation of sandstone formations was made possible by the introduction of hydrofluoric acid (HF) to the industry with the patent taken by Standard Oil in 1933. Nevertheless, it was discovered that HF was causing precipitation problems, and the first successful acidizing of sandstone took place in 1940 with the Dowell Company mixing HF with HCl (Smith and Hendrickson 1965). It should be noted that HCl was the first acid used for matrix acidizing more than a century ago, and it is still the most common acid used.

Use of HCl in Carbonate Acidizing

Because of the rapid dissolution of carbonates, acidizing in carbonate reservoirs is usually aimed to bypass the damage, which is called carbonate matrix acidizing. HCl is mainly used to stimulate carbonate formations due to its high reactivity with carbonate rocks such as limestone ($CaCO_3$), dolomite ($CaMg(CO_3)_2$) and siderite ($FeCO_3$) (Muecke 1982);

$CaCO_3 + 2HCl \rightarrow CaCl_2 + CO_2 + H_2$. ..... (1)

$CaMg(CO_3)_2 + 4HCl \rightarrow CaCl_2 + MgCl_2 + 2CO_2 + 2H_2O$. ..... (2)

$FeCO_3 + 2HCl \rightarrow FeCl_2 + CO_2 + H_2O$. ..... (3)

HCl is usually used in concentrations of 15%, 20%, and 28% in the industry. The amount of mineral dissolved by these different acid concentration is almost same, but the main difference is their reaction rates and volumes (Coulter Jr. et al. 1987).

Dissolution of limestone and dolomite is mass transfer limited above 32^o F and 302^o F respectively (Hoefner and Fogler 1989). It was shown that diffusion controlled (i.e. mass transfer limited) reaction between HCl and carbonate leads to formation of highly conductive channels called wormholes (Buijse 1997).

Wormhole Mechanism in Carbonate Acidizing

Wormholes are formed by the reaction of acid inside rock pores and wormholes and fluid loss from wormholes to formation (Buijse 1997). Damköhler number, N_{Da}, is used to characterize the formation of wormholes in carbonate rocks, and it is defined as the ratio of the net rate of dissolution by acid to the rate of convective transport of acid. At high Damköhler number values, face dissolution occurs while at low Damköhler number values ramified wormholes forms (Fredd and Fogler 1998a). In his later work, Fredd (2000) further categorized wormhole patterns into 5 types, which are face dissolution, conical wormholes, dominant wormholes, ramified wormholes and uniform wormholes. They occur with increasing injection rates respectively from face dissolution to uniform wormholes. **Fig. 1** shows these structures according to their depths of

penetration, and clearly dominant wormholes are desired in matrix acidizing of carbonates.

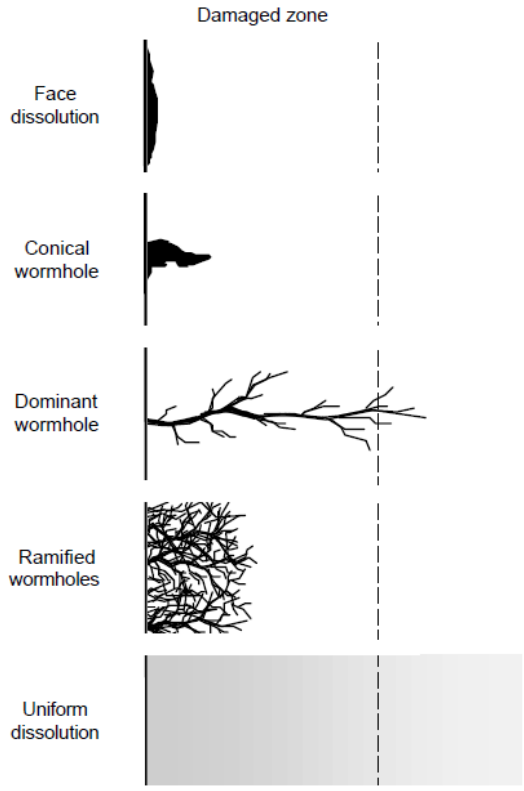

Fig. 1–Wormhole structures and their relative depths of penetration (Fredd 2000)

Problems Associated with the Use of HCl in Carbonate Acidizing

Matrix acidizing of carbonate requires low injection rates for preventing fracturing of the formation. Although the high dissolving power of HCl is beneficial in matrix acidizing of carbonate rocks, rapid spending of HCl may prevent acid from deep penetration into the formation at low injection rates (Fredd and Fogler 1998a). As a result, face dissolution and/or conical shaped wormholes can be formed (Fig. 1). Effects of this

rapid spending of HCl is more profound at elevated temperatures as the reaction rate becomes faster (Buijse et al. 2003).

Another problem stated by Harris et al. (1966) is that HCl is highly corrosive and can only be used with corrosion inhibitors efficiently up to 225^{o}F. Above this temperature, corrosion inhibitors only work for 2 hours, and either higher injection rates or a pre-flush to cool down the formation is required.

Use of HCl in Sandstone Acidizing

Sandstone acidizing aims to remove near-wellbore damage by dissolving silica (SiO_2), clays (e.g. $Al_2Si_2O_5(OH)_4$), feldspars (e.g. $NaAlSi_3O_8$) and carbonates ($CaCO_3$) through the use of mud acid which is generally composed of HF and HCl and their reactions are given by (Muecke 1982);

$$SiO_2 + 4HF \rightarrow SiF_4 + 2H_2O. \quad (4)$$

$$Al_2Si_2O_5(OH)_4 + 18HF \rightarrow 2H_2SiF_6 + 2AlF_3 + 9H_2O. \quad (5)$$

$$NaAlSi_3O_8 + 22HF \rightarrow 3H_2SiF_6 + AlF_3 + NaF + 8H_2O. \quad (6)$$

$$CaCO_3 + 2H^+ \rightarrow Ca^{++} + CO_2 + H_2O. \quad (7)$$

In their study Gatewood et al. (1970) stated that acidizing the damaged sandstone reservoirs with HF results in good production increase, while acidizing the undamaged sandstone reservoirs with HF can barely cover the cost of acidizing. They also concluded that increasing formation temperature and clay concentration decreases the acid penetration and increasing the initial HF concentration increases the acid penetration. Concentrations of HF and HCl in mud acid for sandstone acidizing usually varies between 2 to 6% and 8 to 12% respectively (Coulter Jr. et al. 1987).

Precipitate Problem in Sandstone Acidizing

Treating sandstone rocks through acidizing is much more complex than carbonate rocks. Even though the purpose of acidizing the formation is to increase the permeability, it is possible to have a decrease in permeability after acidizing sandstone formations. Two possible mechanisms for this decrease described by Hill et al. (1981) as precipitation of reaction products and (or) fines migration. This precipitation was reported as a result of secondary and tertiary reactions following the primary reaction (Eqs. 4, 5, 6 and 7) between HF and minerals found in sandstone (Gdanski 1999; Li et al. 1998; Ziauddin et al. 1999). The secondary reaction, as shown in Eqs. 8 and 9, takes place between fluosilicic acid and aluminosilicate (K-feldspar, illite etc.) (Li et al. 1998);

$$SiF_6^{2-} + 6KAlSi_3O_8 + 18H^+ + 10H_2O \rightarrow 6K^+ + 6AlF^{2+} + 18H_2SiO_3 + H_4SiO_4. \quad \ldots. (8)$$

$$SiF_6^{2-} + KAl_3Si_3O_{10}(OH)_2 + 6H^+ + 4H_2O \rightarrow K^+ + 3AlF_2^+ + 4H_4SiO_4. \quad \ldots\ldots\ldots\ldots\ldots. (9)$$

Silica gel forms as a result of elimination of aluminum from aluminosilicate through tertiary reaction, which is shown in Eq. 10 (Li et al. 1998);

$$AlF_2^+ + KAlSi_3O_8 + 4H^+ + 4H_2O \rightarrow K^+ + 2AlF^{2+} + 3H_4SiO_2. \quad \ldots\ldots\ldots\ldots\ldots\ldots\ldots\ldots (10)$$

HCl-Clay Interactions in Sandstone Acidizing

In sandstone acidizing, in order to prevent the possible precipitation of CaF_2, a preflush of HCl is usually used before pumping HF-HCl mixture when the amount of calcium carbonate ($CaCO_3$) is not negligible (5-10%) (Coulter Jr. et al. 1987; Muecke 1982).

As it was first stated by Gdanski and Peavy (1986), HCl does not react only with carbonates within the sandstone formations, but also reacts with aluminosilicates. This

interaction between aluminosilicates and HCl was explained by Bryant and Buller (1990) as the extraction of aluminum (Al) and weakening of crystal structure of the minerals, and the development of a siliceous leached layer on the surface of the minerals resulting in fines migration.

In their detailed study on acid-sensitive aluminosilicates, Hartman et al. (2006) examined the dissolution of analcime (a type of zeolite) and three types of clay minerals which are kaolinite, chlorite, and illite in HCl. Accordingly, dissolution reaction takes place as leaching of Al and dissolution and precipitation of Silicon (Si). It was found that, dissolution process occurs at a much faster rate with zeolite than clays. Their explanation for this difference was the difference in their mineral structures. Since zeolites have more complex crystalline structure as opposed to simple, layered structure of clay minerals **(Fig. 2)**, they provide more surface area for reaction and the reaction between acids occurs much faster.

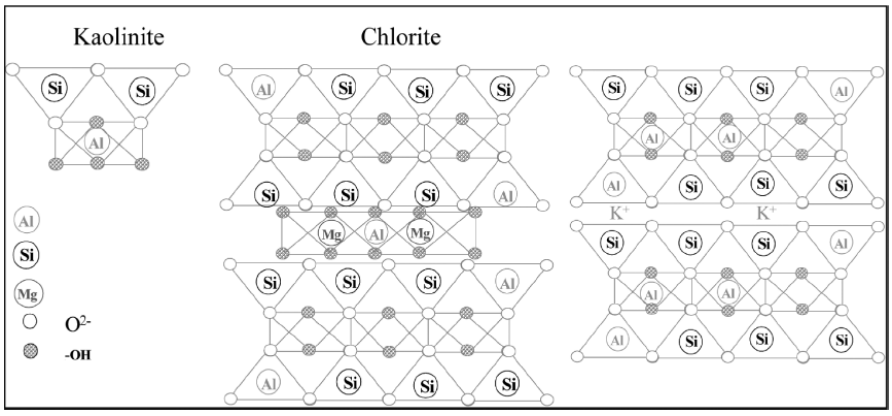

Fig. 2–Mineral structures of clays (Hartman et al. 2006)

Alternatives of HCl in Carbonate and Sandstone Acidizing

Organic Acids

Weak organic acids such as formic acid, acetic acid have been used as an alternative to HCl (Buijse et al. 2003; Fredd and Fogler 1998a). Since organic acids are weak acids with low H^+ concentration, they react with carbonates at a slower rate than HCl and are suitable to use in wells with high bottomhole temperatures (Coulter Jr. et al. 1987). Therefore, organic acids can provide deeper penetration than HCl in carbonate reservoirs at low injection rates.

$$2\mathrm{HOrg} + \mathrm{CaCO_3} \rightarrow \mathrm{CaOrg_2} + \mathrm{H_2O} + \mathrm{CO_2}. \quad \text{(11)}$$

Limitations of Organic Acids

Organic acids are not as efficient as HCl since their reaction with carbonate is reversible (Eq. 11) under reservoir conditions, meaning that they are thermodynamically limited. Chatelain et al. (1976) showed that 60% of a 15 wt% acetic acid solution remained unreacted when it was injected into carbonate at 250^{o}F. It was reported that corrosion caused by organic acids is also an issue, especially at high temperatures (Bybee 2002; Frenier et al. 2001; Scribner 2001). Another limitation of organic acids is that, they cannot be used at high concentrations since their calcium salts, like calcium acetate and calcium formate, have low solubility. Moreover, the cost of organic acids is considerably higher than HCl (Chang et al. 2008).

Chelating Agents

Chelating agents have been used for removal of calcium and iron scales in oil wells as well as stimulating carbonate reservoirs. The mechanism for the stimulation with

chelating agents, however, is different than acids. Chelating agents are capable of forming stable metal/ligand chelates with metals such as calcium and iron which are commonly found in oil reservoirs. Chelating agents, which have enough bonding sites, surround the coordination sites of metal ion in aqueous solution to form these chelates (Shaughnessy and Kline 1983). Polyaminocarboxylic acids such as EDTA, can form highly stable chelates with both calcium and iron ions (Fredd and Fogler 1998a). For this reaction to happen, polyaminocarboxylic acids undergo a stepwise loss of protons to reach their fully ionized state (Eqs. 12 through 15).

$H_4Y \rightleftharpoons H_3Y^{-1} + H^+$, ……..…. (12)

$H_3Y^{-1} \rightleftharpoons H_2Y^{-2} + H^+$, ……..…. (13)

$H_2Y^{-2} \rightleftharpoons HY^{-3} + H^+$, ……..…. (14)

$HY^{-3} \rightleftharpoons Y^{-4} + H^+$, ……..…. (15)

The dissolution of calcium by EDTA occurs by combination of hydrogen ion attack (Eq. 16) and chelation of free calcium ion (Eq. 17) at pH of 4-5 (Shaughnessy and Kline 1983). The combined reaction of chelation and hydrogen ion attack is given in Eq. 18.

$2H^+ + CaCO_3 \rightleftharpoons Ca^{+2} + H_2O + CO_2$, ……..…….. (16)

$Ca^{+2} + H_2Y^{-2} \rightleftharpoons CaY^{-2} + H^+$, ……..……..…….. (17)

$H_2Y^{-2} + CaCO_3 \rightleftharpoons CaY^{-2} + H_2O + CO_2$. ……..…….. (18)

Chelating agents are also considered as an alternative to HCl like in the case of organic acids. Comparing to HCl, it was shown that, chelating agents do not cause face dissolution at low injection rates. Moreover, they perform better at high temperature and low injection rate conditions (Mahmoud et al. 2011).

Limitations of Chelating Agents

The main concern regarding the use of chelating agents in oil wells is their thermal stabilities at high temperatures. Sokhanvarian et al. (2016) studied the thermal stability of 4 types of chelating agents, which are GLDA, NTA, HEDTA, and EDTA. They concluded that, chelating agents are susceptible to thermal degradation at temperatures over 350^{o}F. Another limitation of most common chelating agents is their potential risk to health and environment. For example, EDTA and DTPA are not biodegradable and NTA is known as animal carcinogen (Frenier et al. 2003). Lastly, higher cost is another limitation that chelating agents have (Wilson 2015).

Kinetic Studies for Acid-Carbonate Reactions

Kinetic studies for an acid-carbonate system consist of calculating the rock dissolution rate, reaction rate constant, reaction order, and diffusion coefficient and activation energy. These parameters are used in simulation of acid treatments to obtain optimum acid injection rate, acid concentration and shut-in time (Taylor et al. 2004). Rotating Disk Apparatus (RDA) has been the widely used method to calculate reaction constants for different types of acids (de Rozieres 1994; Fredd and Fogler 1998b; Lund and Fogler 1975; Lund et al. 1973; Rabie et al. 2010; Rabie et al. 2014; Taylor et al. 2004;

Taylor and Nasr-El-Din 2009). RDA can also assist determining the type of reaction, whether it is mass transfer (diffusion) limited or surface reaction limited.

Mass Transfer Limited and Surface Reaction Limited Reactions

Solid-liquid reactions, such as acid-carbonate reaction, occur in the following three steps; (1) diffusion of liquid to the solid-liquid interface, (2) reaction between liquid and solid at the solid-liquid interface, and (3) diffusion of liquid from the solid-liquid interface (Lund et al. 1973). Slowest step determines the reaction type as either mass transfer limited or surface reaction limited. In other words, if the slowest step is the diffusion of liquid to or from the interface, then the reaction is said to be mass transfer limited and if the slowest step is the surface reaction, then the reaction is said to be surface reaction limited (Taylor and Nasr-El-Din 2009).

In an RDA study, reaction rate constants are plotted against the square root of the solid disk angular velocity for laminar conditions. If this plot has a positive slope, the reaction is decided to be mass transfer limited. At higher velocities, where the effect of velocity decreases, the slope approaches to zero. When velocity has no control over the reaction anymore, slope becomes zero and the reaction is called surface reaction limited (Boomer et al. 1972) **(Fig. 3**).

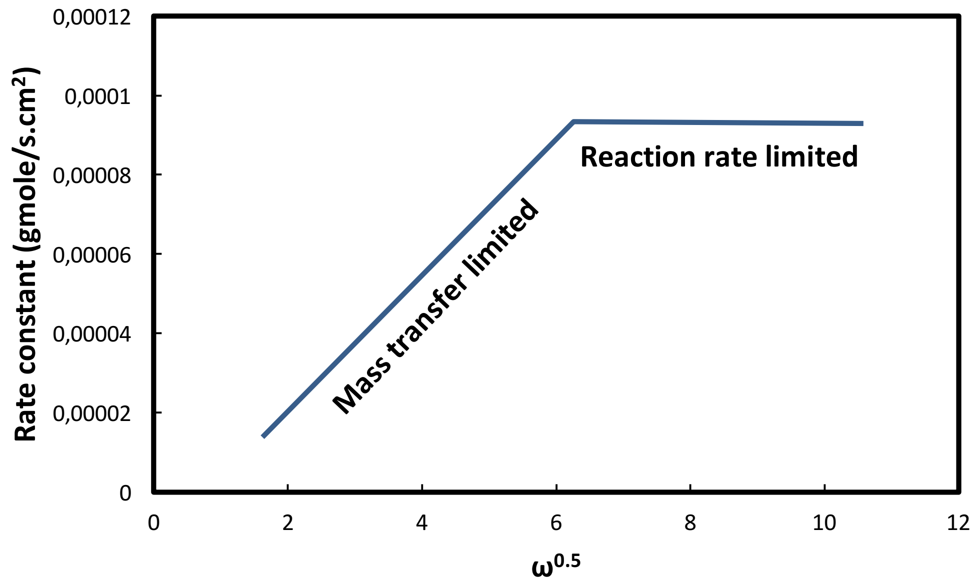

Fig. 3–Plot of reaction rate vs. square root of rotational speed indicating reaction types

Reaction Constants

Newman (1966) presented the equation of rate of mass transfer for Newtonian fluids in laminar flow regime in Eq. 19. In an RDA study, rate of mass transfer, bulk concentration of acid, disk rotational speed, and kinematic viscosity of the acid is known and diffusion coefficient is calculated accordingly. It should be noted that, surface concentration of acid is approximated to zero for mass transfer limited reactions.

$$J_{mt} = \frac{0.62048\, S_c^{-2/3} (\upsilon\omega)^{1/2}}{1+02980\, S_c^{-1/3} + 0.1451\, S_c^{-2/3}} * (C_b - C_s), \ldots \qquad (19)$$

where,

J_{mt} = rate of mass transfer of reactant to rotating disk, gmole/s.cm^2

υ = kinematic viscosity, cm^2/s

ω = disk rotational speed, rad/s

C_b = bulk concentration of acid, gmole/cm^3

C_s = surface concentration of acid, gmole/cm^3

Sc = Schmidt number=υ/D, dimensionless

D = diffusion coefficient, cm^2/s

Reaction order for surface reaction limited reactions can be calculated by using Eq. 20 which is a power law expression (Lund et al. 1973).

$$-r_{HCl} = kC_s^n, \quad \ldots\ldots (20)$$

where,

$-r_{HCl}$ = rate of consumption, gmole/s.cm^2

k = specific reaction rate, (gmole/s.cm^2) (gmole/cm^3)$^{-n}$

n = reaction order, dimensionless

Activation energy can be calculated by using Arrhenius equation. For surface reaction limited reactions and mass transfer limited reactions Eqs. 21 and 22 can be used respectively.

$$k = k_0 \exp(-E_a/RT), \quad \ldots\ldots (21)$$

$$D = D_0 \exp(-E_a/RT), \quad \ldots\ldots (22)$$

where,

k_0 = pre-exponential factor in units of k

D_0 = pre-exponential factor in units of D

E_a = activation energy, kJ/gmole

R = 8.314 kJ/gmole.K

T = temperature, K

A Novel In-Situ Generated Acid

Organic acids and chelating agents have been used to substitute HCl to address the limitations of HCl at high temperature and low injection rate applications of carbonate acidizing. However, organic acids and chelating agents are weak acids compared to HCl. In this study, a novel in-situ generated acid system is investigated. The new acid system is based on HCl and consequently, its dissolution power is comparable with HCl. Without sacrificing the strength of the acid, the retardation mechanism of the in-situ generated HCl provides slower reaction rates, which in return results in dominant wormholes with no face dissolution. Another advantage of in-situ generated HCl is causing less corrosion to metal tubulars (Sokhanvarian et al. 2017).

Qualitative observations, such as face dissolution, breakthrough volume, can be obtained from coreflood tests done with acid-carbonate systems. RDA analysis is used, to get the reaction constants (reaction rate constant, diffusion coefficient and activation energy) of the acid to quantify and confirm these observations.

The objective of this study is to (1) investigate the performance of the in-situ generated HCl with coreflood tests in sandstone cores (as pre-flush) and carbonate cores (both dolomite and limestone) at 300^{o}F, (2) determine the reaction constants of in-situ generated HCl with RDA analysis, and (3) compare the performance of in-situ generated HCl with 15 wt% regular HCl according to the results of coreflood and RDA tests.

CHAPTER II

EXPERIMENTAL METHODS

Materials

In-situ generated HCl and 15 wt% regular HCl (ACS grade, 36-37 wt%) were the two acids tested in this study with coreflood experiments. Deionized (DI) water (18.2 MΩ.cm at room temperature) and KCl were mixed to prepare 5 wt% brine, which was used as pre and post flush fluid in coreflood tests and to saturate cores. The additives used are shown in **Table 1**, while physical properties of fluids measured at 75^{o}F are shown in **Table 2**. The cores used in this study were obtained from Bandera sandstone, Grey Berea sandstone, Silurian dolomite and Indiana limestone with a length of 6 in. and a diameter of 1.5 in. Their mineral composition is shown in **Table 3**.

Marble disks, having 0 vol% porosity, were cut to dimensions of 1.5 in. diameter and 0.65 in. height. Mineralogy of these marble disks was 99 wt% calcite. After cutting, the disks were smoothed by first using sandpaper and second soaking in 0.1 M HCl for 30 minutes. Then, the disks were washed with deionized (DI) water (18.2 MΩ.cm at 25℃) and kept in DI water until the time they were used.

Additive	Concentration, gpt
Corrosion inhibitor	6
Corrosion inhibitor intensifier	40
Iron control agent	8
Non-emulsifier	3

Table 1–Amounts of additives used in acid compositions

Acid Used	Viscosity, cp	Density, g/cm^3	pH	HCl Concentration, wt%
15 wt% regular HCl	1.220	1.073	0	15
In-situ generated HCl	1.596	1.107	0	16.3
15 wt% regular HCl + additives	1.30	1.082	0	18.76
In-situ generated HCl + additives	1.92	1.14	0	19.54
5 wt% KCl	0.910	1.049	-	-

Table 2–Physical properties of fluids used in this study

	Grey Berea Sandstone (wt%)	Bandera Sandstone (wt%)	Silurian Dolomite (wt%)	Indiana Limestone (wt%)
Quartz	86	57	0.38	1.7
Dolomite	1	16	96	0.4
Calcite	2	-	0.04	97.3
Illite	1	10	-	-
Kaolinite	5	3	-	-
Chlorite	2	1	-	-
K-Feldspar	3	-	-	-
Plagioclase	-	12	-	-
Ankerite	-	-	3	-
Siderite	-	-	0.04	-
Albite	-	-	0.99	-

Table 3–Mineral composition of cores used in this study

Core Preparation

Core samples were first dried at 220°F for four hours and then saturated with 5 wt% KCl for four hours. The dry and saturated weights were each recorded and using the density of 5 wt% KCl, the porosity of the cores was calculated.

Coreflood

Using a nitrogen cylinder, a back-pressure regulator was used to apply 1200 psi of back pressure for keeping CO_2 in the solution. The overburden pressure applied to the core holder was 1500 psi. The pressure range of the differential pressure transducer was 0-300 psi, and it was connected to a computer to record the pressure drop across the core (from the inlet of the core to the outlet of the core). LabVIEW™ software was used to plot pressure drop versus time graph. To inject the acid composition into the core, a precision syringe pump with a maximum allowable pressure of 2000 psi was used. Using an automatic fraction collector, effluents were collected every quarter PV (pore volume) of acid injected. See **Fig. 4** for a schematic of the coreflood setup used in this study.

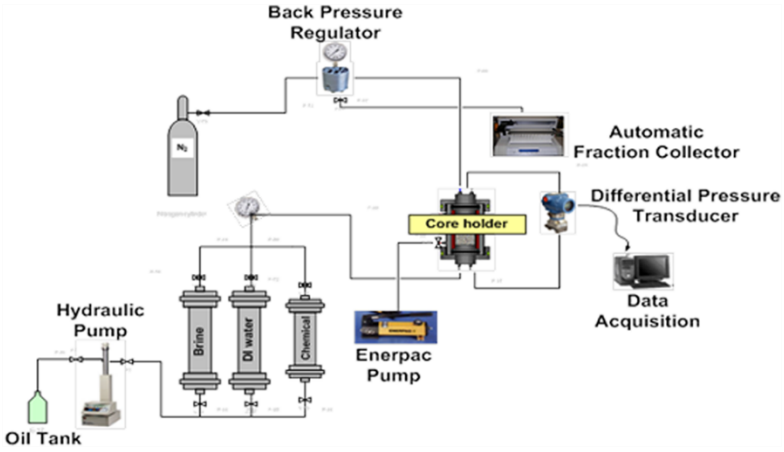

Fig. 4–Coreflood setup (El-Monier and Nasr-El-Din 2013)

Rotating Disk Apparatus (RDA)

In this method, reacting rock is mounted on a spindle with the help of a heat-shrink Teflon® tubing (**Fig. 5**) and is rotated at different rotational speeds in a Hastelloy® vessel filled with reacting fluid, at different temperatures (Taylor et al. 2004). In this study, the operating temperatures were 100^{o}F, 150^{o}F, and 200^{o}F, while rotational speeds of 200 to 1200 revolution per minute (rpm) was used. The pressure inside the reaction vessel was kept between 1000-1300 psi to keep the CO_2 in solution. See **Fig. 6** for the picture of the RDA setup used in this study.

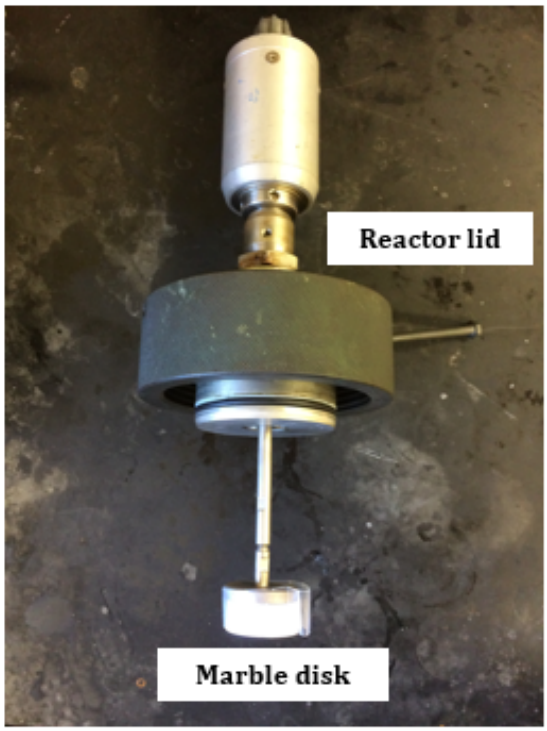

Fig. 5– Photograph of reacting marble disk and reactor lid, which is connected to rotor

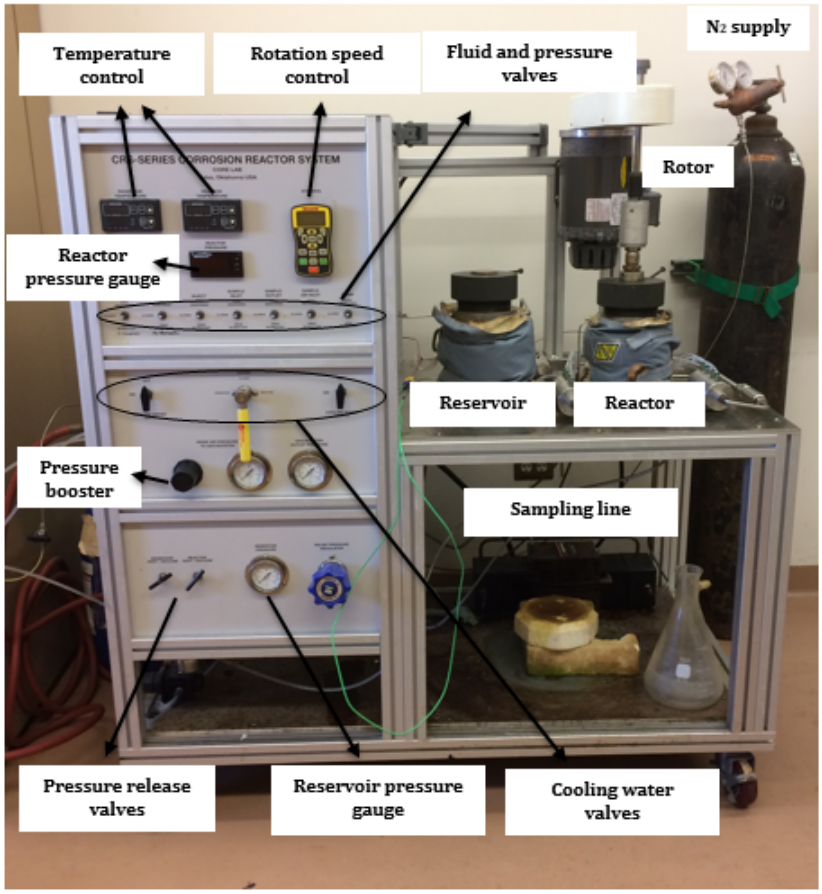

Fig. 6– Photograph of rotating disk apparatus

Computed Tomography (CT Scan)

Medical-grade CT scanner was used for the analysis of the cores. It is adapted for specialized use with drilling cores. Series of standard image files resulted from the data of the scanner were visualized using ImageJ software. These image files were interpreted as porosity profile for sandstone cores, while one whole image of the core was used to detect the wormhole propagation for carbonate cores.

See-Through Cell

The see-through cell is a pressure vessel to heat liquids higher than the boiling point of water (**Fig. 7**). It has a glass window to 'see' inside the cell. The liquid is contained in a glass, graduated cylinder and this cylinder is then placed into the see-through cell. After the metal cap of the see-through cell is sealed, the vessel can be pressurized with a nitrogen source. The system temperature can be set to a certain temperature with a heating jacket. See-through cell allows the user to test the behavior of the liquid with temperature and observe the physical changes during the test.

Fig. 7–Photograph of see-through cell

Inductively Coupled Plasma – Optical Emission Spectroscopy (ICP – OES)

An Optima 7000 ICP-OES Spectrometer was used for elemental analysis on samples collected from RDA and coreflood experiments. Ca, Mg and K concentrations

were measured for dolomite and limestone cores, while for sandstone cores, Ca, Mg, K, Fe, Si, and Al were measured. Dilution factors for coreflood effluents collected from Grey Berea Sandstone, Bandera Sandstone, Silurian Dolomite, and Indiana Limestone were 1000, 2000, and 5000 ppm respectively. Dilution factors for RDA samples were 500 ppm.

Auto Titrator

Metrohm (907 Titrando) titrator was used to measure the core effluent acid concentration. The titration type utilized was strong acid-strong base titration, and 0.1M and 0.5M NaOH were used as a titrant. The weight of the effluent sample was measured and entered into the software interface. The software then calculated the amount of NaOH used to neutralize the acid, and, from there, the weight percent of acid present inside the solution was reported.

pH Measurements

The pH of the core effluent samples was measured using epoxy electrode, and it was calibrated before each measurement with three pH buffers (4, 7, and 10).

Density and Viscosity Measurements

The density of in-situ generated HCl and 15 wt% HCl was measured with DMA 35 portable density meter at room temperature. The kinematic viscosity was measured with a capillary viscometer. The capillary tube used was 0C type. After putting the fluid into this tube, the viscosity timings were recorded at different temperatures. These values were multiplied by the constant, 0.003 to calculate kinematic viscosity. Finally, it was multiplied by the density of the fluid to obtain the absolute viscosity.

CHAPTER III

RESULTS AND DISCUSSION*

Coreflood Studies

In this chapter, performances of the novel in-situ generated HCl and 15 wt% HCl were analyzed and compared with a series of coreflood experiments. In these experiments, effects of temperature, injection rate and the amount of acid injected were observed. Sandstone cores (Grey Berea Sandstone and Bandera Sandstone) were used to measure the performances of both acids in a preflush stage and porosity and permeability changes were measured. Carbonate cores (Silurian Dolomite and Indiana Limestone) were used to measure the performances of both acids in the main stage and wormhole propagations were examined. Pressure drop vs. time was plotted with the help of LabVIEW^{TM} software.

For sandstone cores, 5 wt% KCl was injected with an injection rate of 3 cm^3/min through production direction until a stabilized pressure drop was observed in the software. Then, the direction was switched to the injection direction and the desired amount of acid was injected with the desired injection rate. Effluents were collected every 0.2 PV after the start of acid injection. After the acid injection, brine was injected with an injection rate of 3 cm^3/min first in the injection direction for 2 PV and then in the production direction

* Reprinted with permission from "A New In-Situ Generated Acid System for Carbonate Dissolution in Sandstone and Carbonate Reservoirs" by Khatere Sokhanvarian, Thanakrich Pummarapanthu, Emre Arslan, Hisham Nasr-El-Din, Nicole Shimek, Kern Smith, 2017. SPE International Conference on Oilfield Chemistry, 3-5 April, Montgomery, Texas, USA, Copyright [2017] by Society of Petroleum Engineers.

until the pressure drop was stabilized and the effluents became colorless. Permeability ratio was decided from stabilized pressure drop values before and after acid injection using Darcy's equation. Porosity profiles of cores, before and after the acid treatment, were obtained by performing CT scan on the cores in dry and saturated conditions.

For carbonate cores, 5 wt% KCl was again injected with an injection rate of 3 cm^3/min through production direction until the pressure drop was stabilized. Afterwards, a maximum of 5 PV of acid was injected in the injection direction to observe the breakthrough when the pressure drop suddenly dropped to 0. Effluents were collected every 0.2 PV after the start of the acid injection. After the breakthrough, brine was injected with an injection rate of 3 cm^3/min first in the injection direction for 2 PV and then in the production direction until the effluents became colorless. Wormhole propagation was captured by performing CT scans on cores after the acid treatment.

In the first subsection, a summary of previous coreflood experiments is provided, which were done with in-situ generated HCl and 15 wt% HCl at 250 and 300^{o}F. The possible reason for poor performances at 300^{o}F is addressed in the next subsection. In the following subsections, results of coreflood tests, done with Bandera sandstone, Grey Berea sandstone, Silurian dolomite, and Indiana limestone at 300^{o}F, were given and compared with the results of previous coreflood tests. The performances of the in-situ generated HCl and 15 wt% HCl was also compared for all core types.

Summary of Previous Coreflood Tests Done at 250 and 300^{o}F

During the course of this project, series of coreflood tests were carried out. This study focuses more on the coreflood experiments done at 300^{o}F. For convenience,

previous experiments done at 250 and 300°F is summarized under this section and results are compared in detail in the coming sections.

At the beginning of the project, coreflood tests were done with Grey Berea sandstone, Bandera sandstone, and Silurian dolomite at 250 and 300°F (Sokhanvarian et al. 2017). The novel in-situ generated HCl and 15 wt% HCl was used in these tests and 5 PV of acid was injected with an injection rate of 1 cm^3/min for each case.

Coreflood tests done with Grey Berea sandstone indicated that at 250°F, in-situ generated HCl performed better than 15 wt% HCl. At this temperature, there was a 164% permeability improvement with the new in-situ generated HCl, while 15 wt% HCl did not change permeability at all. On the other hand, at 300°F, both acids showed a damaging trend. In situ-generated HCl caused 11% permeability decrease and 15 wt% HCl caused severe damage to the core as the pressure drop did not stabilize. These results are shown in **Table 4**.

Core ID	Acid	Temperature, °F	k_f/k_i
G-6-22	In-situ generated HCl	250	2.64
G-6-27	15 wt% HCl	250	1.0
G-6-21	In-situ generated HCl	300	0.89
G-6-17	15 wt% HCl	300	Pressure drop did not stabilize

Table 4–Grey Berea sandstone coreflood tests. 5 PV of acid was injected with 1 cm^3/min

Bandera sandstone has more illite and carbonate than Grey Berea sandstone in its mineral composition. Illite is a very sensitive clay type and can plug the pore throats by swelling in the presence of HCl. However, the high concentration of carbonate in Bandera sandstone can overcome this effect and result in better permeability and porosity

improvement. In **Table 5**, the results of coreflood tests of Bandera sandstone are given. It is seen in this table that at 250°F, both in-situ generated HCl and 15 wt% HCl improved permeability. When the temperature was increased to 300°F, both acids showed a decline in their performances.

Core ID	Acid	Temperature, °F	k_f/k_i
BG-6-12	In-situ generated HCl	250	1.72
BG-6-6	15 wt% HCl	250	2.17
BG-6-7	In-situ generated HCl	300	1.00
BG-6-5	15 wt% HCl	300	1.51

Table 5–Bandera sandstone coreflood tests. 5 PV of acid was injected with 1 cm^3/min

Wormhole propagation and injected PV of acid to reach breakthrough were the two main parameters to investigate carbonate acidizing. Although in-situ generated HCl reached breakthrough after 3 PV of injection into Silurian dolomite at 250°F, 15 wt% HCl could not penetrate the 6 inch long core after 5 PV of injection at the same temperature. In fact, in-situ generated HCl created a single, dominant wormhole, while 15 wt% HCl caused face dissolution (**Fig. 8**). Increasing the temperature to 300°F however, decreased the performances of both acids as they could not reach breakthrough after 5 PV of injection. Results of Silurian dolomite coreflood studies are tabulated in **Table 6**.

Core ID	Acid	Temperature, °F	PV to breakthrough (BT)
SD-6-40	In-situ generated HCl	250	3
SD-6-42	15 wt% HCl	250	Did not reach BT after 5 PV
SD-6-41	In-situ generated HCl	300	Did not reach BT after 5 PV
SD-6-37	15 wt% HCl	300	Did not reach BT after 5 PV

Table 6–Silurian dolomite coreflood tests. Injection rate of acids was 1 cm^3/min

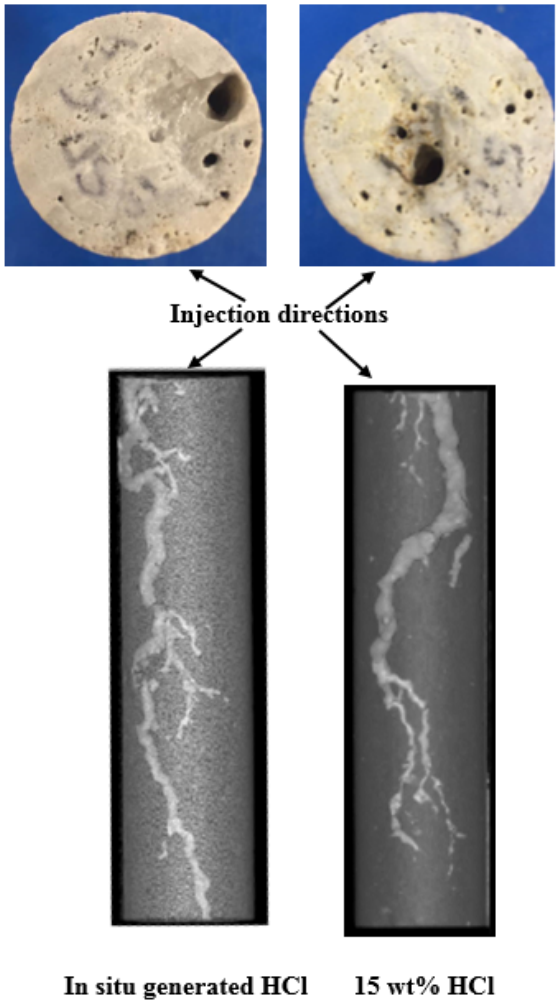

Fig. 8–Silurian dolomite cores after injecting in-situ generated HCl and 15 wt% HCl at 250^{o}F with an injection rate of 1 cm^{3}/min

Addressing the Performance Reduction of In-Situ Generated HCl at High Temperature

Results provided for the previous coreflood tests indicated that the new in-situ generated HCl displayed better performance at 250^{o}F, comparing to 15 wt% HCl. However, increasing the temperature to 300^{o}F decreased the performance of in-situ

generated HCl dramatically. To address this situation, pH and HCl concentrations of effluents collected at 250 and 300^{o}F were compared. In **Fig. 9** and **Fig**. 10, the change in pH and H^{+} concentration with respect to cumulative PV of acid injected is given for in-situ generated HCl at 250 and 300^{o}F for Grey Berea sandstone and Bandera sandstone respectively. A decrease in pH to 0 and an increase in H^{+} concentration is an indication of acidity in the collected effluents. Therefore, it was inferred that there was an excess acid which remained unreacted at 250^{o}F. On the other hand, at 300^{o}F, almost all of the in-situ generated HCl seemed spent.

To confirm these interpretations, a decomposition experiment was conducted with see-through cell. The cell was heated to 300^{o}F and in-situ generated HCl was put in this cell. A pressure of 400 psi was applied with the help of a nitrogen cylinder to keep the CO_2 in solution. At the end of 4 hours of heating, pH was measured as 7.61 and H^{+} concentration was 0 vol%. Moreover, a white precipitate was observed during heating and after cooling (**Fig. 11**).

This experiment showed that in-situ generated HCl was decomposing very quickly at high temperatures and forming a chloride salt precipitation. Since it is known that chloride salts are soluble in water, it can be removed by increasing the amount of brine injected after the treatment. In the following coreflood experiments, this problem is addressed by increasing the injection rate of acid and decreasing the PV of acid injected. At the end, an optimum injection rate for in-situ generated HCl was determined.

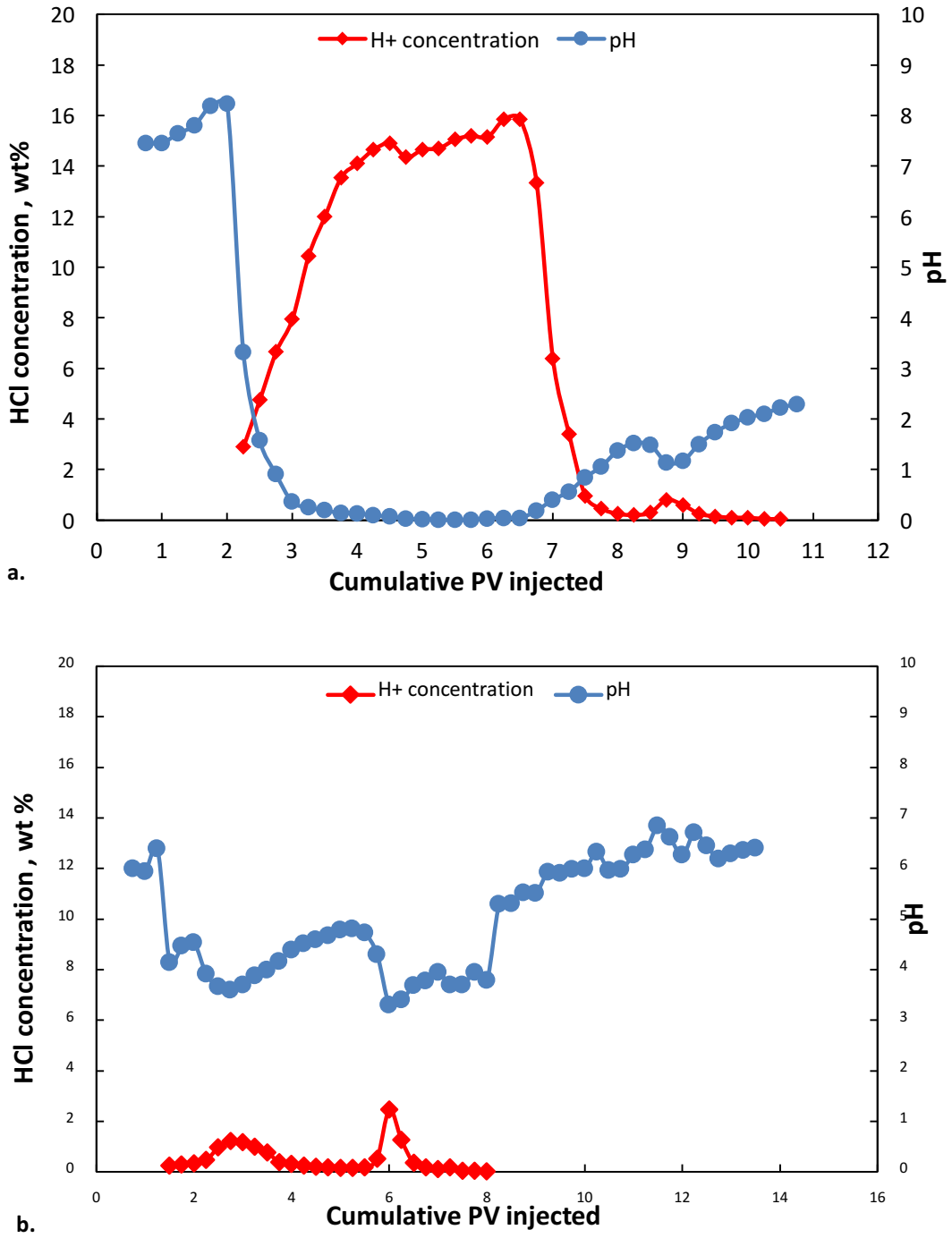

Fig. 9–pH and H^+ concentration values for coreflood experiment of **Grey Berea sandstone** at a. 250 and b. 300°F. 5 PV of in-situ generated HCl was injected with 1 cm^3/min injection rate.

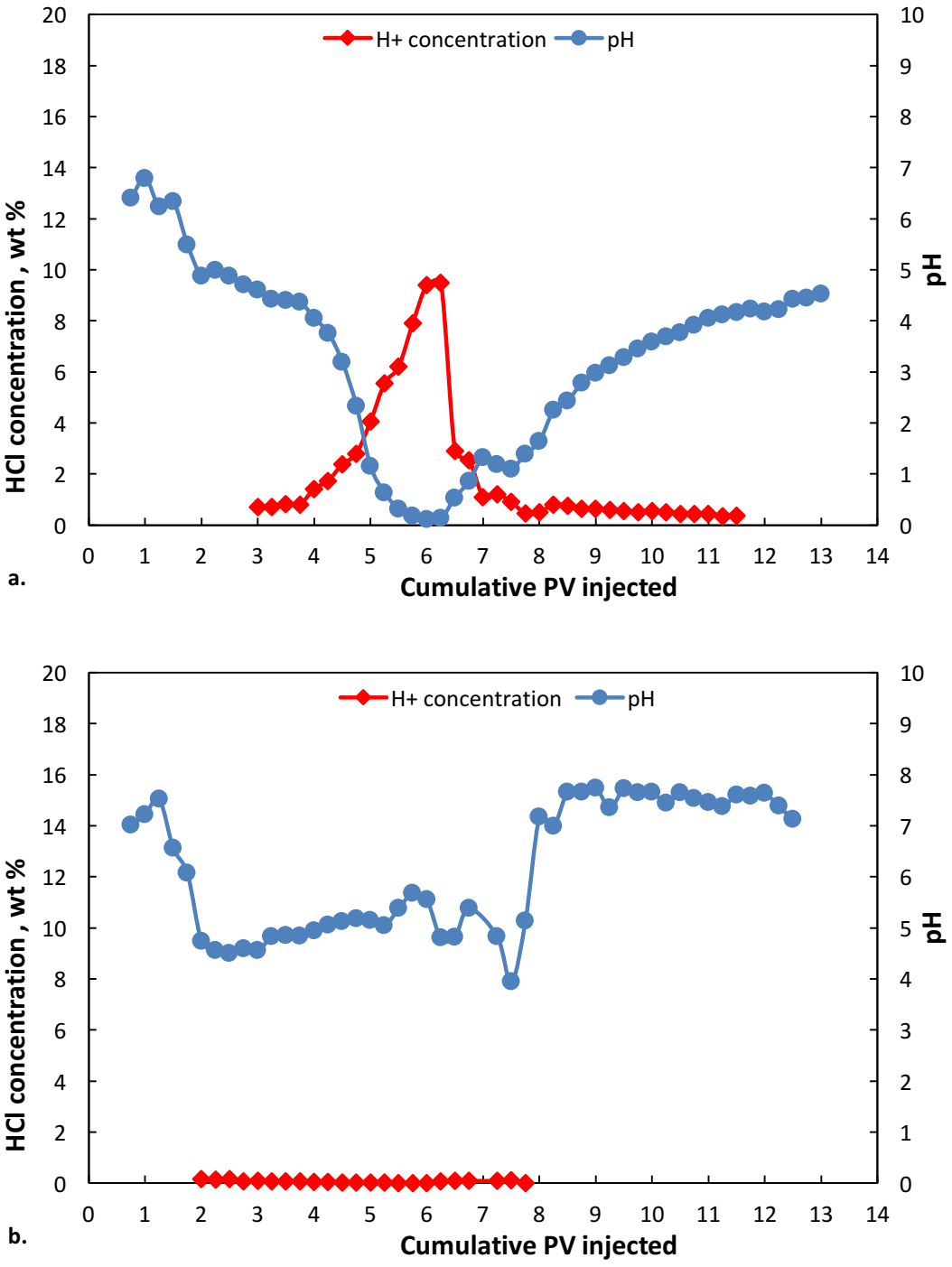

Fig. 10–pH and H^+ concentration values for coreflood experiment of **Bandera sandstone** at a. 250 and b. 300°F. 5 PV of in-situ generated HCl was injected with 1 cm^3/min injection rate.

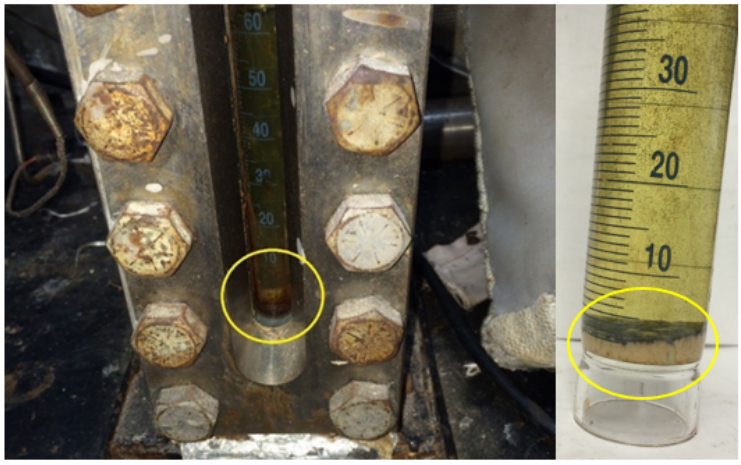

(a) During heating (b) After cooling

Fig. 11–Pictures of in-situ generated HCl taken (a) during heating inside the see-through cell, (b) after cooling at the end of see-through cell. In both cases a white precipitate is visible.

Coreflood Experiments Done with Grey Berea Sandstone at 300^{o}F

Treatment with In-Situ Generated HCl (5 cm^3/min – 1 PV – G-6-20)

Considering the effects of a possible precipitate inside the core, the coreflood experiment with in-situ generated HCl and Grey Berea sandstone at 300^{o}F was repeated. In this test, the injection rate was increased from 1 cm^3/min to 5 cm^3/min. By increasing the injection rate, residence time of the acid inside the core was decreased and thus it was aimed to minimize the formation of precipitates inside the core. Moreover, the amount of acid injected was decreased from 5 PV to 1 PV because there was 2 to 4 PV of excess acid remained unreacted in the previous coreflood tests at 250^{o}F.

These modifications proved successful, and permeability of Grey Berea sandstone was increased by 17% with in-situ generated HCl at 300^{o}F. There was an 11% damage in the previous case at the same temperature (**Table 7**).

Core ID	Flow rate, cm^3/min	PV of in-situ generated HCl	k_f/k_i
G-6-21	1	5	0.89
G-6-20	5	1	1.17

Table 7–Comparison of permeability change for coreflood tests of Grey Berea sandstone after the treatment with in-situ generated HCl at 300°F

ICP analysis was carried out to correlate the coreflood results (**Fig. 12**). The presence of calcium and magnesium ions was a sign of carbonate dissolution and the main reason for permeability improvement. Iron concentration was around 10,000 mg/L at its peak. The presence of iron ions is an indication of dissolution of illite and chlorite clays found in the Grey Berea sandstone. K^+ concentration was decreased during acid injection and increased again when injection switched back to 5 wt% KCl.

Brine (5 wt% KCl) was injected as pre-flush and its pH was around 7. After the injection of in-situ generated HCl followed by post-flush with brine, pH decreased to around 4.5 (**Fig. 13**). This means that almost all of the acid was spent in the core to dissolve carbonates present in sandstone. When the injection switched back to brine, pH increased to 6 on average.

Finally, a CT scan analysis was done after the acid treatment and the porosity profile was drawn along the length of the core (**Fig. 14**). On the same plot, average porosity (17.85%) was also included as a line, which was obtained by measuring the dry and saturated weight of the core. It was observed that the porosity increased significantly, around 1.5% on average. The increase was more evident at the inlet of the core. Porosity increase is also an indication of carbonate dissolution and is parallel to permeability improvement.

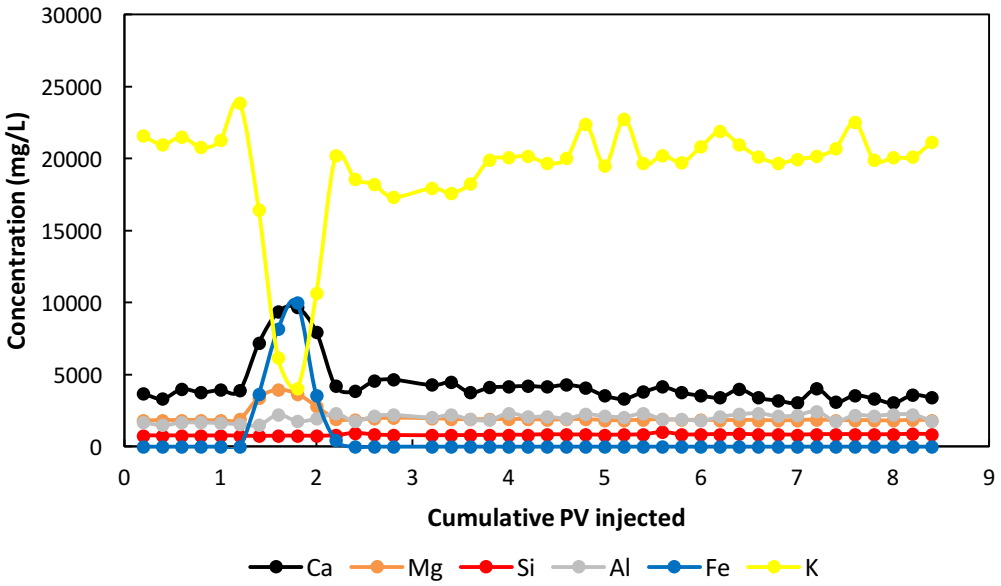

Fig. 12–ICP analysis of effluent samples from Grey Berea sandstone (G-6-20) after the treatment with in-situ generated HCl at 300°F (5 cm^3/min – 1 PV)

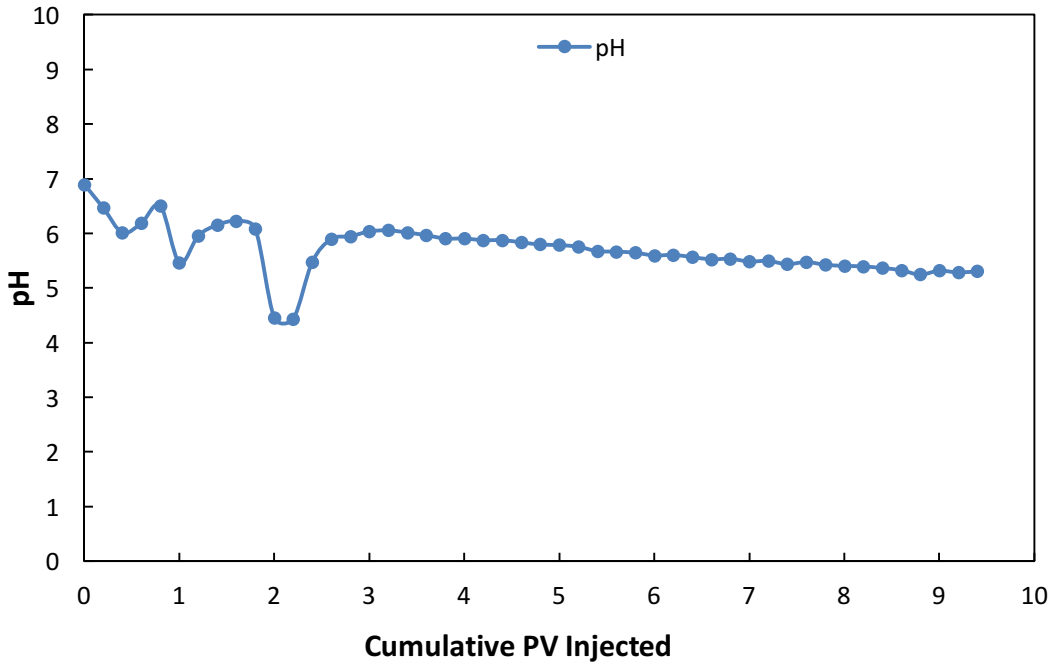

Fig. 13–pH of effluent samples from Grey Berea sandstone (G-6-20) after the treatment with in-situ generated HCl at 300°F (5 cm^3/min – 1 PV)

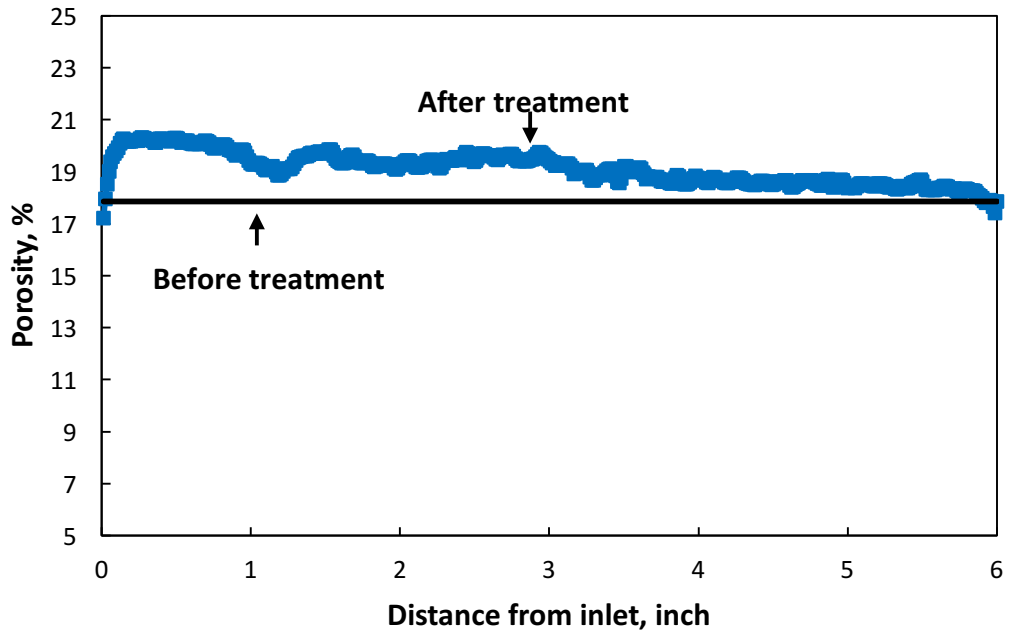

Fig. 14–Porosity profile of Grey Berea sandstone (G-6-20) before and after the treatment with in-situ generated HCl at 300°F (5 cm^3/min – 1 PV)

Coreflood Experiments Done with Bandera Sandstone at 300°F

Treatment with In-Situ Generated HCl (2 cm^3/min – 2 PV – BG-6-8)

For Bandera sandstone, the injection rate was first increased to 2 cm^3/min and the injected amount of acid was decreased to 2 PV. In fact, this experiment was the first intended to optimize the injection rate of in-situ generated HCl. The pressure drop profile in **Fig. 15** showed that this modification did not provide any permeability improvement. There was a 3% damage observed in this case, which was the same for the treatment done at 300°F with 1 cm^3/min injection rate and 5 PV of acid (**Table 8**).

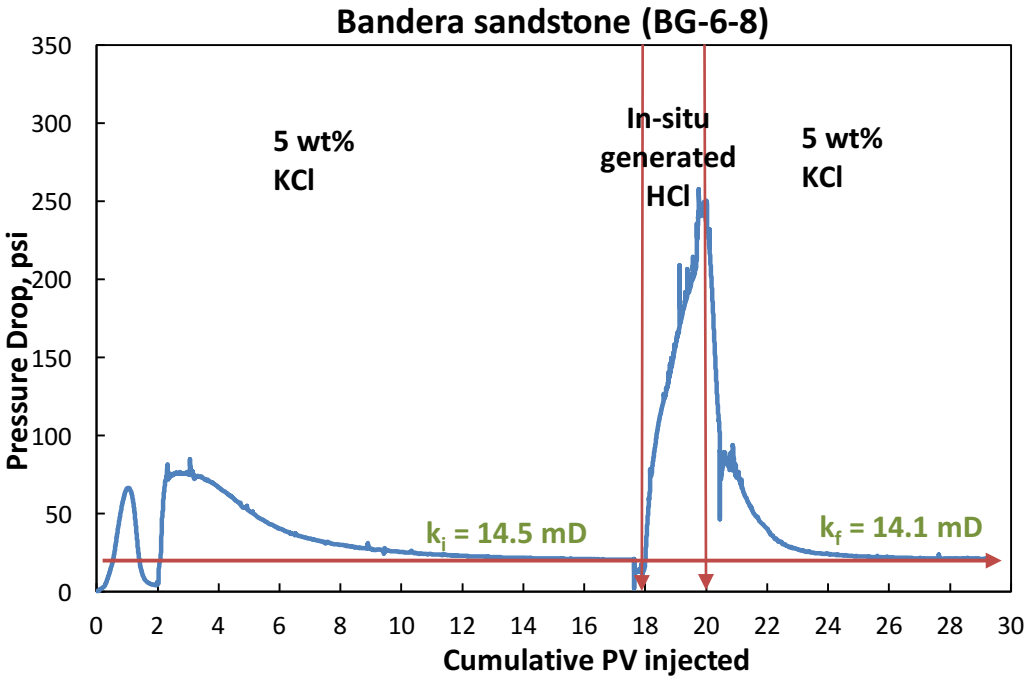

Fig. 15–Pressure drop profile of Bandera sandstone (BG-6-8), treated with in-situ generated HCl at 300°F (2 cm^3/min – 2 PV)

Core ID	Flow rate, cm^3/min	PV of in-situ generated HCl	k_f/k_i
BG-6-7	1	5	0.97
BG-6-8	2	2	0.97

Table 8–Comparison of permeability change for coreflood tests of Bandera sandstone after the treatment with in-situ generated HCl at 300°F (BG-6-7 and BG-6-8)

ICP analysis was carried out to correlate the coreflood results (**Fig. 16**). The presence of calcium and magnesium ions was a sign of carbonate dissolution. Iron concentration was around 2,500 mg/L at its peak. The presence of iron ions is an indication of dissolution of illite and chlorite clays found in the Bandera sandstone. K^+ concentration was decreased during acid injection and increased again when injection switched back to 5 wt% KCl.

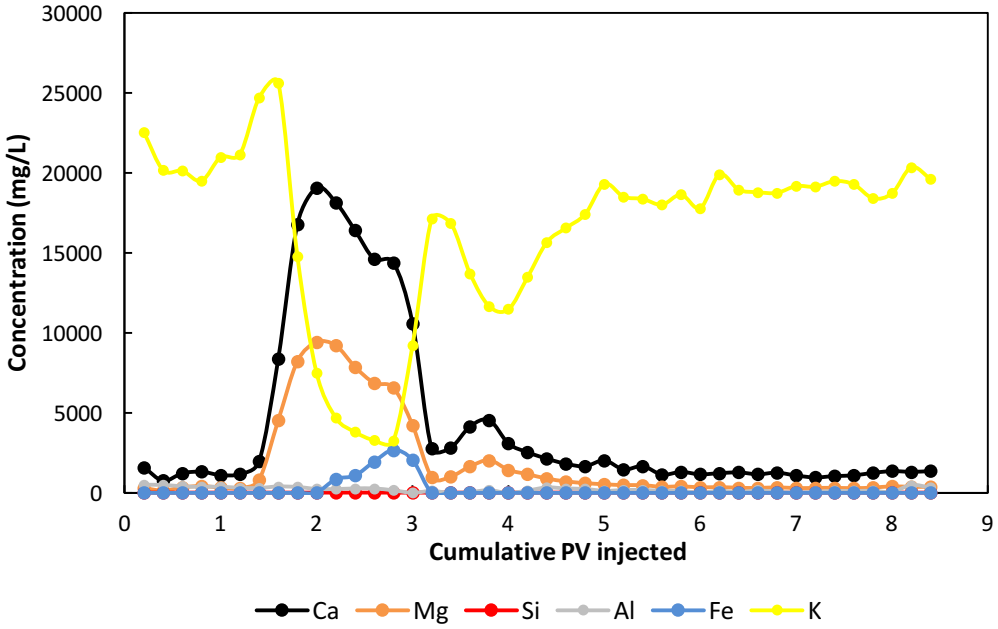

Fig. 16–ICP analysis of effluent samples from Bandera sandstone (BG-6-8) after the treatment with in-situ generated HCl at 300°F (2 cm^3/min – 2 PV)

Brine (5 wt% KCl) was injected as pre-flush and its pH was 7. After the injection of in-situ generated HCl followed by post-flush with brine, pH remained almost constant around 6.5 on average except for 2 data points (**Fig. 17**). This means that almost all of the acid was spent in the core to dissolve carbonates present in sandstone, and therefore no live acid was observed in the returning fluid.

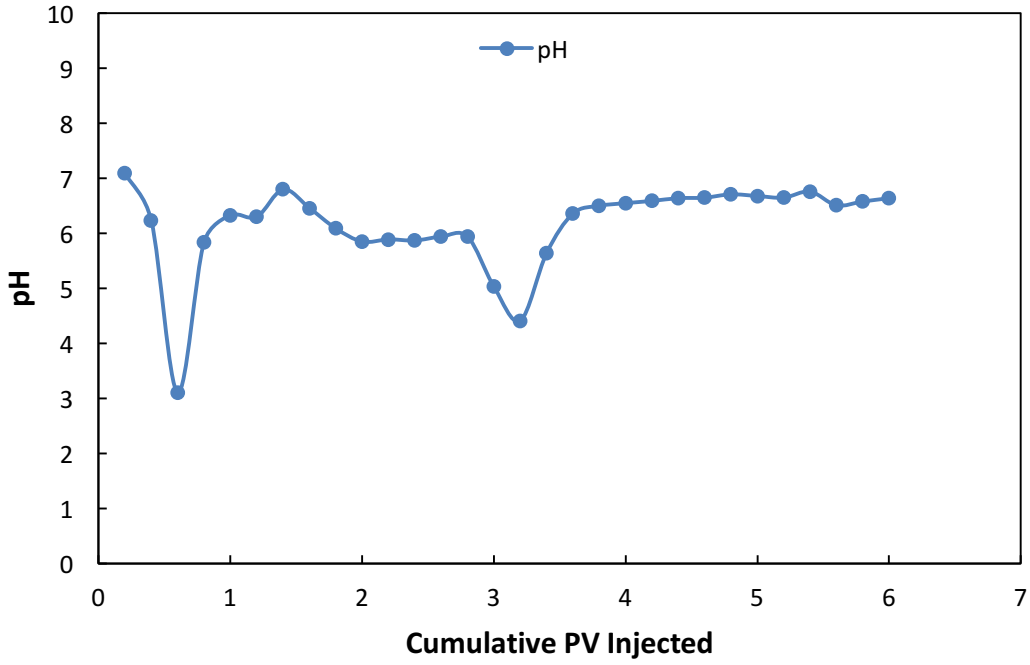

Fig. 17–pH of effluent samples from Bandera sandstone (BG-6-8) after the treatment with in-situ generated HCl at 300°F (2 cm^3/min – 2 PV)

Finally, a CT scan analysis was done after the acid treatment and the porosity profile was drawn along the length of the core (**Fig. 18**). On the same plot, average porosity (17.76%) was also included as a line, which was obtained by measuring the dry and saturated weight of the core. The plot shows a porosity increase up to 3% at the face of the core. After this peak at the face, porosity started to decline, and after around 2.5 inches it fell below the original porosity as a result of possible damage. This information was another indication that residence time of acid inside the rock plays an important role for acidizing treatments of sandstone.

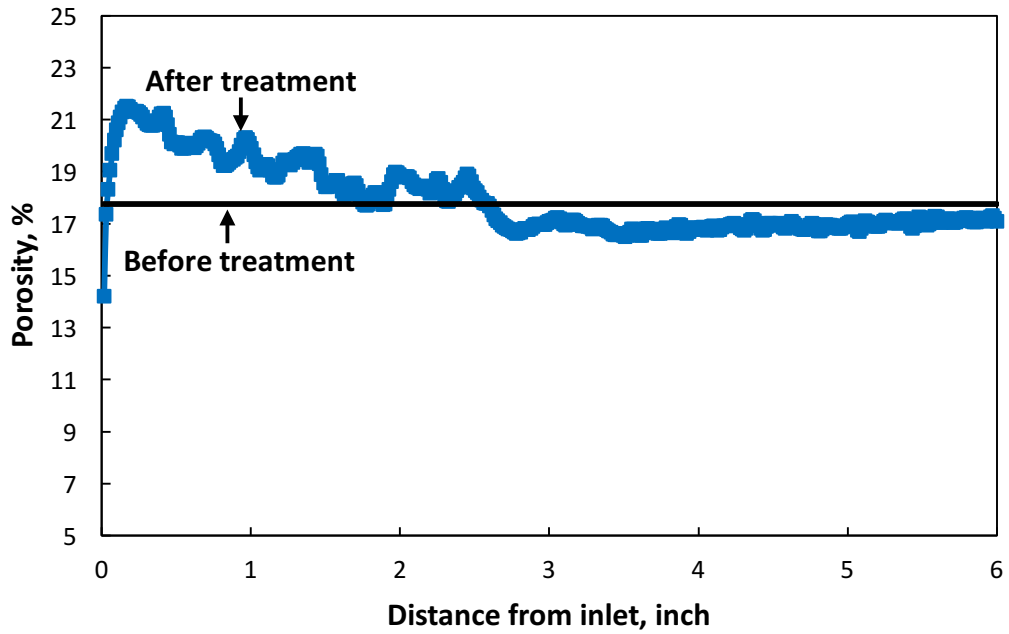

Fig. 18–Porosity profile of Bandera sandstone (BG-6-8) before and after the treatment with in-situ generated HCl at 300°F (2 cm^3/min – 2 PV)

Treatment with In-Situ Generated HCl (5 cm^3/min – 1 PV – BG-6-3)

It was understood that acidizing Bandera sandstone with 2 PV of in-situ generated HCl at 2 cm^3/min was not successful at 300°F. Therefore, another coreflood experiment was performed, this time increasing the injection rate to 5 cm^3/min and decreasing the amount of injected in-situ generated HCl to 1 PV. In this case, a 4% increase in permeability was observed after the treatment (**Fig. 19**). When compared to previous experiments, in which 3% damage was seen, this improvement was promising (**Table 9**).

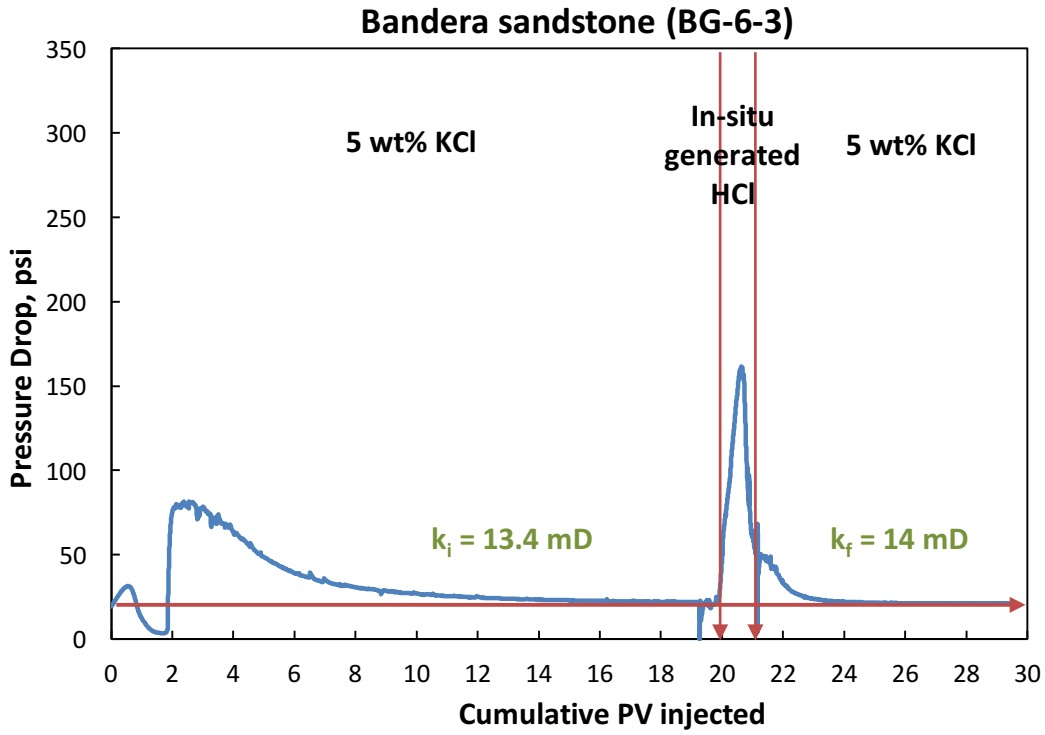

Fig. 19–Pressure drop profile of Bandera sandstone (BG-6-3), treated with in-situ generated HCl at 300°F (5 cm^3/min – 1 PV)

Core ID	Flow rate, cm^3/min	PV of in-situ generated HCl	k_f/k_i
BG-6-7	1	5	0.97
BG-6-8	2	2	0.97
BG-6-3	5	1	1.04

Table 9–Comparison of permeability change for coreflood tests of Bandera sandstone after the treatment with in-situ generated HCl at 300°F (BG-6-7, BG-6-8, and BG-6-3)

ICP analysis was carried out to correlate the coreflood results (**Fig. 20**). The presence of calcium and magnesium ions was a sign of carbonate dissolution. Iron concentration was around 0 throughout the experiment. This could be interpreted as possible iron precipitation in the pores of the core. Another possibility could be illite and

chlorite remaining undissolved. The latter could be more logical since kaolinite and feldspar seemed also to remain undissolved as there was no Al^{+3} or Si^{+4} observed. K^{+} concentration was decreased during acid injection and increased again when injection switched back to 5 wt% KCl.

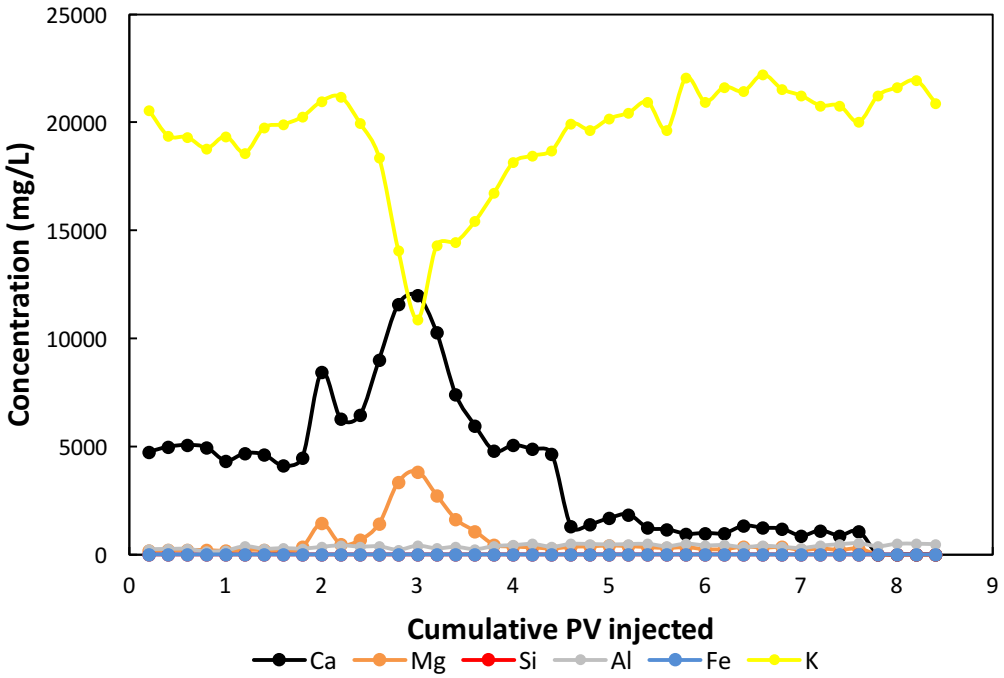

Fig. 20–ICP analysis of effluent samples from Bandera sandstone (BG-6-3) after the treatment with in-situ generated HCl at 300°F (5 cm^3/min – 1 PV)

Brine (5 wt% KCl) was injected as pre-flush and its pH was 7. After the injection of in-situ generated HCl followed by post-flush with brine, pH remained almost constant around 6.5 on average except for one data point (**Fig. 21**). This means that almost all of the acid was spent in the core to dissolve carbonates present in sandstone, and therefore no live acid was observed in the returning fluid.

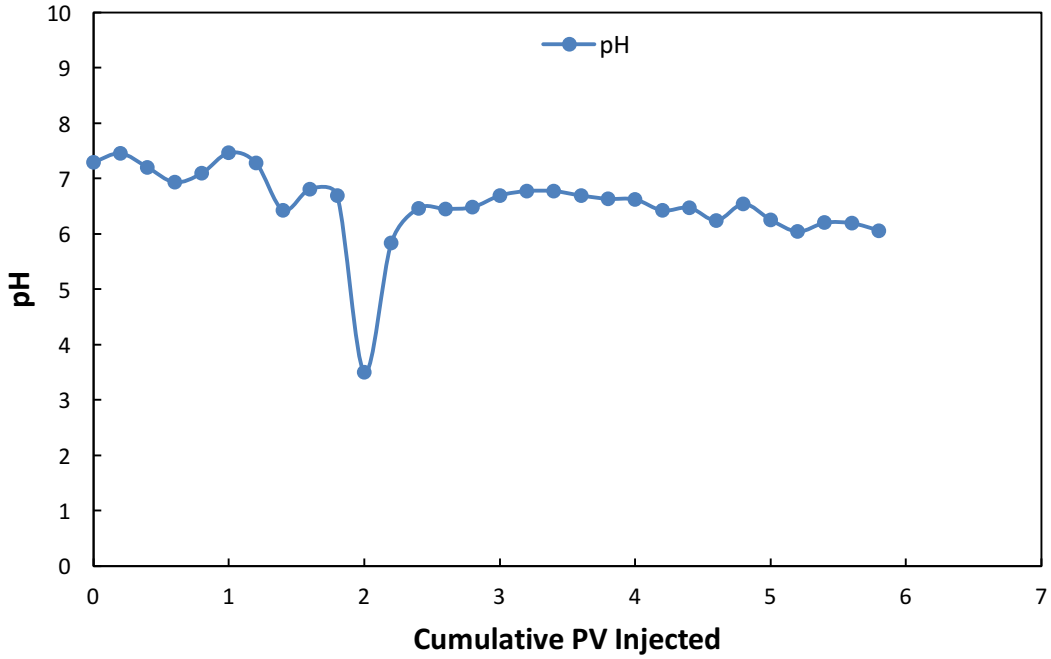

Fig. 21–pH of effluent samples from Bandera sandstone (BG-6-3) after the treatment with in-situ generated HCl at 300°F (5 cm^3/min – 1 PV)

Finally, a CT scan analysis was done after the acid treatment and the porosity profile was drawn along the length of the core (**Fig. 22**). On the same plot, average porosity (17.74%) was also included as a line, which was obtained by measuring the dry and saturated weight of the core. The plot shows a significant porosity increase up to 4.5% at the face of the core. After this peak at the face, porosity started to decline, and after around 1 inch it fell below the original porosity as a result of possible damage. The 4% increase in permeability can be attributed to this porosity increase observed within the 1 inch of the core.

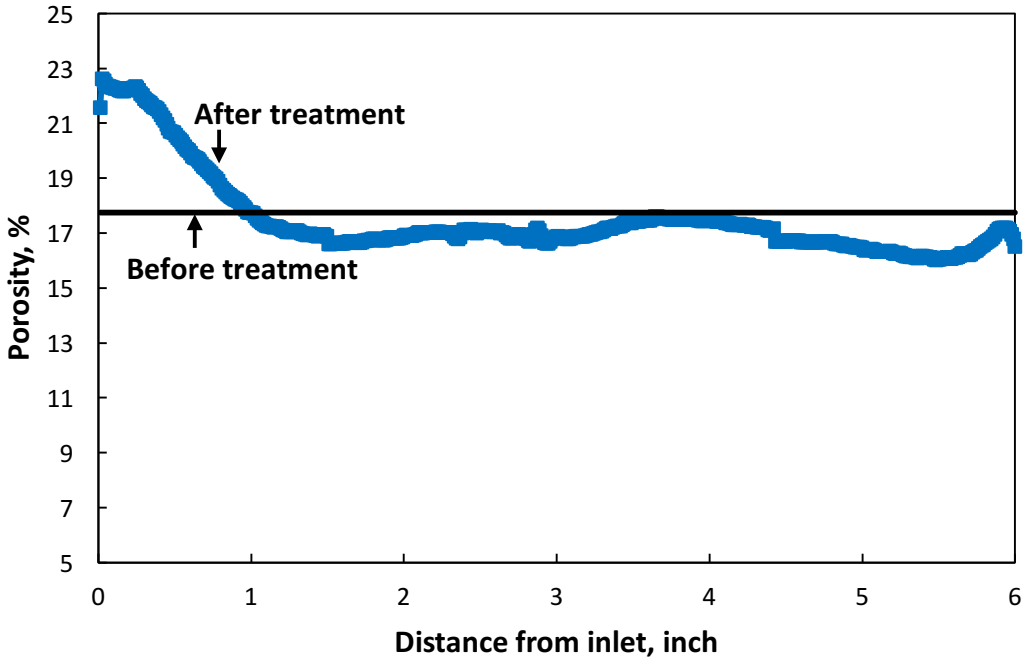

Fig. 22–Porosity profile of Bandera sandstone (BG-6-3) before and after the treatment with in-situ generated HCl at 300°F (5 cm^3/min – 1 PV)

Treatment with In-Situ Generated HCl (5 cm^3/min – 2 PV – BG-1)

Increasing the injection rate from 1 cm^3/min to 5 cm^3/min provided a 7% increase in performance of in-situ generated HCl (3% damage vs. 4% permeability improvement). However, this increase was still not comparable with 15 wt% HCl. Therefore, it was decided to double the amount of acid injected to 2 PV while keeping the injection rate as 5 cm^3/min. The pressure drop profile indicated a 37% increase in permeability, which was a significant achievement (**Fig. 23**).When compared to previous cases, there was more acid available to react with decreased residence time inside the core, which in return provided the optimum conditions for acidizing Bandera sandstone with in-situ generated HCl (**Table 10**).

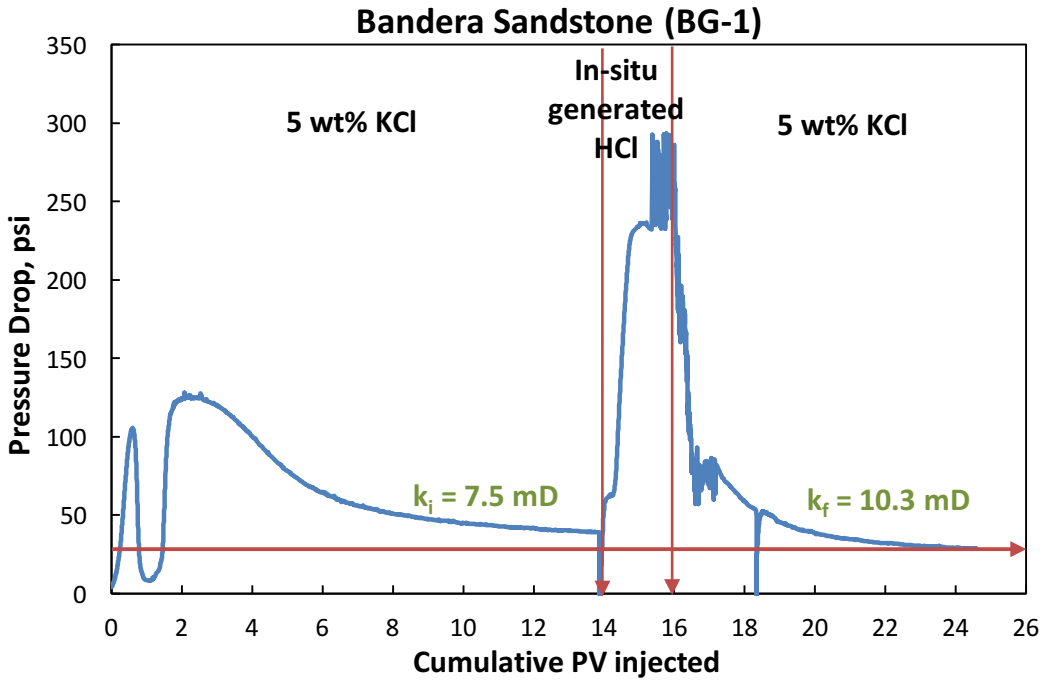

Fig. 23–Pressure drop profile of Bandera sandstone (BG-1), treated with in-situ generated HCl at 300°F (5 cm^3/min – 2 PV)

Core ID	Flow rate, cm^3/min	PV of in-situ generated HCl	k_f/k_i
BG-6-7	1	5	0.97
BG-6-8	2	2	0.97
BG-6-3	5	1	1.04
BG-1	5	2	1.37

Table 10–Comparison of permeability change for coreflood tests of Bandera sandstone after the treatment with in-situ generated HCl at 300°F (BG-6-7, BG-6-8, BG-6-3, and BG-1)

ICP analysis was carried out to correlate the coreflood results (**Fig. 24**). The presence of calcium and magnesium ions was a sign of carbonate dissolution. Iron concentration was around 25,000 mg/L at its peak. The presence of iron ions is an indication of dissolution of illite and chlorite clays found in the Bandera sandstone.

Aluminum (Al^{+3}) was also seen in the ICP results, which can be attributed to kaolinite and feldspar dissolution. K^{+} concentration was decreased during acid injection and increased again when injection switched back to 5 wt% KCl.

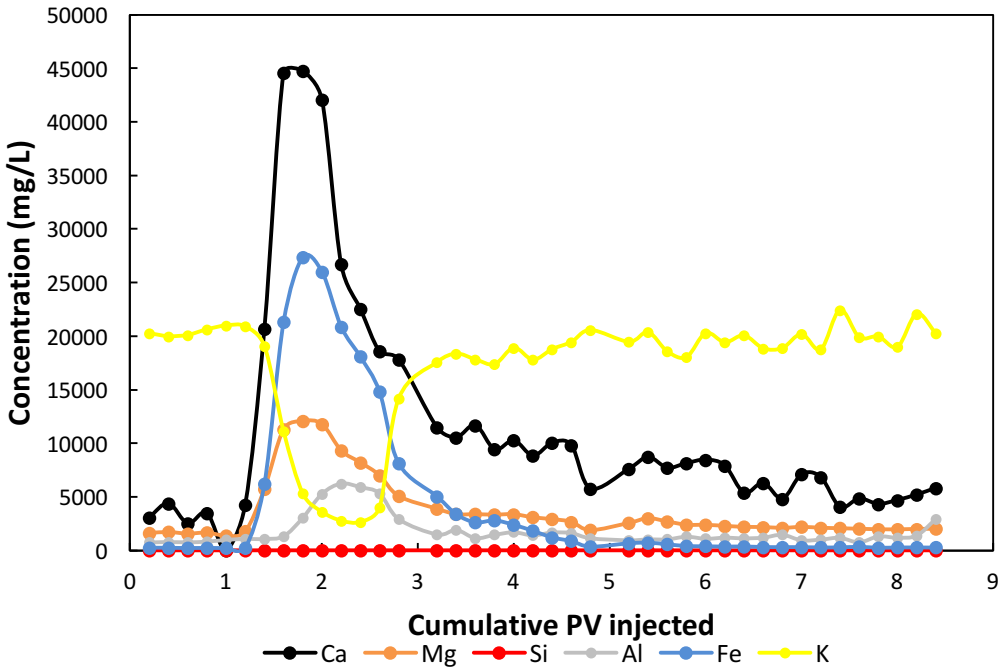

Fig. 24–ICP analysis of effluent samples from Bandera sandstone (BG-1) after the treatment with in-situ generated HCl at 300°F (5 cm^3/min – 2 PV)

At this point, a comparison between the three cases (BG-6-8, BG-6-3, and BG-1), in terms of calcium, magnesium and iron concentrations is necessary to better understand the effects of injection rate and the amount of acid injected on the dissolution of minerals. In **Fig. 25**, it is seen that injection of 2 PV in-situ generated HCl at 5 cm^3/min dissolved the most minerals, which is in agreement with the increase in permeability.

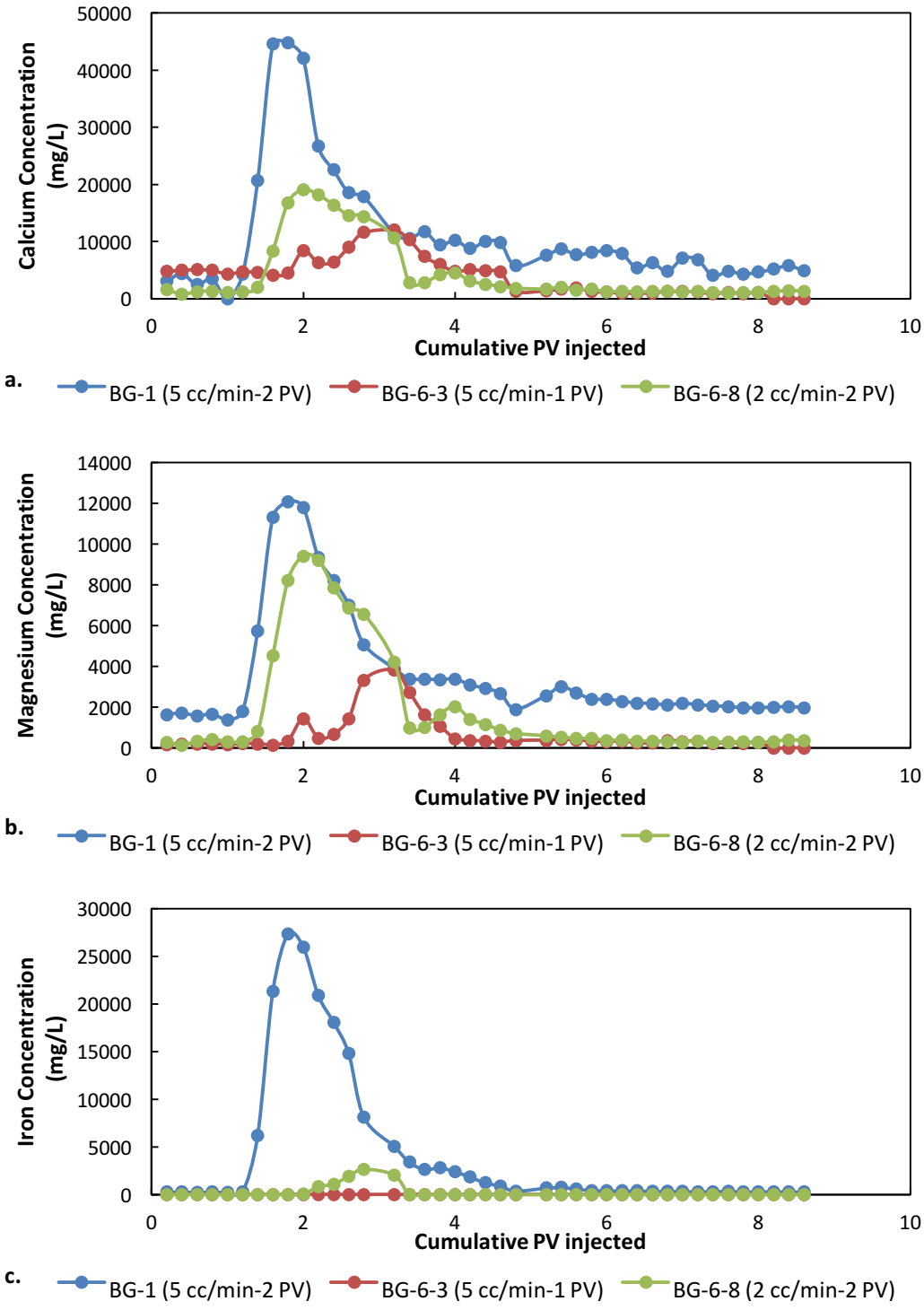

Fig. 25–Comparison of concentration of minerals dissolved (a. calcium, b. magnesium, c. iron) after acidizing Bandera sandstone with in-situ generated HCl at 300°F

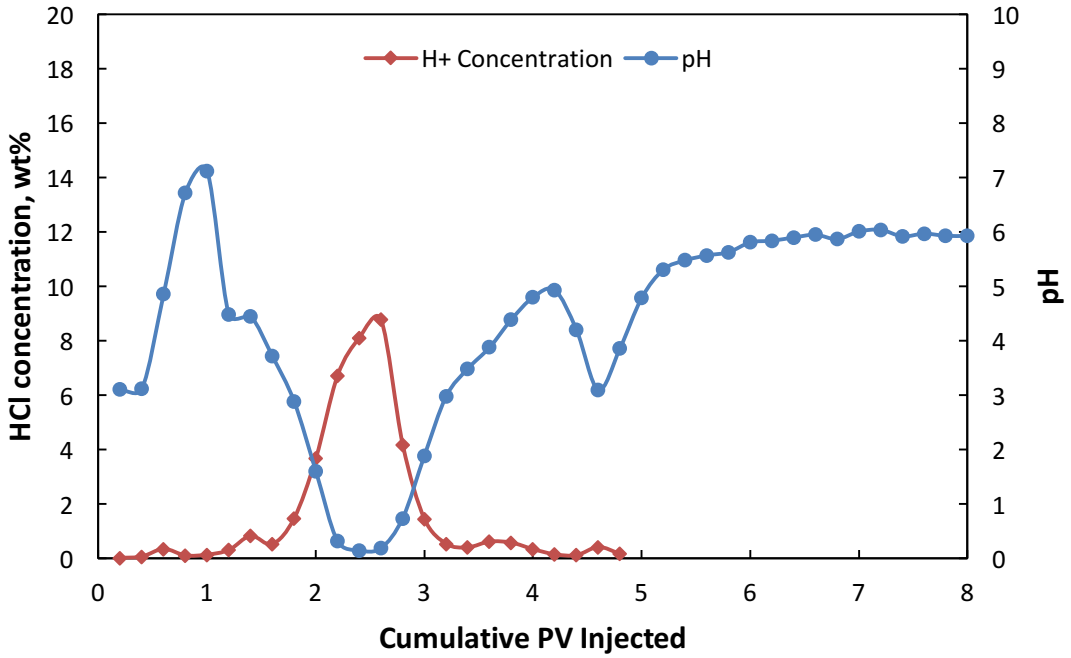

Fig. 26–pH and H^+ concentration of effluent samples from Bandera sandstone (BG-1) after the treatment with in-situ generated HCl at 300°F (5 cm^3/min – 2 PV)

Brine (5 wt% KCl) was injected as pre-flush, and its pH was 7. After the injection of in-situ generated HCl, pH started to decline, and decreased to 0. Parallel to the decrease in pH, H^+ concentration increased up to 10 wt% (**Fig. 26**). Finally, brine was injected as post-flush, and pH was stabilized at around 6 while H^+ concentration was decreased to 0. When pH and H^+ concentrations were interpreted with ICP results and pressure drop profile, it was inferred that most of the acid was spent to dissolve the minerals inside the core. Some of the acid remained unreacted, and was collected as live acid.

CT scan analysis was done after the acid treatment and the porosity profile was drawn along the length of the core (**Fig. 27**). On the same plot, average porosity (17.15%) was also included as a line, which was obtained by measuring the dry and saturated weight of the core. The plot shows a significant porosity increase, which is around 2% on average.

The increase was more evident at the inlet of the core. Porosity increase was also in agreement with the pressure drop profile, ICP analysis, pH and H^+ concentrations, and all results indicated that acidizing of Bandera sandstone with in-situ generated HCl at 300°F was successful.

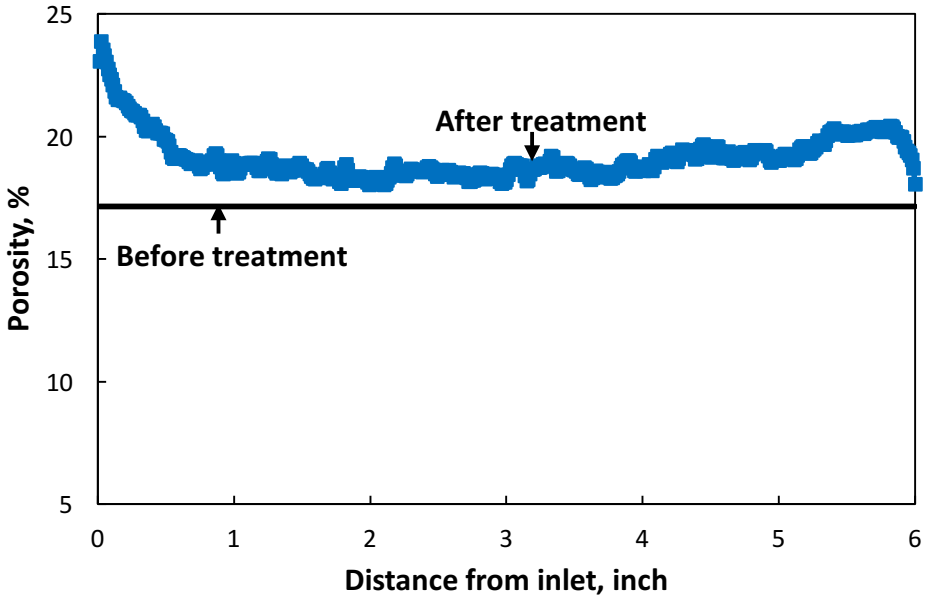

Fig. 27–Porosity profile of Bandera sandstone (BG-1) before and after the treatment with in-situ generated HCl at 300°F (5 cm^3/min – 2 PV)

Treatment with 15 wt% HCl (5 cm^3/min – 2 PV – BG-2)

The optimum injection parameters for acidizing the Bandera sandstone with in-situ generated HCl at 300°F was obtained as 5 cm^3/min and 2 PV. Using the same injection parameters, Bandera sandstone was acidized with 15 wt% HCl at 300°F. The pressure drop profile indicated that this treatment resulted in 30% permeability improvement (**Fig. 28**). When the performances of 15 wt% HCl and in-situ generated HCl was compared in terms of permeability increase, it was seen that the latter performed better (**Table 11**).

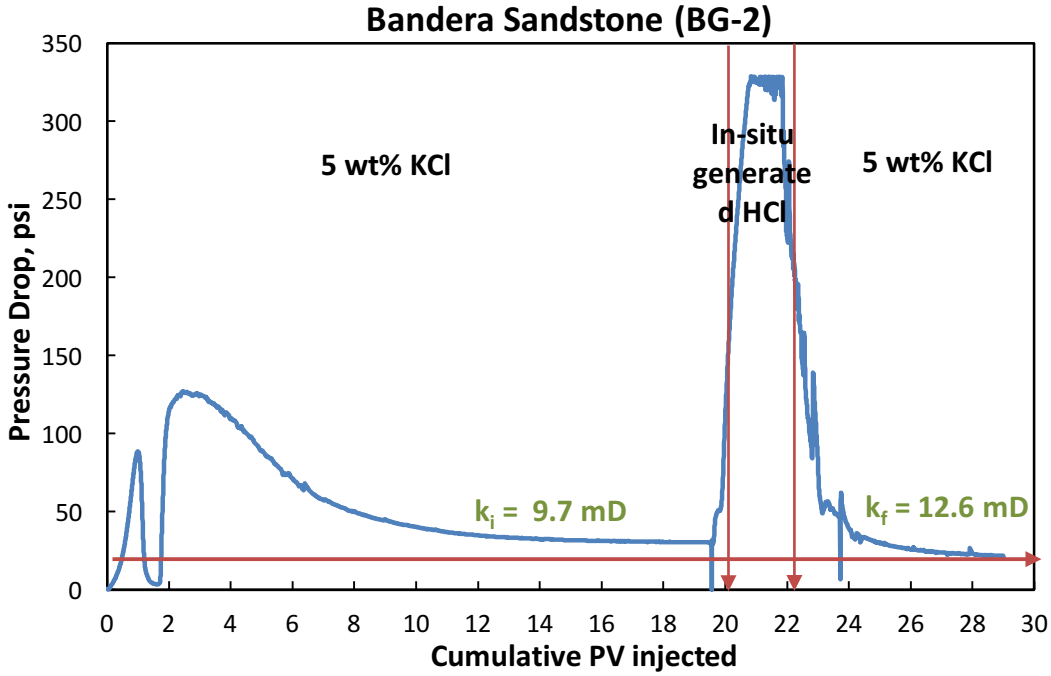

Fig. 28–Pressure drop profile of Bandera sandstone (BG-2), treated with 15 wt% HCl at 300°F (5 cm^3/min – 2 PV)

Core ID	Acid	Flow rate, cm^3/min	PV injected	k_f/k_i
BG-1	In-situ generated HCl	5	2	1.37
BG-2	15 wt% HCl	5	2	1.30

Table 11–Comparison of the change in permeability of Bandera sandstone after acidizing with in-situ generated HCl and 15 wt% HCl at 300°F

ICP analysis was carried out to correlate the coreflood results (**Fig. 29**). The presence of calcium and magnesium ions was a sign of carbonate dissolution. Iron concentration was around 60,000 mg/L at its peak. The presence of iron ions is an indication of dissolution of illite and chlorite clays found in the Bandera sandstone. Aluminum (Al^{+3}) was also seen in the ICP results, which can be attributed to kaolinite and

feldspar dissolution. K^+ concentration was decreased during acid injection and increased again when injection switched back to 5 wt% KCl.

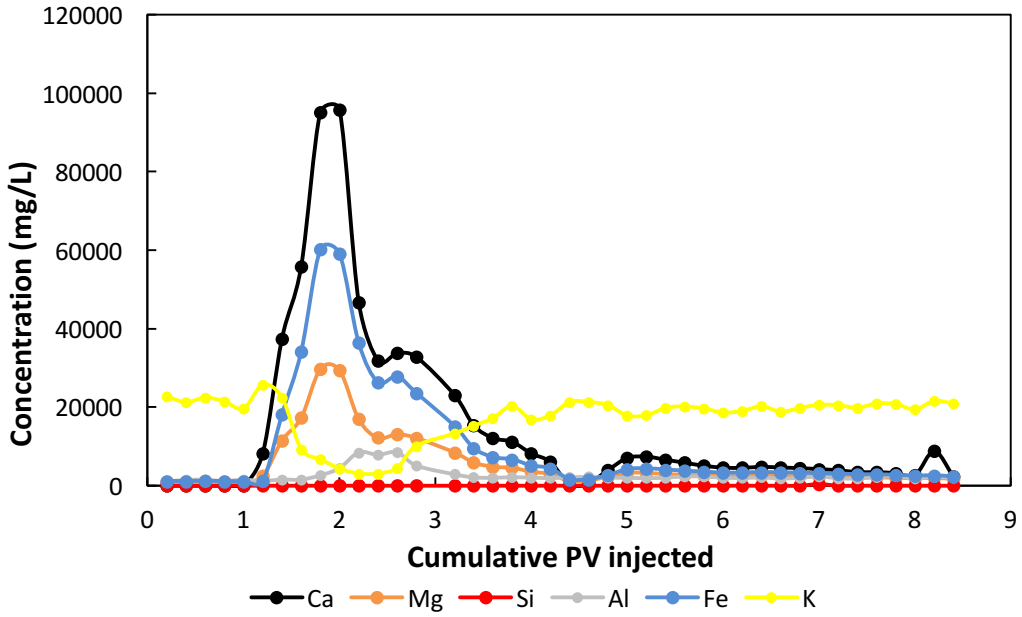

Fig. 29–ICP analysis of effluent samples from Bandera sandstone (BG-2) after the treatment with 15 wt% HCl at 300°F (5 cm^3/min – 2 PV)

It should be noted that 15 wt% HCl dissolved around two times more minerals than in-situ generated HCl according to ICP results (**Fig. 30**). This was a sign of the high dissolving power of HCl and yet, in-situ generated HCl delivered a higher permeability increase than regular HCl. This can be interpreted as HCl caused more precipitates than it dissolved at 300°F. High dissolving power can be a disadvantage of HCl especially in carbonate acidizing; this concept will be discussed more in the coming sections.

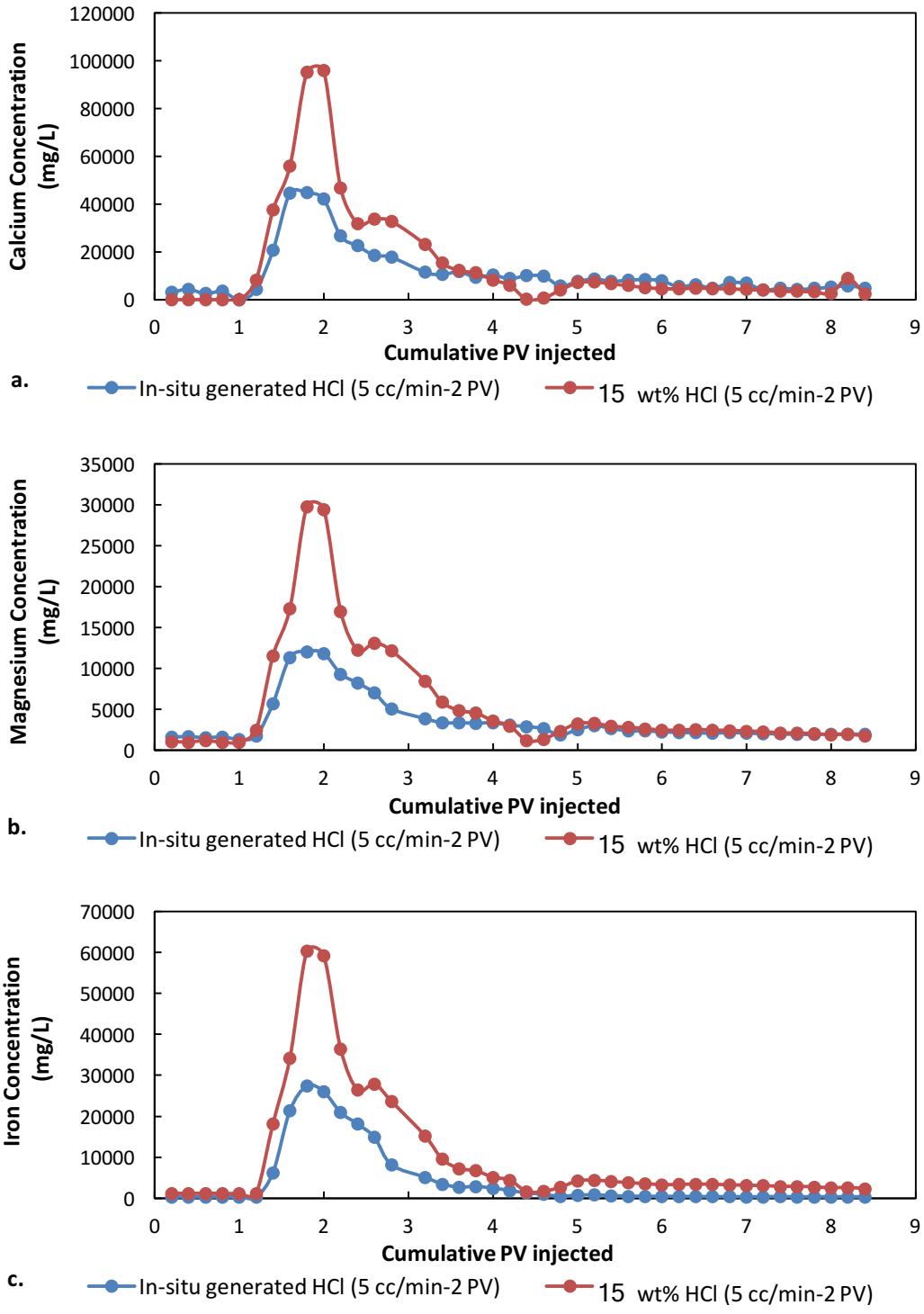

Fig. 30–Comparison of concentration of minerals dissolved (a. calcium, b. magnesium, c. iron) after acidizing Bandera sandstone with in-situ generated HCl and 15 wt% HCl at 300°F

Brine (5 wt% KCl) was injected as pre-flush and its pH was 7. After the injection of in-situ generated HCl, pH started to decline, and decreased to 0. Parallel to the decrease in pH, H^+ concentration increased up to 8 wt% (**Fig. 31**). Finally, brine was injected as post-flush and the pH was stabilized at around 4 while H^+ concentration was decreased to 0. When pH and H^+ concentrations were interpreted with ICP results and pressure drop profile, it was inferred that most of the acid was spent to dissolve the minerals inside the core. Some of the acids remained unreacted and it was collected as live acid.

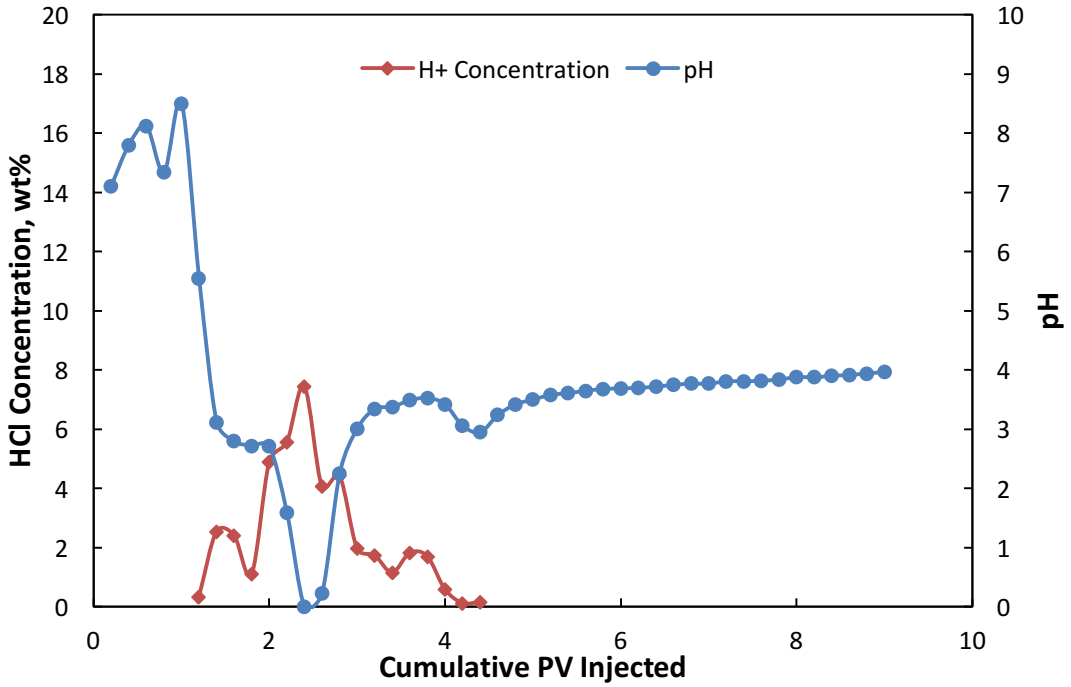

Fig. 31–pH and H^+ concentration of effluent samples from Bandera sandstone (BG-2) after the treatment with 15 wt% HCl at 300°F (5 cm^3/min – 2 PV)

Coreflood Experiments Done with Silurian Dolomite at 300° F

Treatment with In-Situ Generated HCl (2 cm³/min – SD-6-35)

Dolomite, $CaMg(CO_3)_2$, is a type of carbonate rock with the formula. The previous coreflood experiments with Silurian dolomite were conducted with an injection rate of 1 cm^3/min at 300°F. In-situ generated HCl could not reach breakthrough after 5 PV of injection at this rate. Therefore, it was decided to increase the injection rate to 2 cm^3/min and repeat the experiment at 300°F. According to the pressure drop profile of this coreflood experiment, in-situ generated HCl reached breakthrough after 3.3 PV of injection (**Fig. 32**).

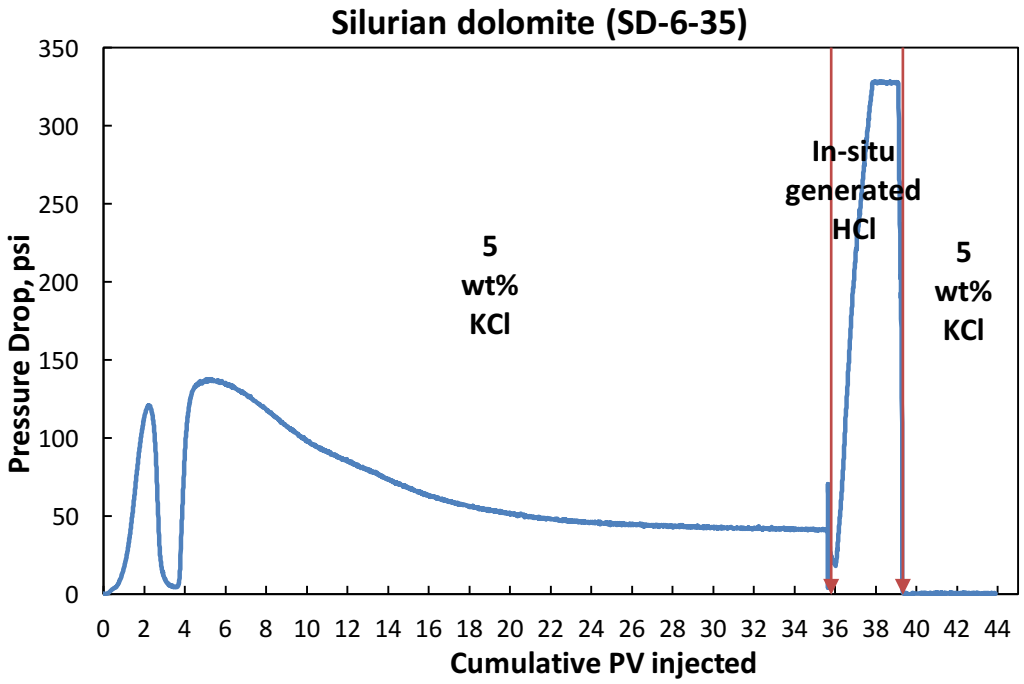

Fig. 32–Pressure drop profile of Silurian dolomite (SD-6-35), treated with in-situ generated HCl at 300°F (2 cm^3/min – reached BT after 3.3 PV)

ICP analysis was carried out to correlate the coreflood results (**Fig. 33**). Calcium concentration was around 45,000 mg/L at its peak, whereas magnesium concentration was around 20,000 mg/L at its peak. K^+ concentration was decreased during acid injection and increased again when injection switched back to 5 wt% KCl.

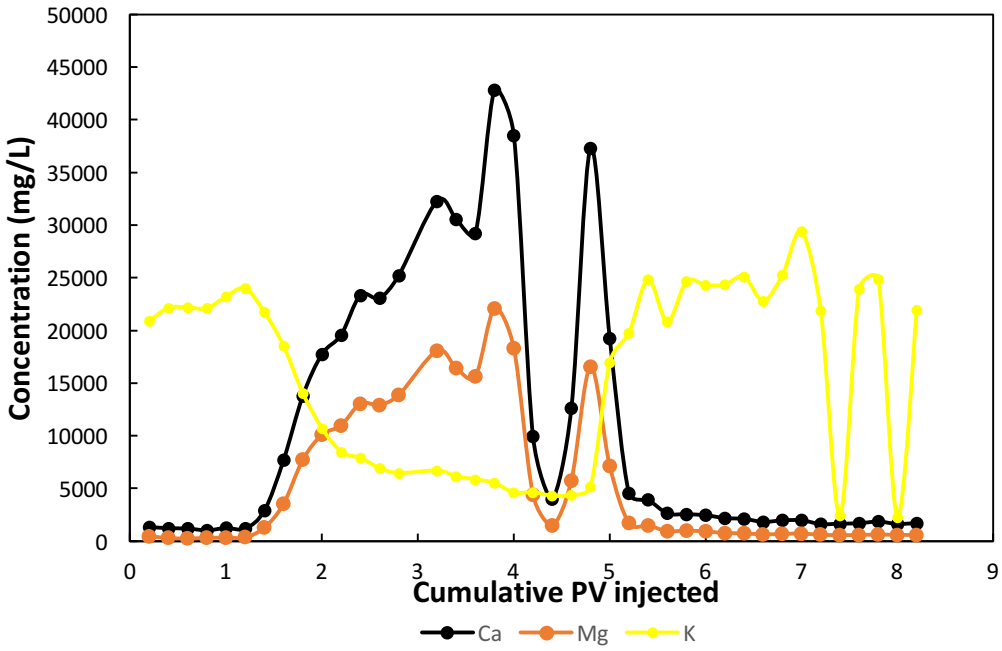

Fig. 33–ICP analysis of effluent samples from Silurian dolomite (SD-6-35) after the treatment with in-situ generated HCl at 300°F (2 cm^3/min – reached BT after 3.3 PV)

Brine (5 wt% KCl) with a pH of 7 was injected as post-flush to clean the remaining acid inside the wormholes. H^+ concentration went up to 15 wt% when pH dropped to 0 (**Fig. 34**). This was the sign that live acid was being collected. Brine was continually injected until the effluents became colorless, in other words until the H^+ concentration was 0. The pH was stabilized at 7 at the end of the experiment.

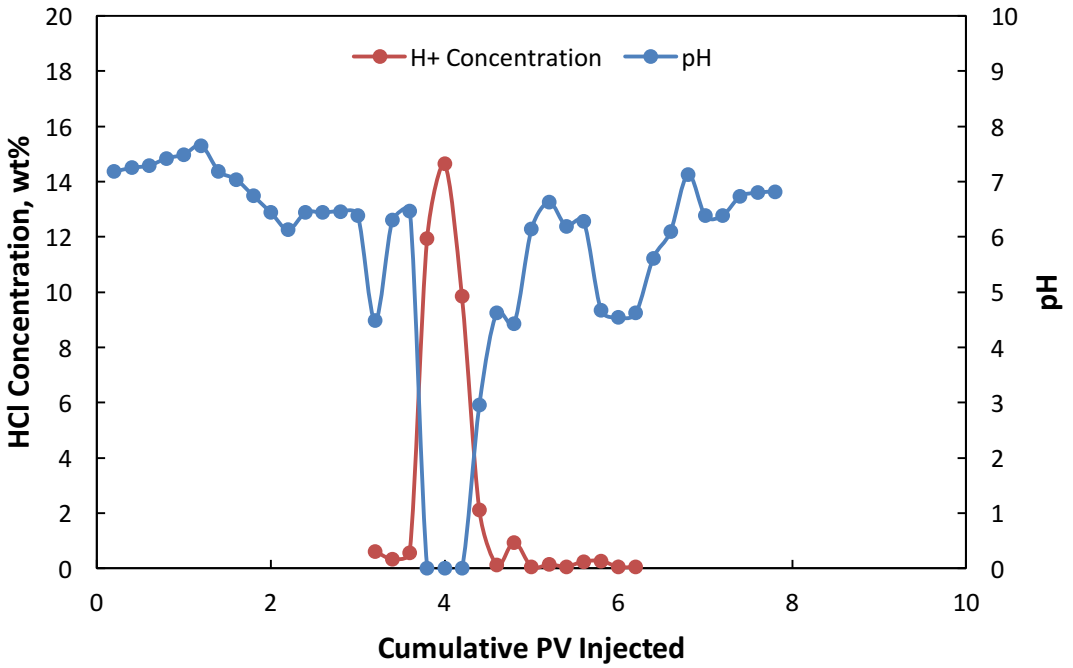

Fig. 34–pH and H^+ concentration of effluent samples from Silurian dolomite (SD-6-35) after the treatment with in-situ generated HCl at 300°F (2 cm^3/min – reached BT after 3.3 PV)

A CT scan was conducted on a Silurian dolomite core after the treatment with in-situ generated HCl at 300°F (**Fig. 35**). The wormhole observed in the CT scan was a single, dominant wormhole. This type of wormhole is the most efficient as was mentioned earlier. Increasing the injection rate from 1 cm^3/min to 2 cm^3/min proved that in-situ generated HCl was very successful in acidizing dolomite at 300°F, and the previous tests were misleading about the performance of the novel acid.

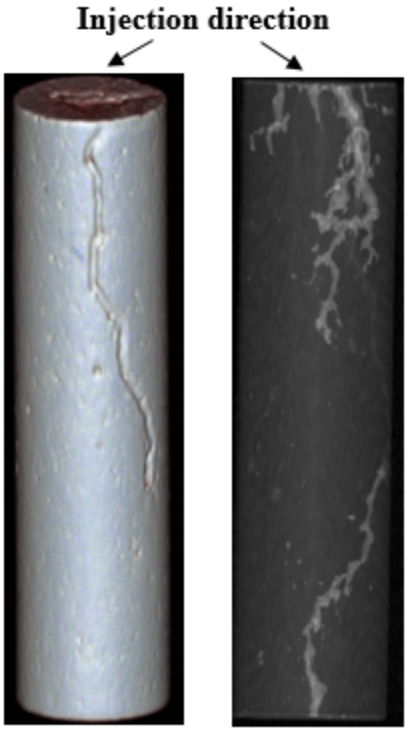

Fig. 35–Wormhole propagation from CT scan for Silurian dolomite treated with in-situ generated HCl at 300°F (2 cm^3/min – reached BT after 3.3 PV)

Treatment with 15 wt% HCl (2 cm^3/min – SD-6-35)

In the previous coreflood experiment done with Silurian dolomite at 300°F, 15 wt% HCl could not reach breakthrough after 5 PV of injection at a rate of 1 cm^3/min. This experiment was also repeated by increasing the injection rate to 2 cm^3/min and results of both acids were compared. The pressure drop profile showed that 15 wt% HCl reached breakthrough after 3.6 PV of injection (**Fig. 36**). Compared to the breakthrough value of in-situ generated HCl, which was 3.3 PV, acidizing with 15 wt% HCl showed a reduced performance in Silurian dolomite at 300°F (**Table 12**).

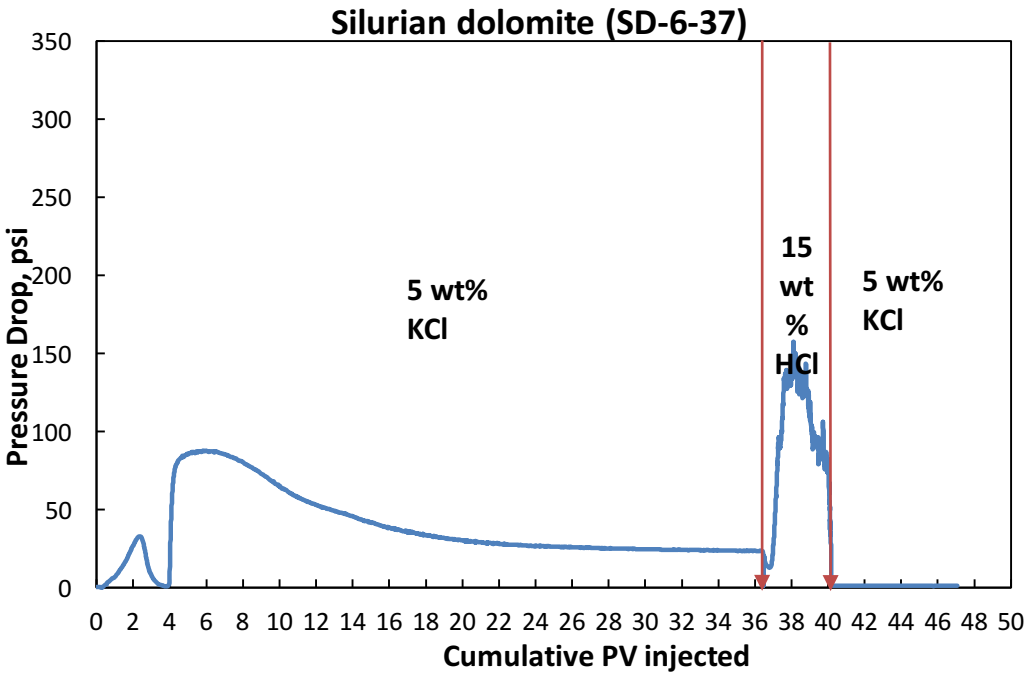

Fig. 36–Pressure drop profile of Silurian dolomite (SD-6-37), treated with 15 wt% HCl at 300°F (2 cm^3/min – reached BT after 3.6 PV)

Core ID	Acid	Temperature, °F	PV to breakthrough (BT)
SD-6-35	In-situ generated HCl	300	3.3
SD-6-37	15 wt% HCl	300	3.6

Table 12–Comparison of the BT values of in-situ generated HCl and 15 wt% HCl in acidizing of Silurian dolomite at 300°F

ICP analysis was carried out to correlate the coreflood results (**Fig. 37**). Calcium concentration was around 70,000 mg/L at its peak, whereas magnesium concentration was around 35,000 mg/L at its peak. K^+ concentration was decreased during acid injection and increased again when injection switched back to 5 wt% KCl.

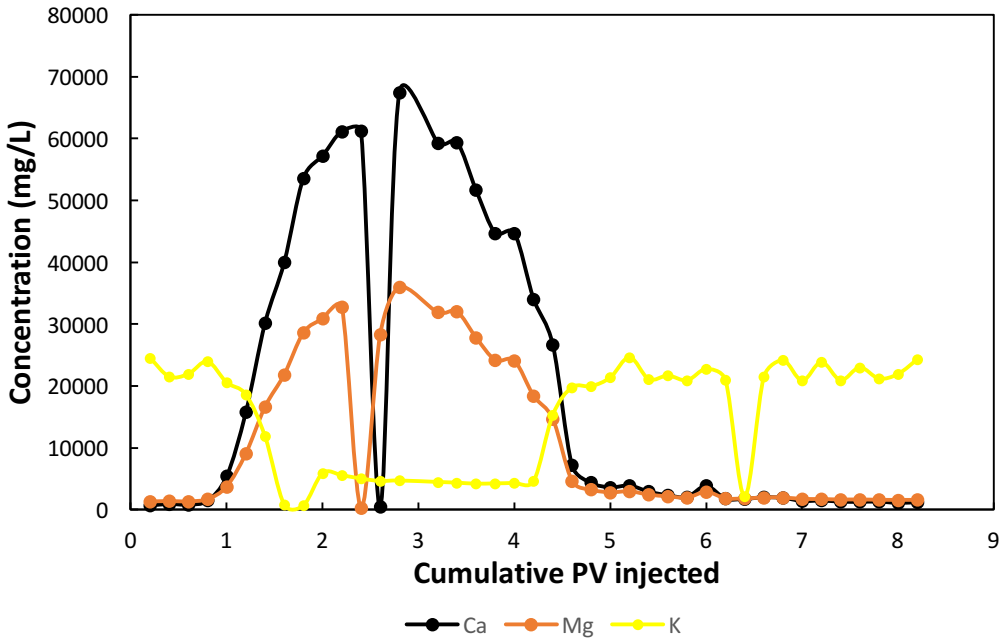

Fig. 37–ICP analysis of effluent samples from Silurian dolomite (SD-6-37) after the treatment with 15 wt% HCl at 300°F (2 cm^3/min – reached BT after 3.6 PV)

Brine (5 wt% KCl) with a pH of 7 was injected as post-flush to clean the remaining acid inside the wormholes. H^+ concentration went up to 4 wt% when pH dropped to 0 (**Fig. 38**). Brine was continually injected until the effluents became colorless, in other words until the H^+ concentration was 0. The pH was stabilized at 4 at the end of the experiment.

A CT scan was conducted on Silurian dolomite core after the treatment with 15 wt% HCl. The wormhole observed in the CT scan was a conical shaped wormhole. This type of wormhole is formed when the acid has a high dissolving power such as regular HCl. When a side by side comparison of CT scans was made, the difference in wormhole type was more visible (**Fig. 39**). Moreover, it is seen in Fig. 39 that regular HCl caused

more face dissolution, which is again associated with its high dissolving power. These results were perfect indicators that in-situ generated HCl had superior performance over the regular 15 wt% HCl for acidizing dolomite at 300°F.

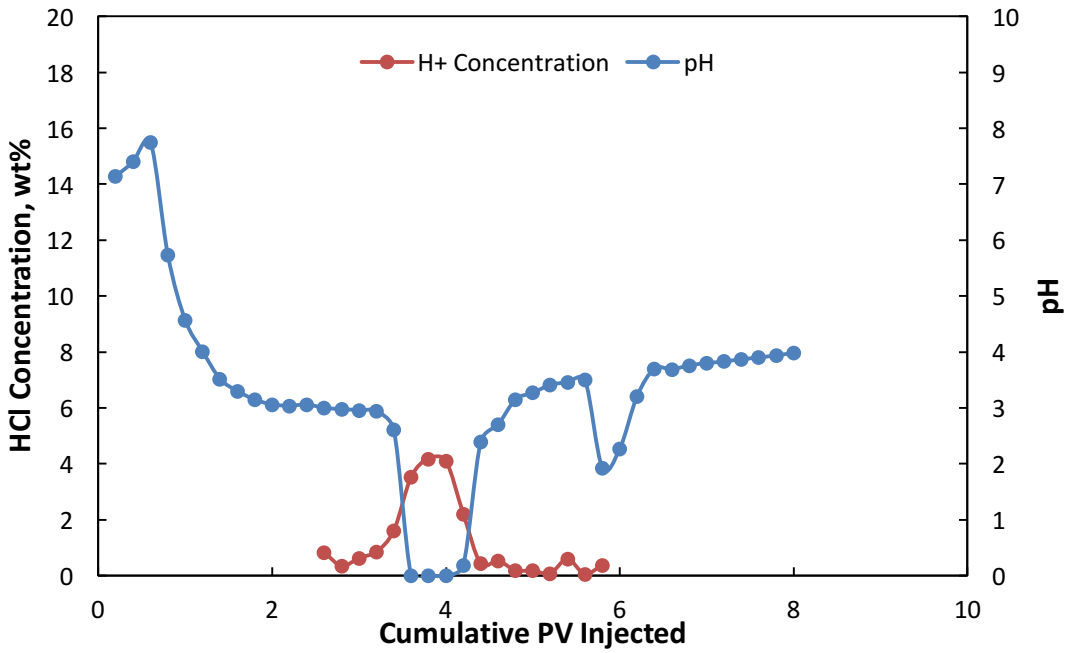

Fig. 38–pH and H^+ concentration of effluent samples from Silurian dolomite (SD-6-37) after the treatment with 15 wt% HCl at 300°F (2 cm^3/min – reached BT after 3.6 PV)

Another sign of the high dissolving power of regular HCl was the concentration of calcium and magnesium dissolved. When the ICP results for Silurian dolomite treated with in-situ generated HCl and 15 wt% HCl was compared, it was seen that 15 wt% HCl dissolved almost two times more minerals than in-situ generated HCl (**Fig. 40**).

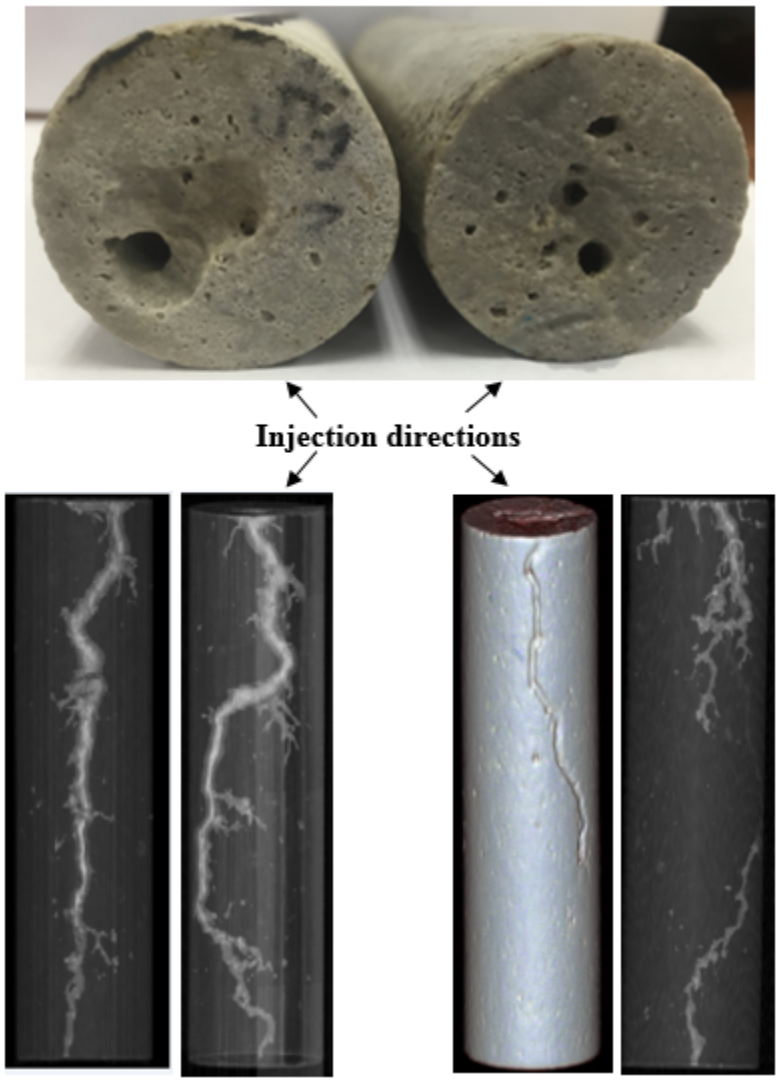

a. 15 wt% HCl **b. In-situ generated HCl**

Fig. 39–Comparison of wormhole propagation in Silurian dolomite cores treated with a. 15 wt% HCl and b. in-situ generated HCl at 300^{o}F

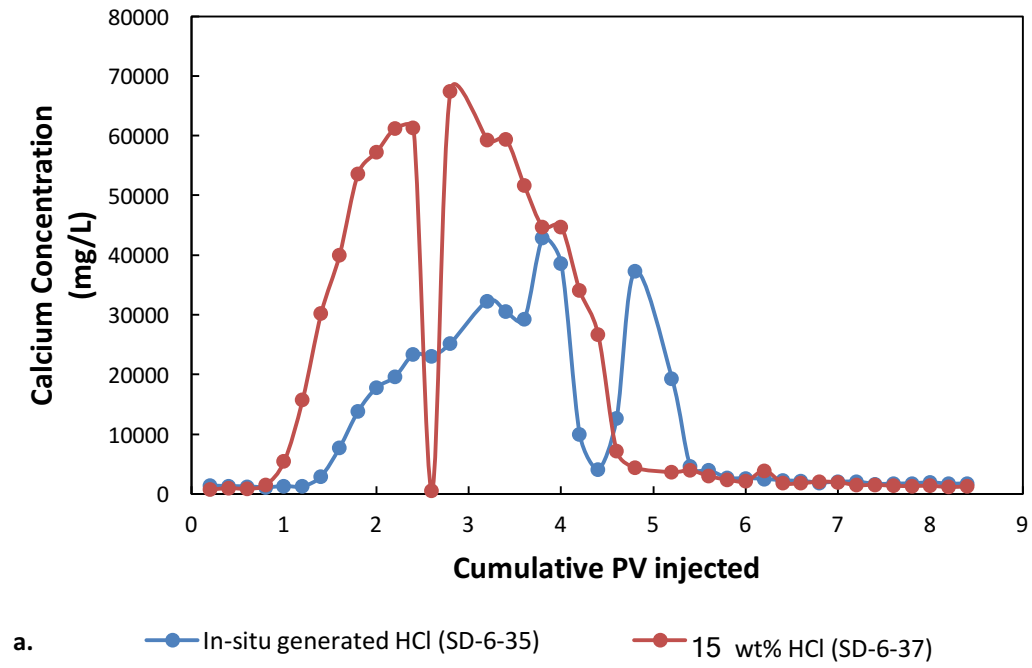

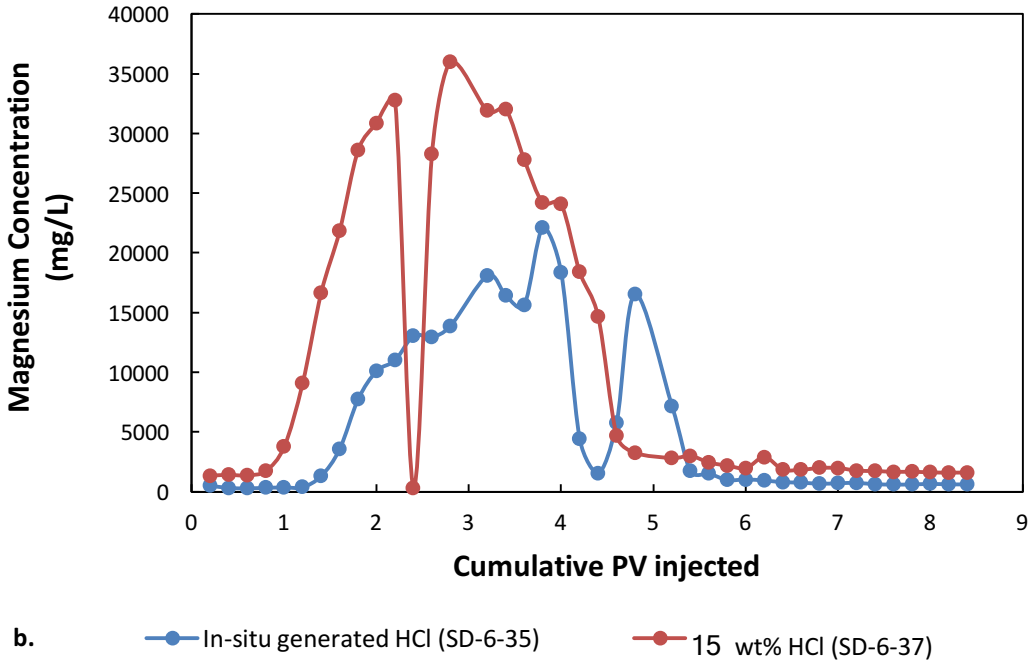

Fig. 40–Comparison of concentration of minerals dissolved (a. calcium, b. magnesium) after acidizing Silurian dolomite with in-situ generated HCl and 15 wt% HCl at 300°F

Coreflood Experiments Done with Indiana Limestone at 300°F

Treatment with In-Situ Generated HCl (2 cm^3/min – L-1-A)

Limestone is another type of carbonate rock with the formula $CaCO_3$. In-situ generated HCl was injected through Indiana limestone core at 300°F. An injection rate of 2 cm^3/min was used, which was the same in the case of Silurian dolomite coreflood. Breakthrough was reached after 1.35 PV of acid injection (**Fig. 41**). It took 3.3 PV of in-situ generated HCl to reach breakthrough in the case of Silurian dolomite. Since the reaction of HCl with dolomite is much slower than limestone, it is expected for dolomite to require more PV to reach breakthrough than limestone.

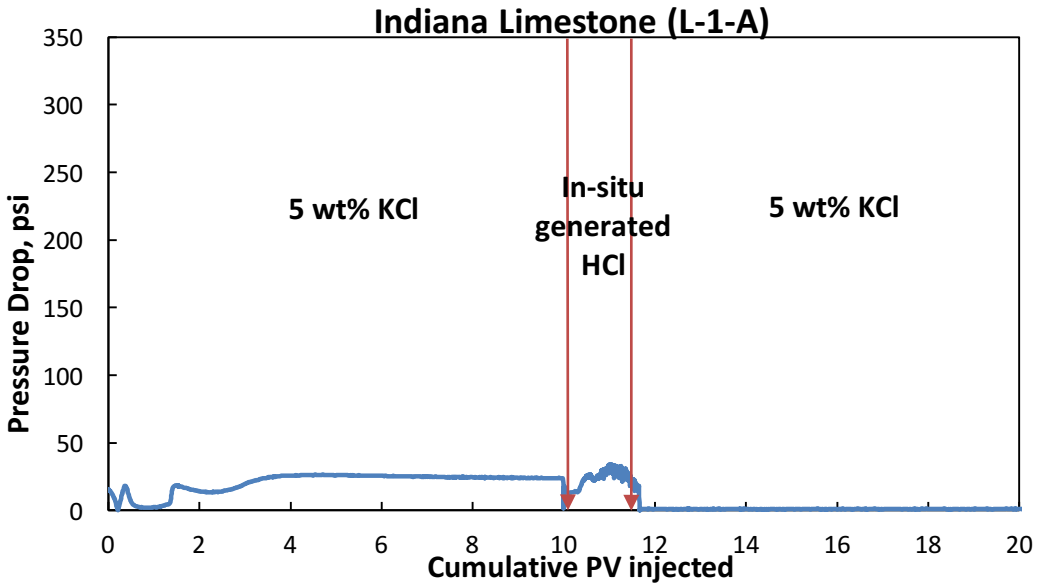

Fig. 41–Pressure drop profile of Indiana limestone (L-1-A), treated with in-situ generated HCl at 300°F (2 cm^3/min – reached BT after 1.35 PV)

ICP analysis was carried out to correlate the coreflood results (**Fig. 42**). Calcium concentration was around 60,000 mg/L at its peak, which indicates carbonate dissolution.

K^+ concentration was decreased during acid injection and increased again when injection switched back to 5 wt% KCl.

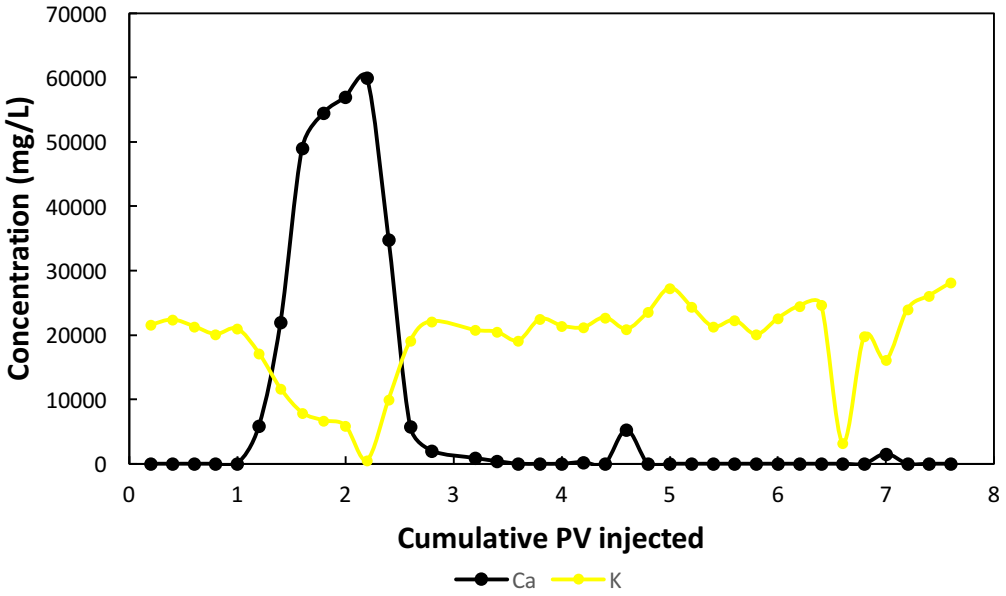

Fig. 42–ICP analysis of effluent samples from Indiana limestone (L-1-A) after the treatment with in-situ generated HCl at 300°F (2 cm^3/min – reached BT after 1.35 PV)

Brine (5 wt% KCl) with a pH of 7 was injected as post-flush to clean the remaining acid inside the wormholes. H+ concentration went up to 5 wt% and pH dropped to a minimum of 3 (**Fig. 43**). Brine was injected until the effluents became colorless, in other words, until the H+ concentration was 0. The pH was increased to around 7 at the end of the experiment.

A CT scan was conducted on Indiana limestone core after the treatment with in-situ generated HCl at 300°F (**Fig. 44**). Carbonate acidizing aims to have dominant wormholes. Like in the case of Silurian dolomite, a single, dominant wormhole was observed in this CT scan as well, which verified the success of the treatment.

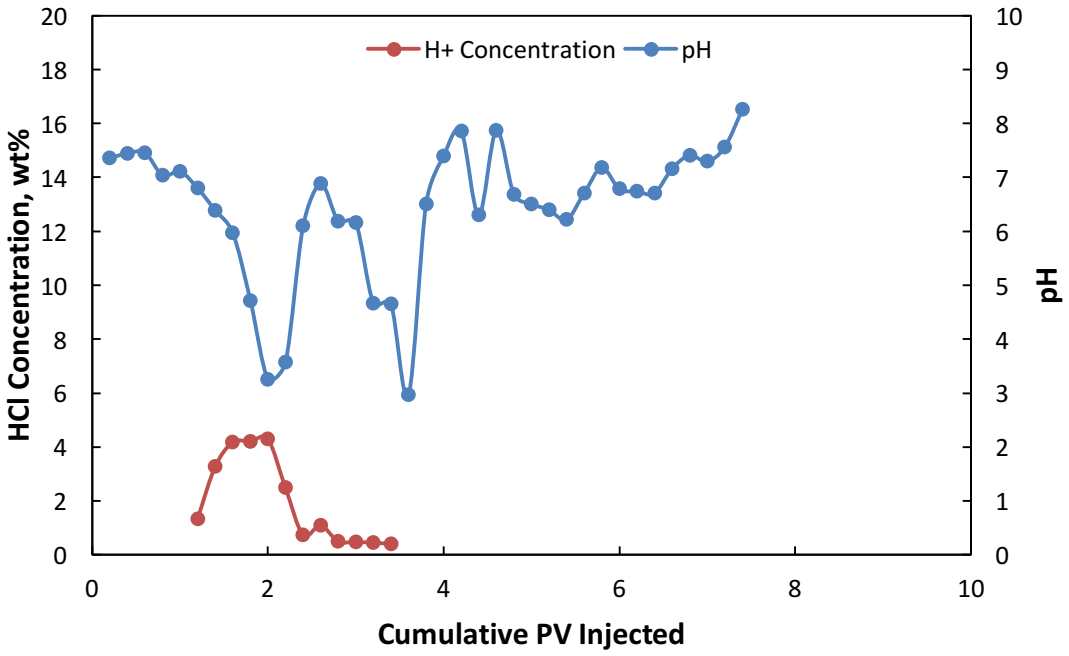

Fig. 43–pH and H^+ concentration of effluent samples from Indiana limestone (L-1-A) after the treatment with in-situ generated HCl at 300°F (2 cm^3/min – reached BT after 1.35 PV)

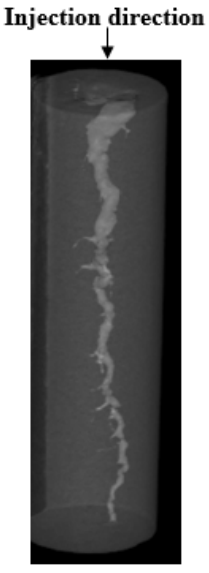

Fig. 44–Wormhole propagation from CT scan for Indiana limestone treated with in-situ generated HCl at 300°F (2 cm^3/min – reached BT after 1.35 PV)

Treatment with 15 wt% HCl (2 cm^3/min – L-1-B)

A final coreflood test was done with Indiana limestone at 300°F by injecting 15 wt% HCl at a rate of 2 cm^3/min. The results were compared with in-situ generated HCl. The pressure drop profile in **Fig. 45** showed that 15 wt% HCl reached breakthrough after 2.01 PV. Compared to the breakthrough value of in-situ generated HCl, which was 1.35 PV, 15 wt% HCl was less successful in acidizing the Indiana limestone at 300°F (**Table 13**).

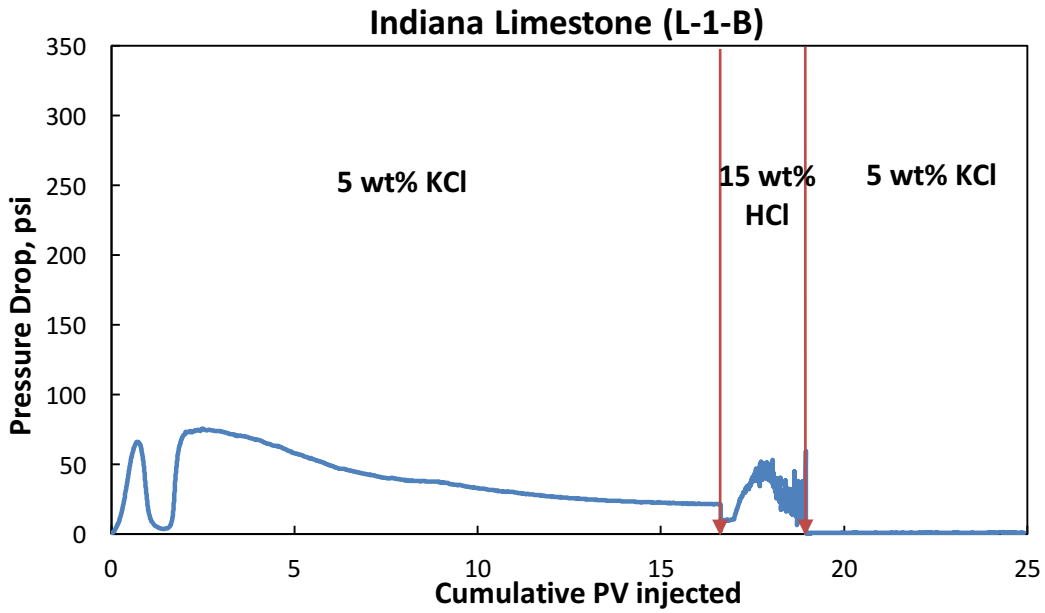

Fig. 45–Pressure drop profile of Indiana limestone (L-1-B), treated with 15 wt% HCl at 300°F (2 cm^3/min – reached BT after 2.01 PV)

Core ID	Acid	Temperature, °F	PV to breakthrough (BT)
L-1-A	In-situ generated HCl	300	1.35
L-1-B	15 wt% HCl	300	2.01

Table 13–Comparison of the BT values of in-situ generated HCl with 15 wt% HCl in acidizing of Indiana limestone at 300°F

ICP analysis was carried out to correlate the coreflood results (**Fig. 46**Fig. 42). Calcium concentration was around 110,000 mg/L at its peak, which indicates carbonate dissolution by 15 wt% HCl. This amount is almost double the concentration of calcium dissolved by in-situ generated HCl, which was around 60,000 mg/L. By looking at these concentrations, once again the high dissolving power of regular HCl was verified with a coreflood experiment of Indiana limestone. K^+ concentration was decreased during acid injection and increased again when injection switched back to 5 wt% KCl.

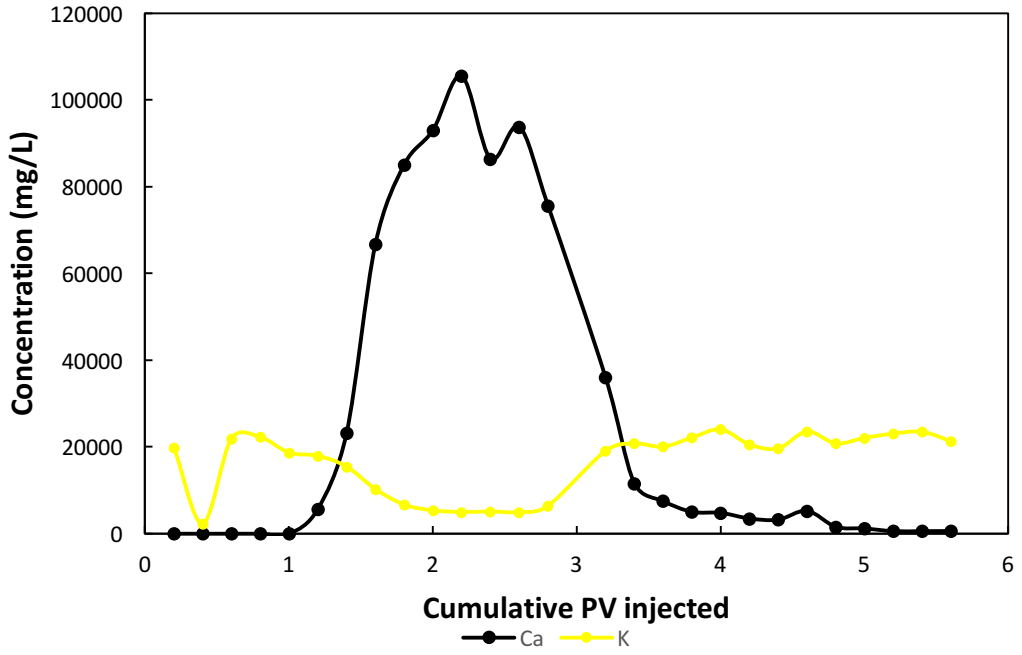

Fig. 46–ICP analysis of effluent samples from Indiana limestone (L-1-B) after the treatment with 15 wt% HCl at 300°F (2 cm^3/min – reached BT after 2.01 PV)

Brine (5 wt% KCl) with a pH of 7 was injected as post-flush to clean the remaining acid inside the wormholes. H+ concentration went up to only 2 wt% and pH dropped to 0 (**Fig. 47**). Brine was continually injected until the effluents became colorless, in other

words, until the H+ concentration was 0. The pH was increased to around 6 at the end of the experiment.

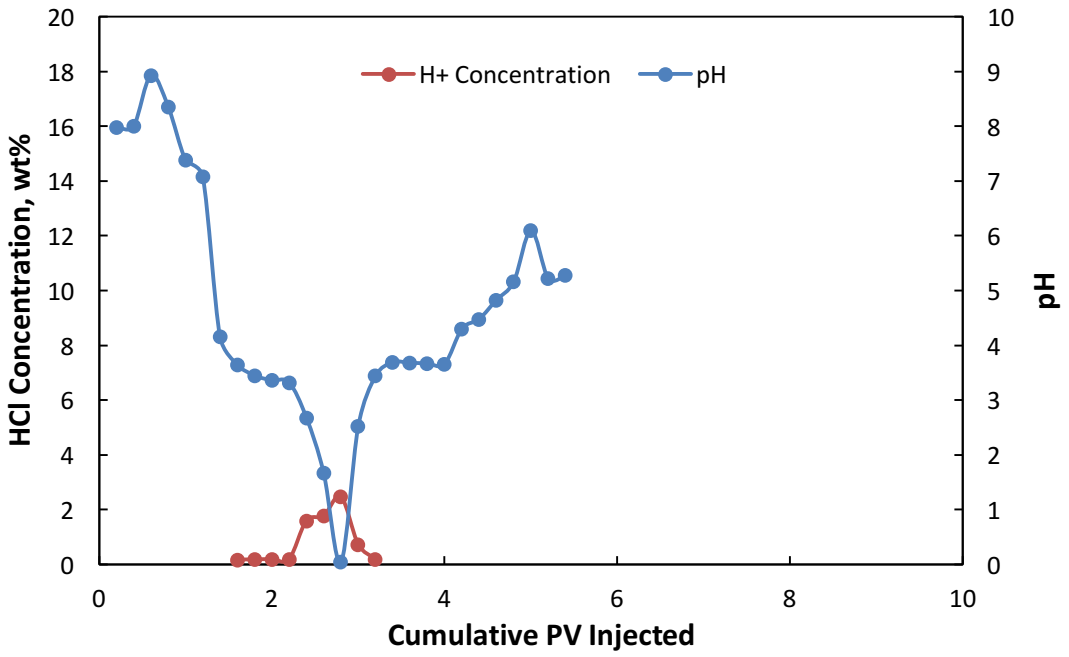

Fig. 47–pH and H^+ concentration of effluent samples from Indiana limestone (L-1-B) after the treatment with 15 wt% HCl at 300°F (2 cm^3/min – reached BT after 2.01 PV)

A CT scan was conducted on Indiana limestone core after the treatment with 15 wt% HCl. The wormhole observed in the CT scan was a conical shaped wormhole. This type of wormhole is formed when the acid has a high dissolving power such as regular HCl. When a side by side comparison of CT scans was made, the difference in wormhole type was more distinct (**Fig. 48**). Moreover, it is seen in Fig. 48 that regular HCl caused more face dissolution, which is again associated with its high dissolving power. These results were perfect indicators that in-situ generated HCl had superior performance over the regular 15 wt% HCl for acidizing limestone at 300°F.

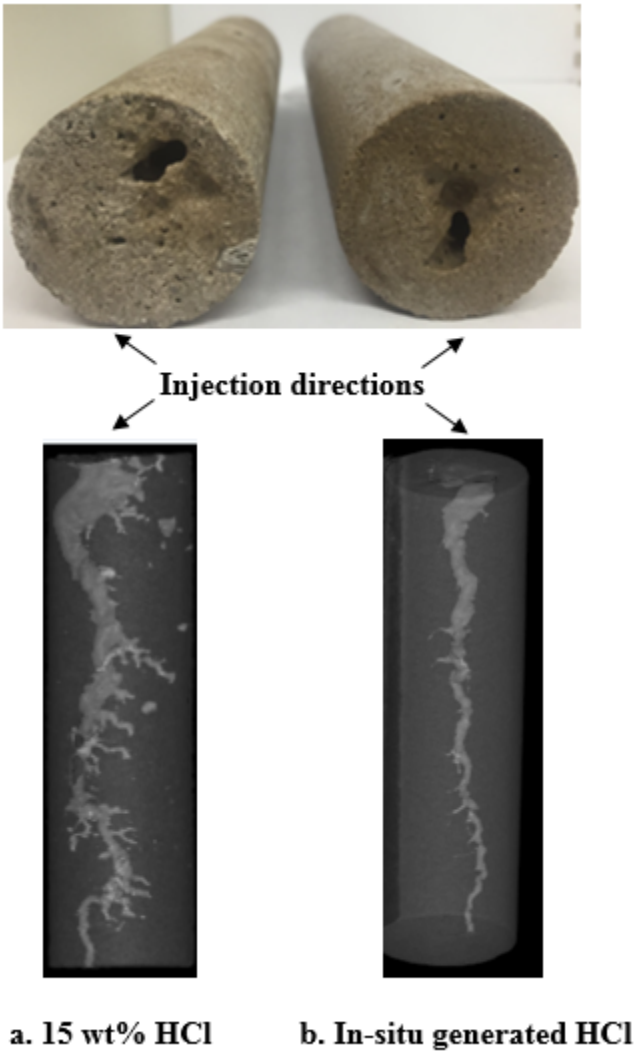

Fig. 48–Comparison of wormhole propagation in Indiana limestone cores treated with a. 15 wt% HCl and b. in-situ generated HCl at 300^{o}F

Rotating Disk Apparatus (RDA) Studies

The results of the coreflood tests, presented in the first chapter, verified that 15 wt% regular HCl had a higher dissolving power than in-situ generated HCl. The indications for this situation were higher concentrations of dissolved minerals and conical shaped wormholes observed during coreflood tests, which were done with 15 wt% regular HCl. However, these observations were qualitative. In order to calculate and define the strength of acid systems used in this study, four sets of RDA experiments were performed. The reaction rate constant, diffusion coefficient and activation energy were the parameters calculated for quantifying the dissolving power of in-situ generated HCl and 15 wt% HCl.

In the first three sets of RDA experiments, the reaction between in-situ generated HCl and a marble disk was tested at 100, 150, and 200^{o}F. For experiments done at 100 and 150^{o}F, six different rotational speeds were used including 200, 400, 600, 800, 1000, and 1200 rpm (revolution per minute). At 200^{o}F, two more experiments were performed at 300 and 700 rpm in addition to these rotational speeds. In the fourth set of RDA experiments, the reaction between 15 wt% regular HCl and a marble disk was tested at 100^{o}F. This time, four different rotational speeds were used including 200, 600,800, and 1200 rpm.

The first section presents the results obtained directly from these four sets of RDA tests. In the second section, calculation of reaction rate constant, diffusion coefficient, and activation energy values of in-situ generated HCl and 15 wt% HCl were given and then these values were compared and discussed.

Summary of RDA Experiments Done with In-Situ Generated HCl and 15 wt% HCl

RDA setup is given in Fig. 5. Using this setup, in-situ generated HCl and 15 wt% regular HCl were tested. The pressure inside the reactor vessel was kept constant between 1000 and 1300 psi. The duration of each experiment was 10 minutes, and 3 mL samples were collected every 1 minute. These samples were diluted with DI water with a dilution factor of 500 ppm. Calcium concentrations of each sample were measured by ICP analysis.

Fig. 49, Fig. **50, and Fig**. **51** show each marble disk after reaction with in-situ generated HCl at 100, 150, and 200^{o}F respectively. **Fig. 52** shows each marble disk after reaction with 15 wt% HCl at 100^{o}F. The state of the disks gave the first idea about the effect of rotational speed on the dissolution rate of marble disks. It was seen that, with increasing rotational speed, the thicknesses of the disks decreased, which was a sign of increasing dissolution rate. However, it was also seen that the thicknesses of the disks after reacting with in-situ generated HCl at 200^{o}F did not change after 800 rpm. The latter case indicates a reaction rate limited reaction while the former case indicates a mass transfer limited reaction (Fig. 3). This will be discussed in the next chapter in more detail.

Calcium concentrations, obtained from ICP analysis, were then plotted against time (**Fig. 53, Fig. 54, Fig. 55, and Fig. 56**). The slope of this plot provided the dissolution rate of calcium in gmole/min. In the reaction between the marble disk (carbonate) and the in-situ generated HCl, 2 moles of H^{+} is spent for each mole of Ca^{+2}. With this fact in mind, spent H^{+} concentrations were calculated from Ca^{+2} concentrations. H^{+} left inside the reactor vessel, which was obtained by subtracting the spent H^{+} concentration from the initial H^{+} concentration (2.906 gmole for in-situ generated HCl and 2.648 gmole for 15

wt% HCl), was plotted against time (**Fig. 57, Fig. 58, Fig. 59, and Fig. 60**). The slope of this plot provided the reaction rate of in-situ generated HCl in gmole/min. Because the surface of disks became non-flat as they reacted with the acid, for some experiments (especially at higher rotational speeds), late data points were discarded. More accurate slope values were obtained this way. R^2 values, along with the equation of the linear trendline, were included on the graphs as well.

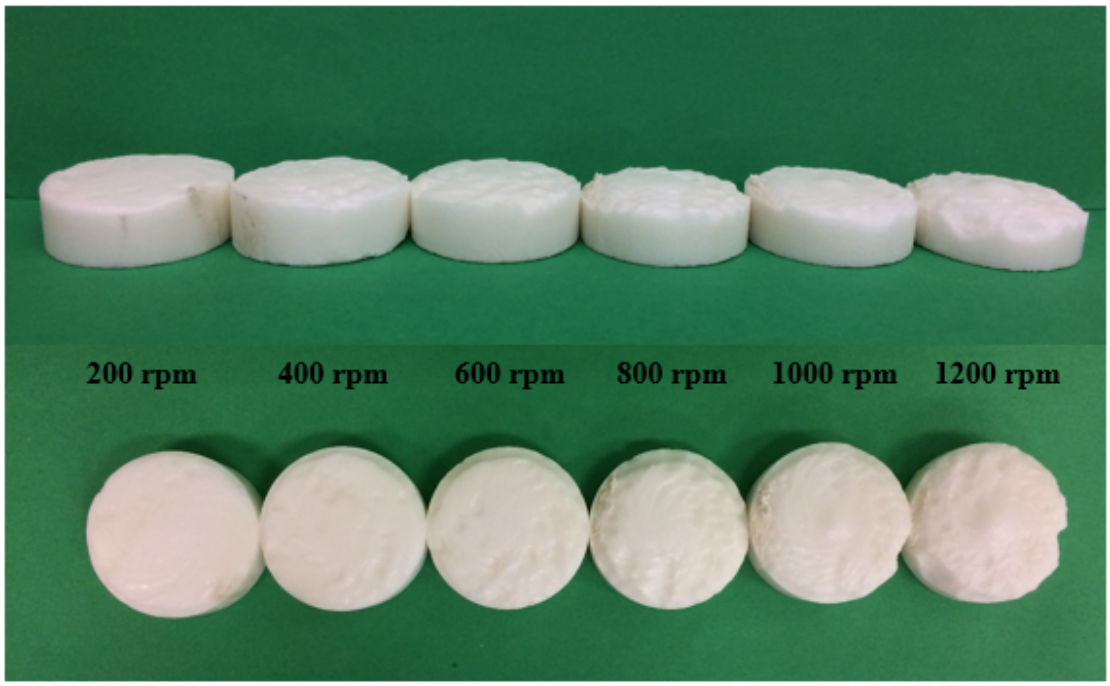

Fig. 49–Marble disks after RDA experiment with in-situ generated HCl at 100^{o}F

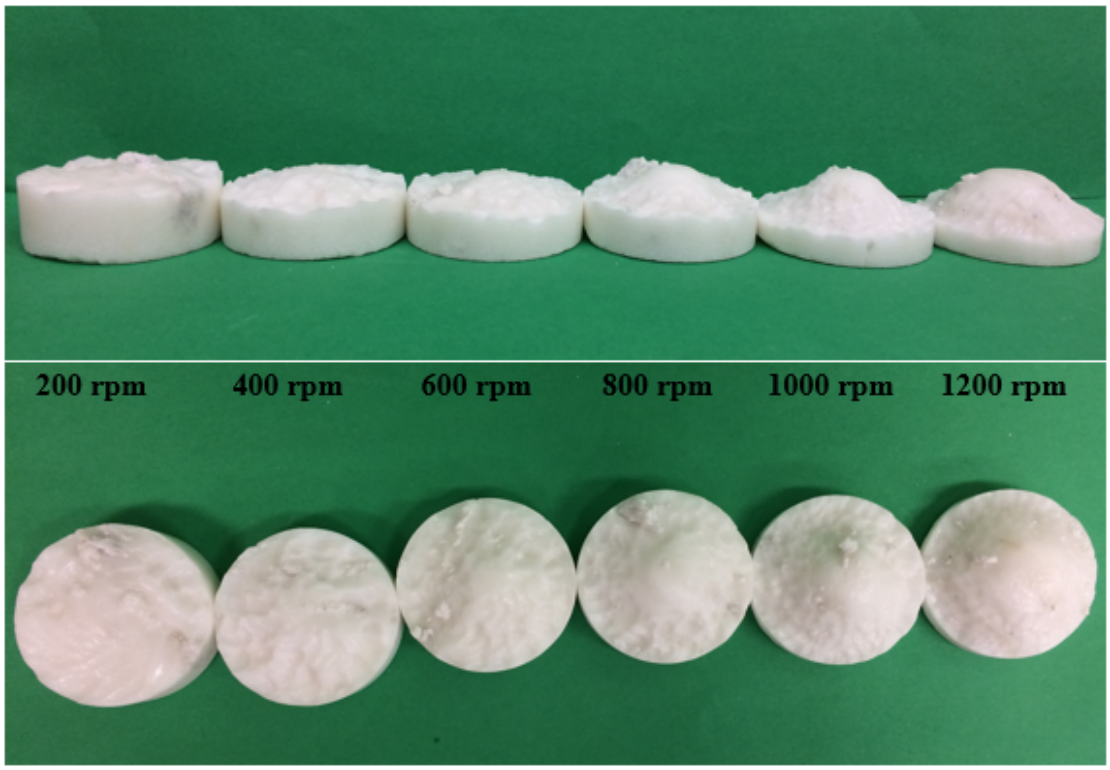

Fig. 50–Marble disks after RDA experiment with in-situ generated HCl at 150°F

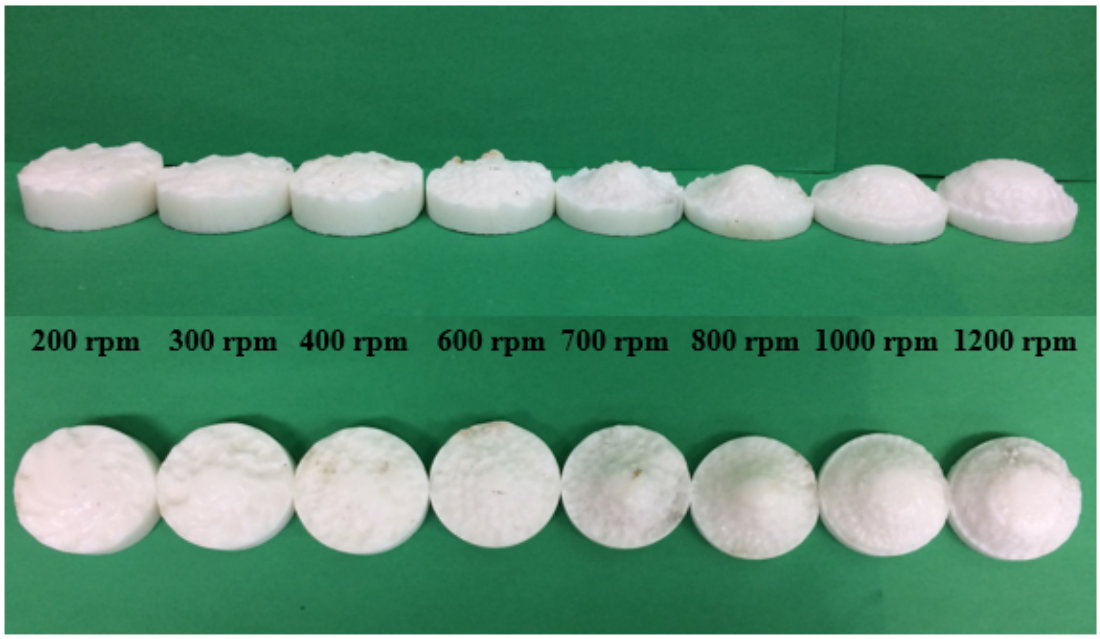

Fig. 51–Marble disks after RDA experiment with in-situ generated HCl at 200°F

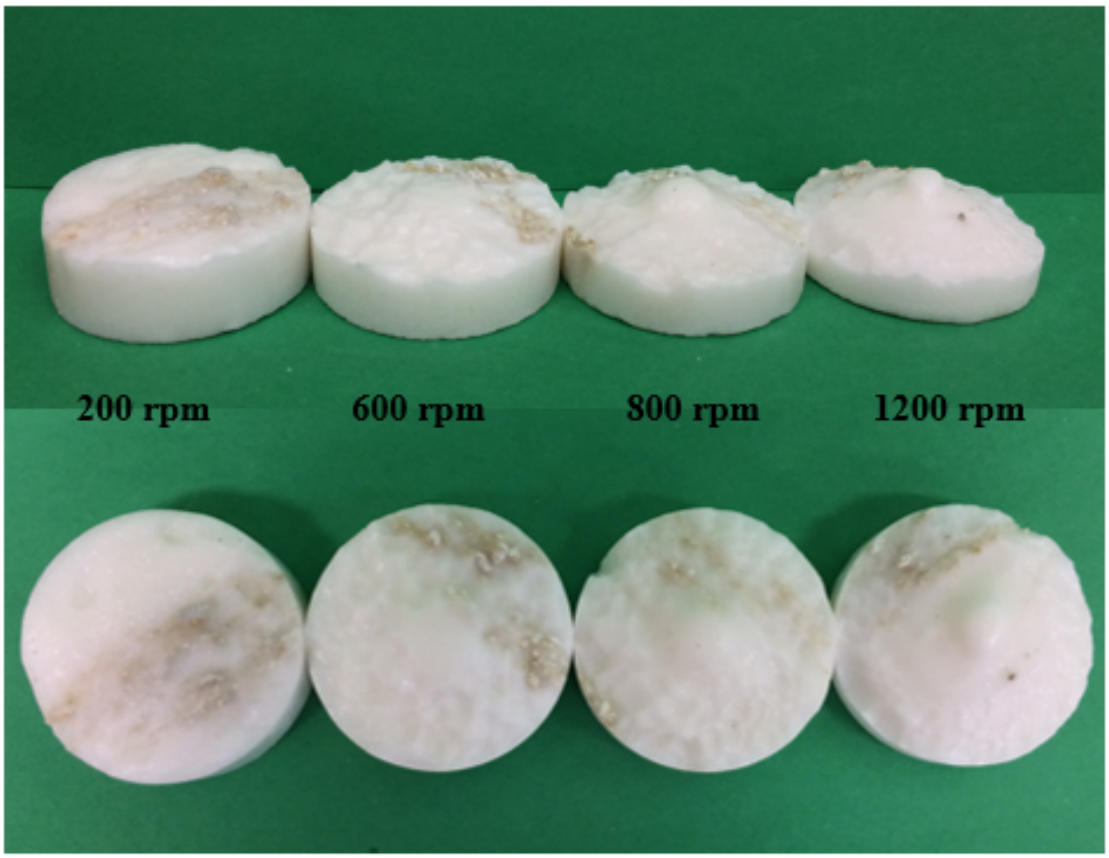

Fig. 52–Marble disks after RDA experiment with 15 wt% HCl at 100^{o}F

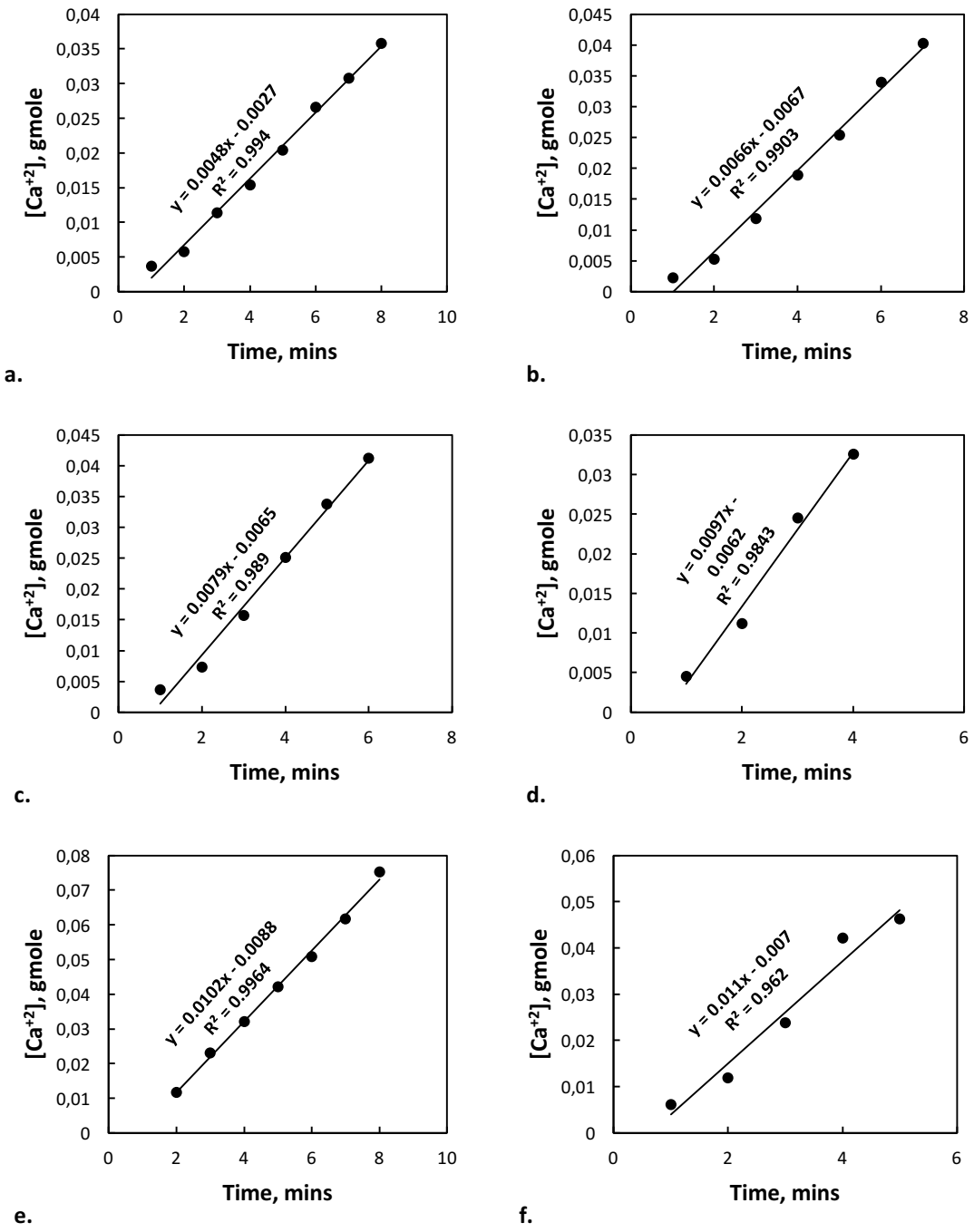

Fig. 53–Dissolved Ca^{+2} concentration vs. time plots for RDA tests done with in-situ generated HCl at 100°F and at a. 200, b. 400, c. 600, d. 800, e. 1000, and f. 1200 rpm

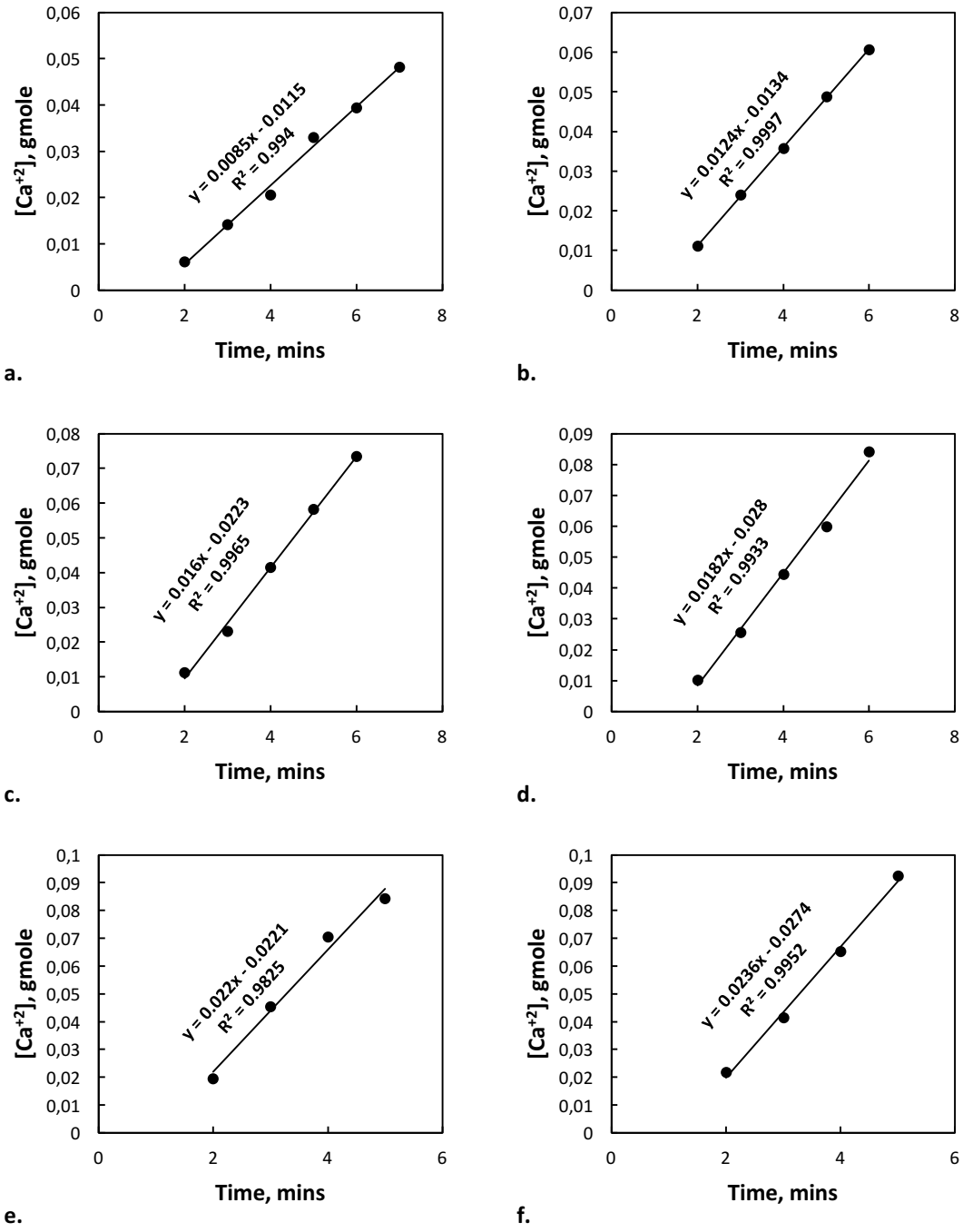

Fig. 54–Dissolved Ca^{+2} concentration vs. time plots for RDA tests done with in-situ generated HCl at 150°F and at a. 200, b. 400, c. 600, d. 800, e. 1000, and f. 1200 rpm

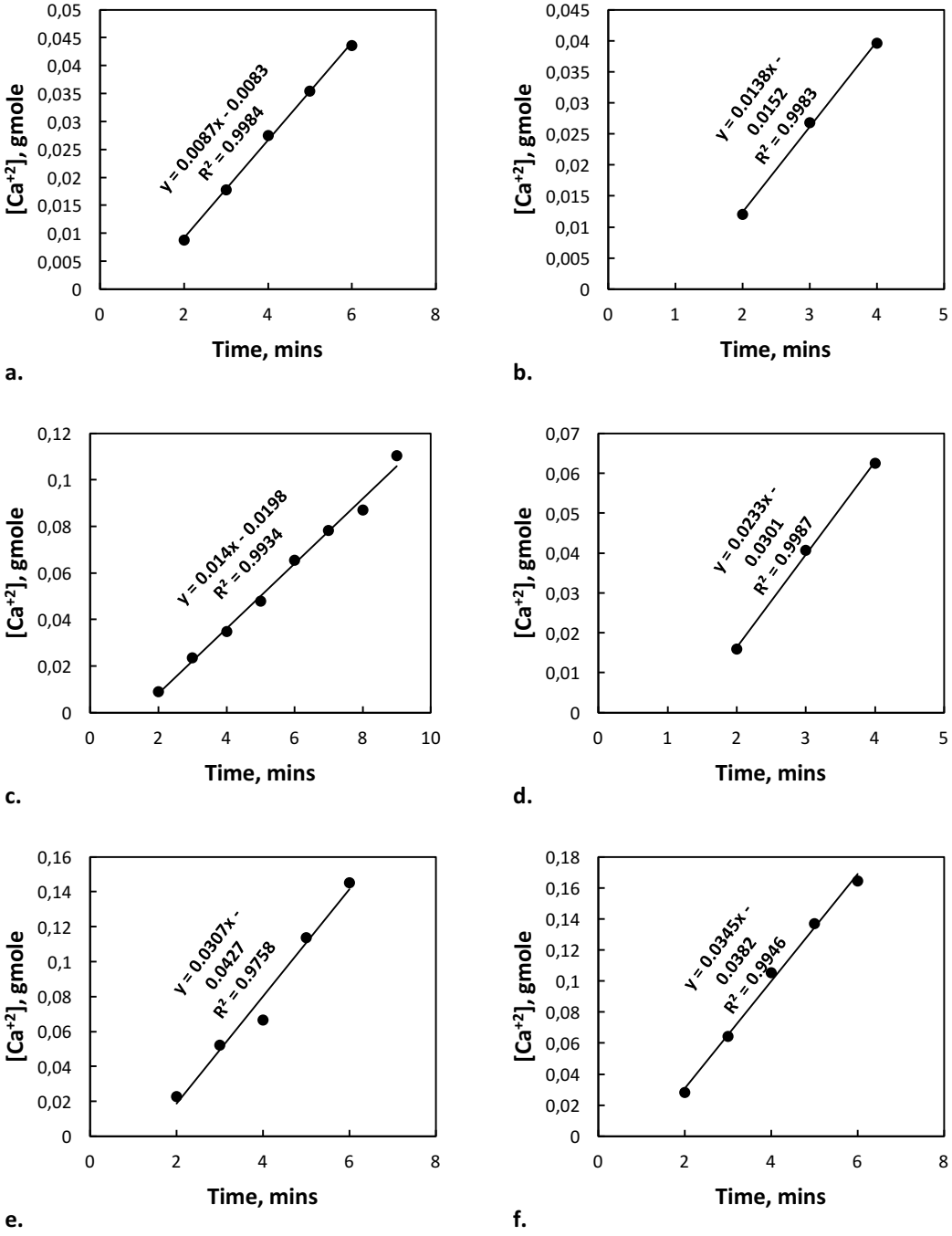

Fig. 55–Dissolved Ca^{+2} concentration vs. time plots for RDA tests done with in-situ generated HCl at 200°F and at a. 200, b. 300, c. 400, d. 600, e. 700, f. 800, g. 1000, and h. 1200 rpm

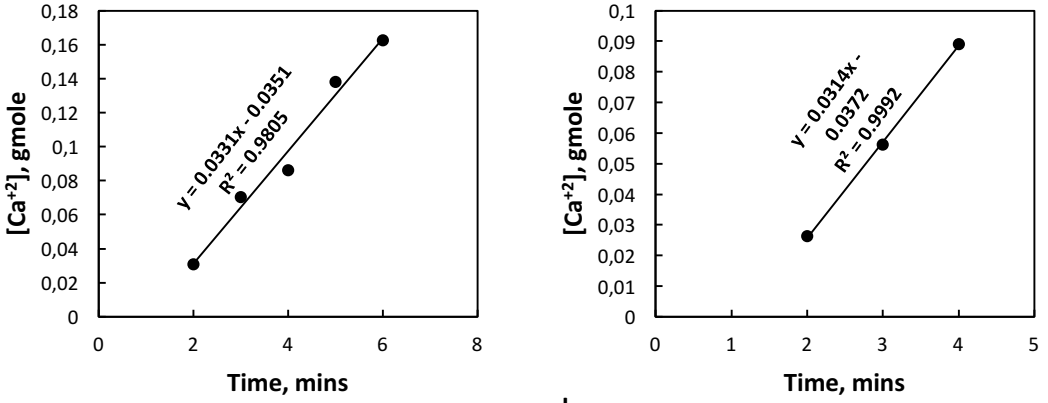

Fig. 55–Continued

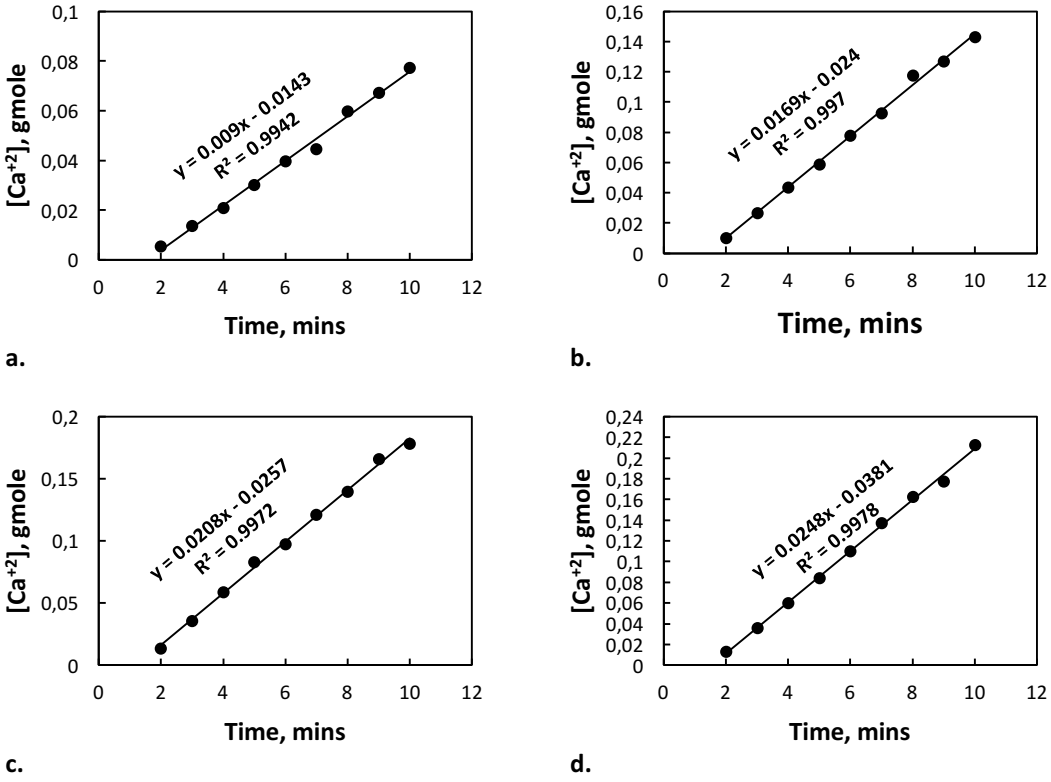

Fig. 56–Dissolved Ca^{+2} concentration vs. time plots for RDA tests done with 15 wt% HCl at 100°F and at a. 200, b. 600, c. 800, and d. 1200 rpm

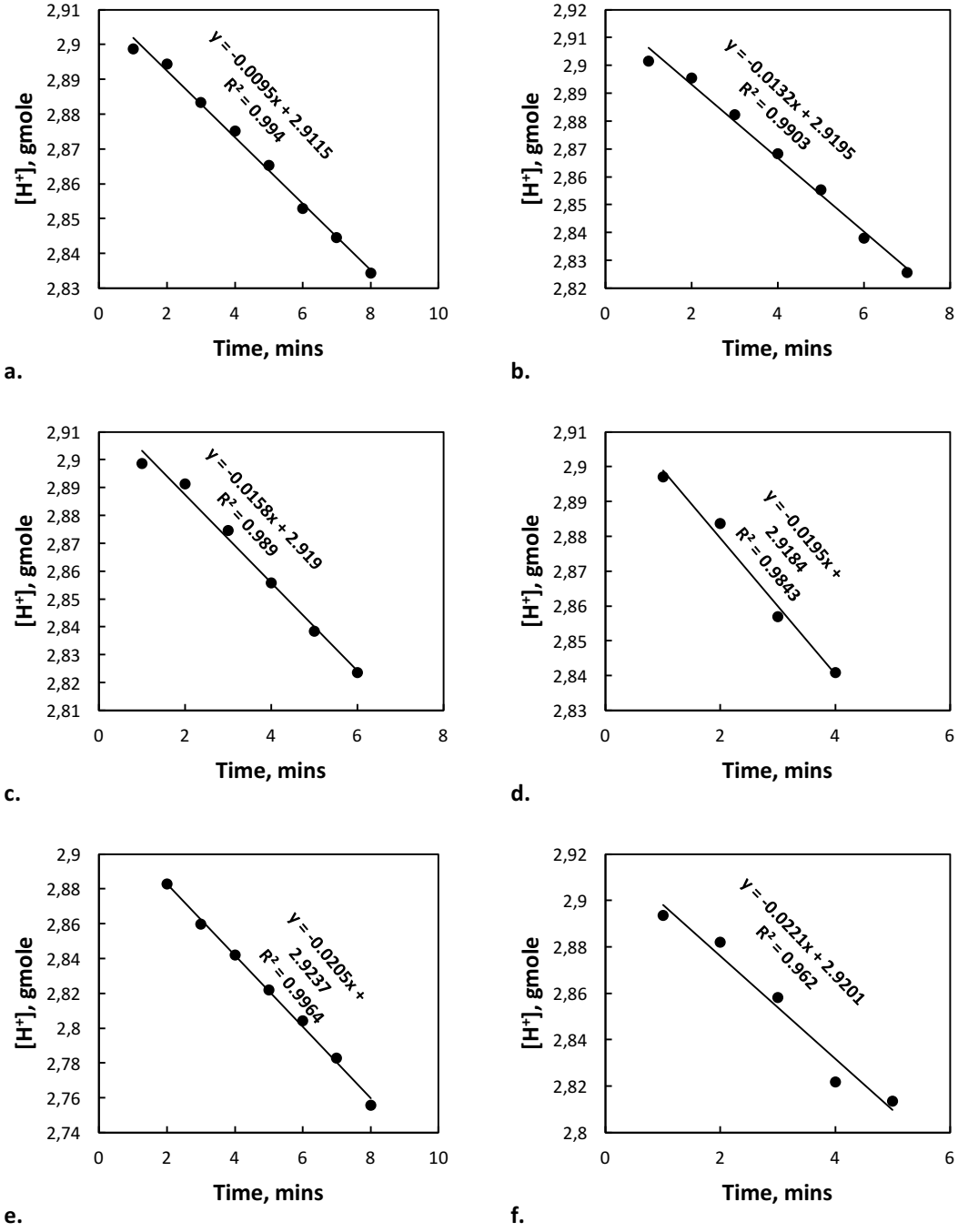

Fig. 57–H^+ concentration left vs. time plots for RDA tests done with in-situ generated HCl at 100°F and at a. 200, b. 400, c. 600, d. 800, e. 1000, and f. 1200 rpm

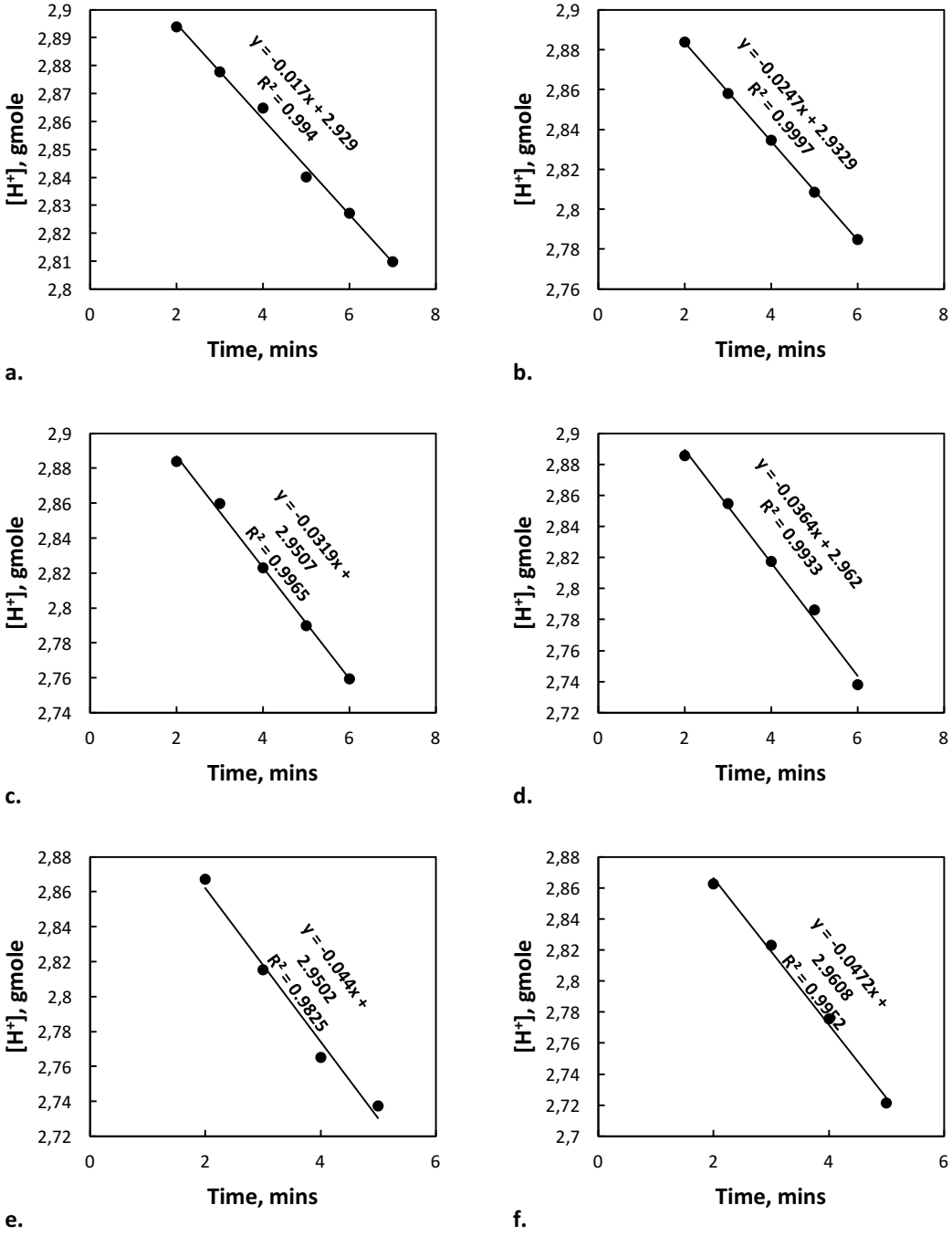

Fig. 58–H^+ concentration left vs. time plots for RDA tests done with in-situ generated HCl at 150°F and at a. 200, b. 400, c. 600, d. 800, e. 1000, and f. 1200 rpm

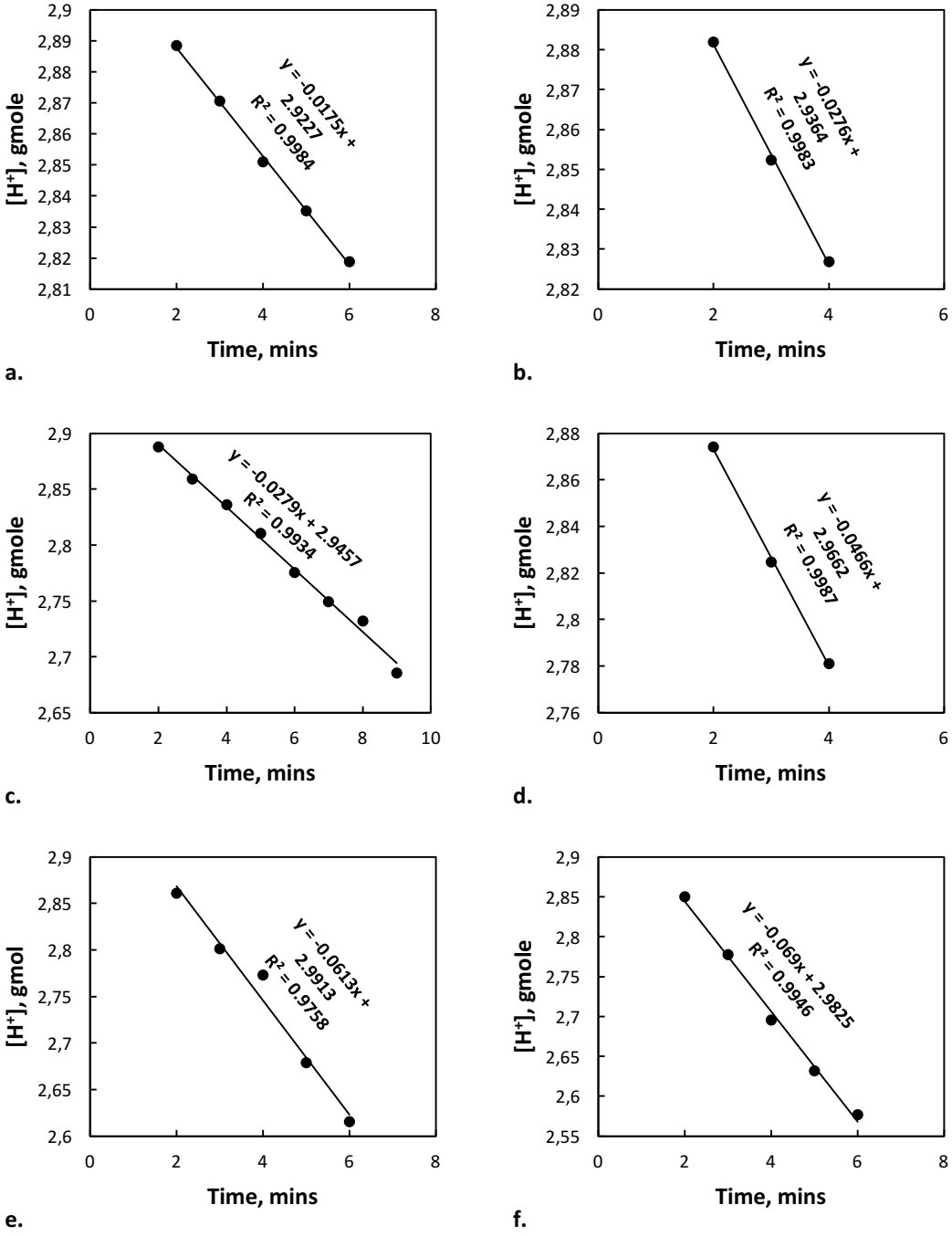

Fig. 59–H^+ concentration left vs. time plots for RDA tests done with in-situ generated HCl at 200^{o}F and at a. 200, b. 300, c. 400, d. 600, e. 700, f. 800, g.1000, and h. 1200 rpm

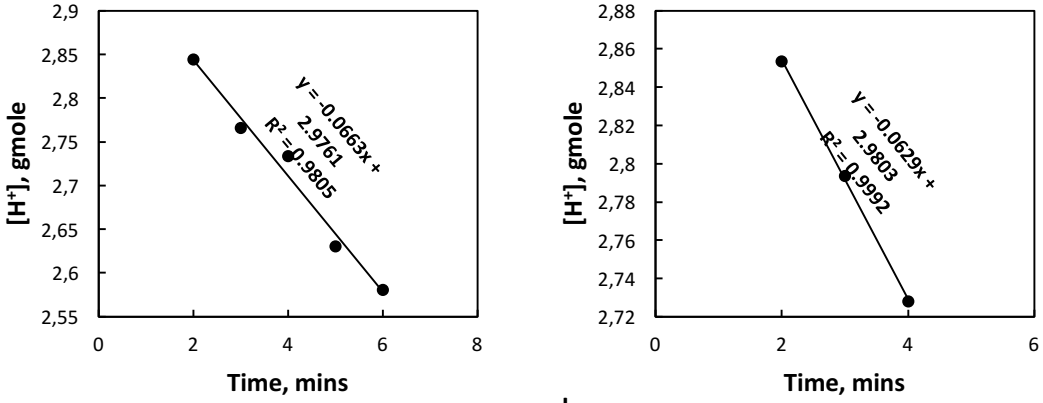

Fig. 59–Continued

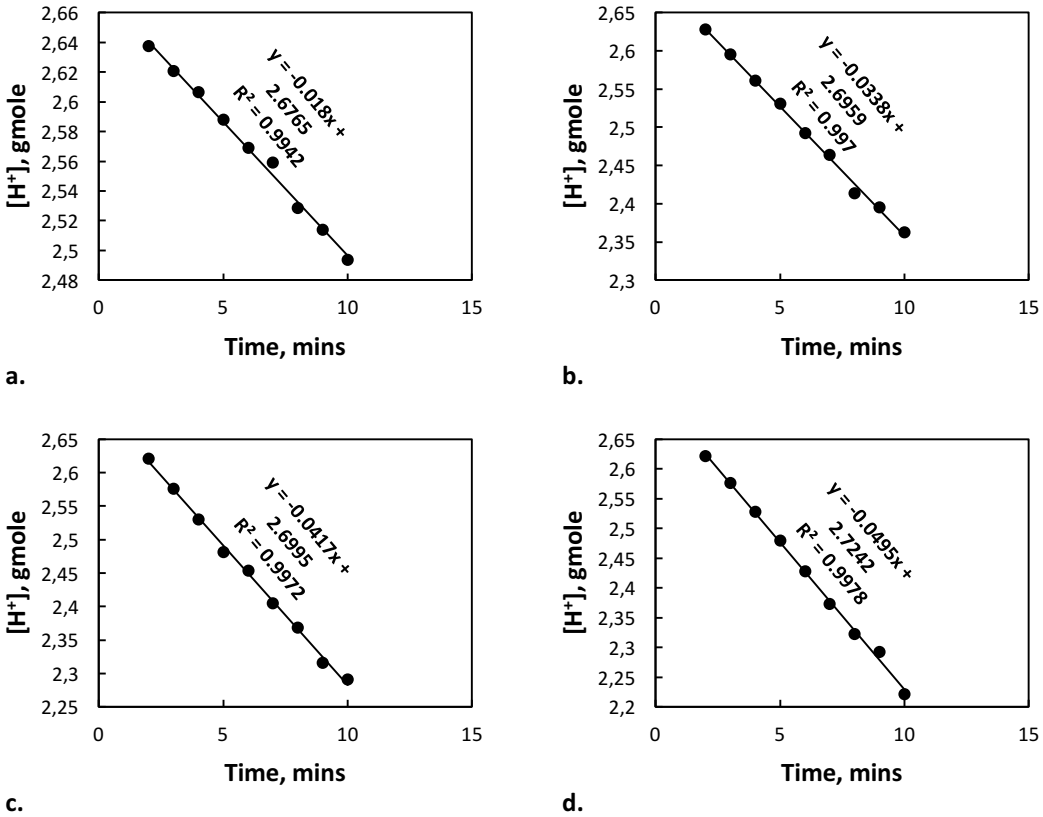

Fig. 60–H^+ concentration left vs. time plots for RDA tests done with 15 wt% HCl at 100°F and at a. 200, b. 600, c. 800, and d. 1200 rpm

Comparison of Reaction Kinetics between In-Situ Generated HCl and 15 wt% HCl

Reaction Rate Constant

The slopes of the graphs given in Fig. 57 through Fig. 60 represent the spending rate of H^+ in gmole/min. After converting the unit into gmole/s, the spending rate of H^+ was inserted into Eq. 23 to calculate the reaction rate:

$$\text{Reaction rate (gmole/s.cm}^2\text{)} = \frac{(\text{H}^+ \text{ spent (gmole/s)/Surface Area (cm}^2\text{))}}{1-\text{porosity (vol\%)}}. \quad \text{(23)}$$

The linear frequency (rpm) for RDA tests was converted into angular frequency ω (rad/s), and the square root of ω ($(rad/s)^{0.5}$) vs. reaction rate (gmole/s.cm^2) was plotted for different rotational speeds (**Fig. 61**). The slope of this plot yielded the reaction rate constant ($J_{mt}/\omega^{0.5}$). It is seen in Fig. 61 that the reaction rate constant for 15 wt% HCl at 100^{o}F was $7.26x10^{-6}$ gmole/s.cm^2.$(rad/s)^{0.5}$. On the other hand, the reaction rate constant for in-situ generated HCl was $2.93x10^{-6}$, $6.99x10^{-6}$, and $1.66x10^{-5}$ gmole/s.cm^2.$(rad/s)^{0.5}$ at 100, 150, and 200^{o}F respectively. The reaction between in-situ generated HCl and calcite was mass transfer limited at all rotational speeds at 100 and 150^{o}F, while at 200^{o}F, the reaction was surface reaction limited after 800 rpm. This change from mass transfer limited reaction to reaction rate limited reaction was unexpected. It may be due to a possible blocking of the reaction sites on the marble disk because of the precipitation of chloride salt mentioned earlier. Reaction rates were also plotted in a column chart against temperature and rotational speed to provide a better comparison (**Fig. 62**).

Reaction rate between HCl and carbonate rock increases with increasing temperature according to Arrhenius equation given in Eq. 22 (Alkhaldi et al. 2009). Low rotational speeds result in a slower transport of mass to the rock surface. Therefore, the

reaction is mass transfer limited at low rotation speeds and it is proportional to reaction rate. On the other hand, the mass transfer boundary layer (surface of marble disk in the case of RDA) decreases as rotational speed increases and thus, the reaction becomes reaction rate limited (Rabie et al. 2010). In other words, reaction rate increases with increasing rotational speed, when the reaction is mass transfer limited.

The effect of temperature and rotational speed on the reaction rate is seen more clearly in Fig. 62. These results were parallel with the literature mentioned above. As the rotation speed was increased, the dissolution rate of the marble disk was also increased. This increase was more dramatic at higher temperatures because increasing the temperature also resulted in an increase in the dissolution rate for all rotation speeds. In fact, 15 wt% HCl at 100°F is 2 times more reactive than in-situ generated HCl at the same temperature and slightly more reactive than in-situ generated HCl at 150°F.

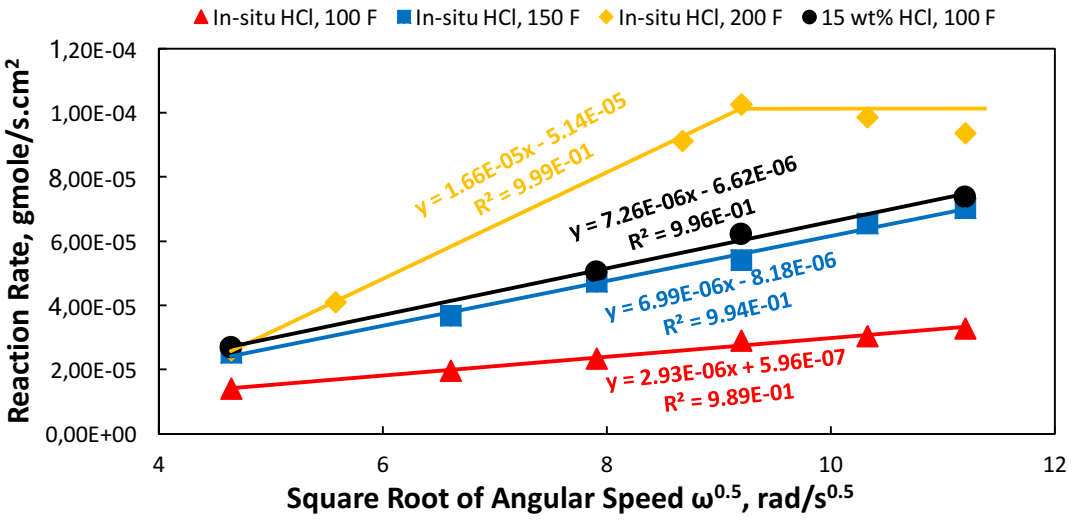

Fig. 61–Reaction rate vs. square root of angular frequency graph for in-situ generated HCl (100°F, 150°F, 200°F) and 15 wt% HCl (100°F).

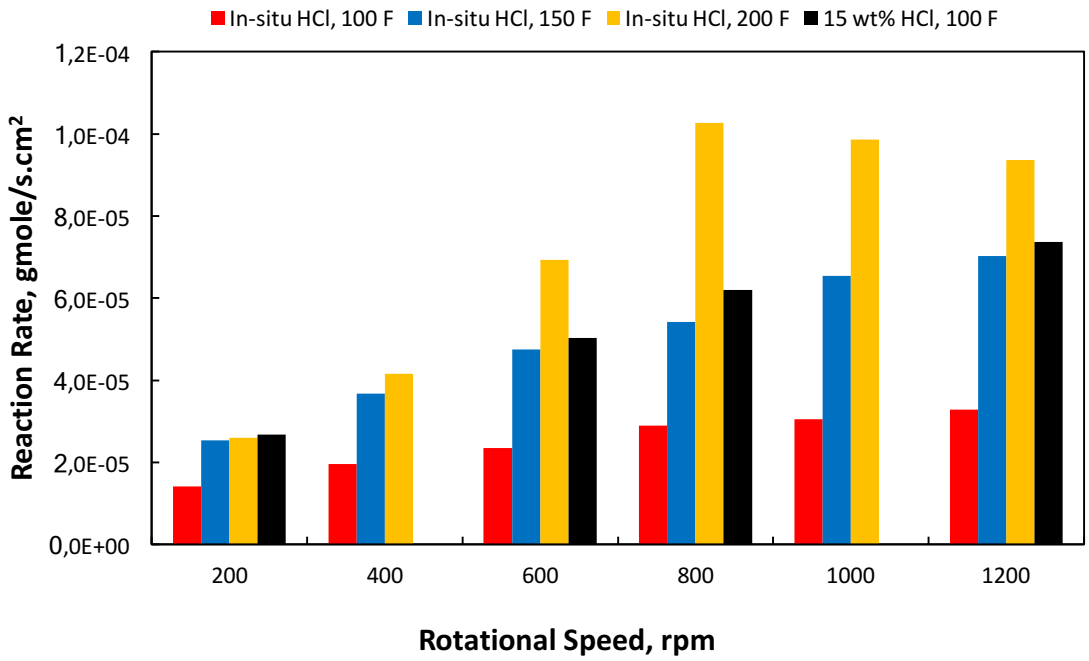

Fig. 62–Effect of temperature and rotational speed on the reaction rate

Diffusion Coefficient

Diffusion coefficient was calculated by using Eq. 19. In this equation, kinematic viscosity (υ) was unknown. Thus, kinematic viscosity of both acids (with additives) were measured at different temperatures (**Fig. 63**) and required values of υ at 100°F, 150°F, and 200°F were obtained by extrapolating the data. The surface concentration of acid (Cs) in the equation was taken to be 0 since the reactions were mass transfer limited within the temperature and rotational speed range studied. After gathering all required variables in Eq. 19 ($J_{mt}/\omega^{0.5}$, υ, C_b), diffusion coefficients for both acids were calculated. Diffusion coefficient for in-situ generated HCl was $7.31x10^{-6}$, $2.51x10^{-5}$, and $8.97x10^{-5}$ cm^2/s at 100, 150, and 200°F respectively. Diffusion coefficient for 15 wt% HCl was $3.13x10^{-5}$ cm^2/s at 100°F. All reaction constants calculated for in-situ generated HCl and 15 wt% HCl are

shown in **Table 14**. Diffusion coefficients of both acids were also graphed in **Fig. 64** for comparison. These results indicated that diffusion coefficient of in-situ generated HCl was increasing with increasing temperature.

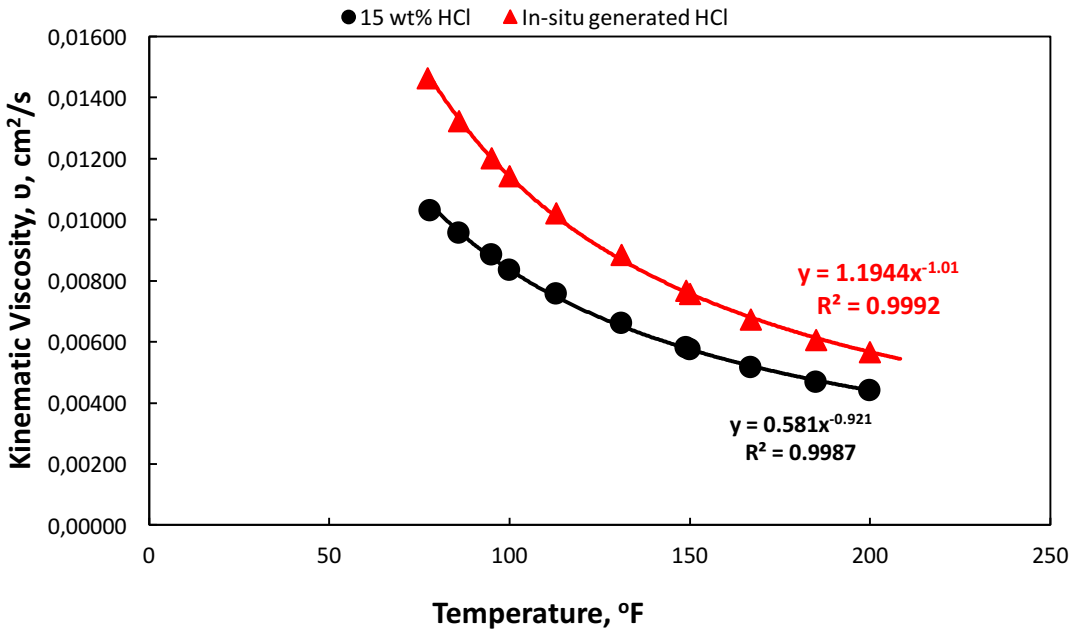

Fig. 63–Measured kinematic viscosity vs. temperature for 15 wt% HCl and in-situ generated HCl

Acid type	**Temperature, (°F)**	**Reaction rate constant, $J_{mt}/\omega^{0.5}$, (gmole/s.cm^2.(rad/s)$^{0.5}$)**	**Diffusion coefficient, D, (cm^2/s)**
15 wt% HCl	100	7.26×10^{-6}	3.13×10^{-5}
In-situ generated HCl	100	2.93×10^{-6}	7.31×10^{-6}
In-situ generated HCl	150	6.99×10^{-6}	2.51×10^{-5}
In-situ generated HCl	200	1.66×10^{-5}	8.97×10^{-5}

Table 14–Kinetic variables calculated for in-situ generated HCl and 15 wt% HCl at 100, 150, and 200°F

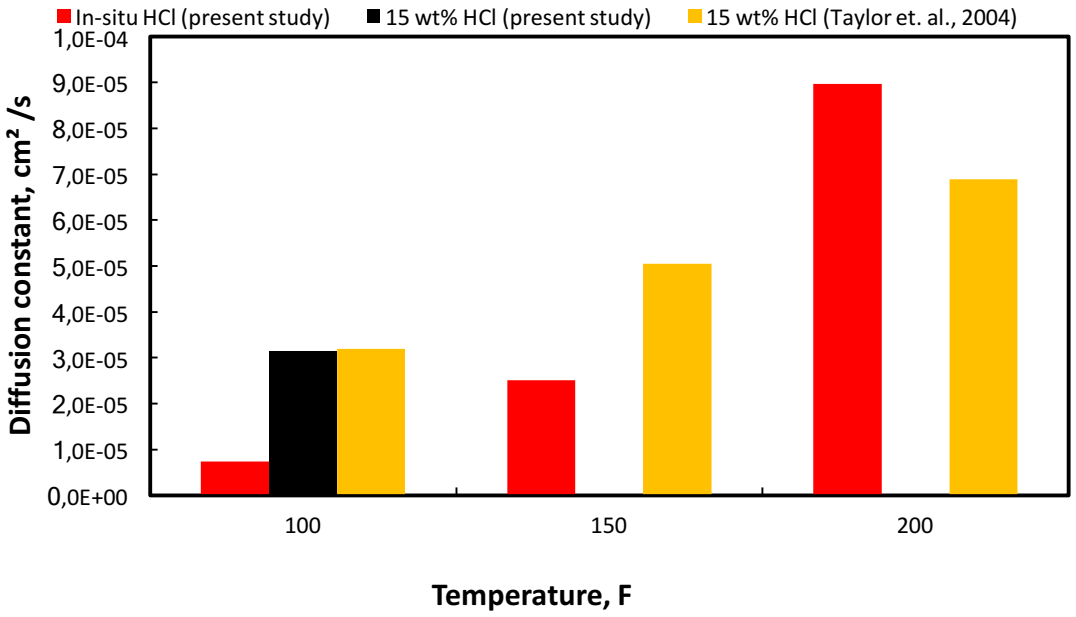

Fig. 64–Comparison of diffusion coefficients for in-situ generated HCl and 15 wt% HCl

The diffusion coefficient for 15 wt% HCl, with additives mentioned in Table 1, at 100°F was found as 3.13×10^{-5} cm^2/s (Table 14). This value was compared with literature to check its accuracy. Taylor et al. (2004) extrapolated Lund and Fogler (1975)'s diffusion coefficient data, for the reaction between HCl and calcite, to 3 different temperature. They used an average increment of 6.65×10^{-7} $cm^2/s/K$, which was gotten from de Rozieres (1994)'s study. This set of extrapolated data was used to calculate the diffusion coefficients of 15 wt% HCl at 100, 150, and 200°F, which were 3.20×10^{-5}, 5.05×10^{-5}, and 6.90×10^{-5} respectively. (**Table 15**). The value at 100°F is close to the measured diffusion coefficient for 15 wt% HCl at 100°F, which was 3.13×10^{-5} cm^2/s. These values are also shown in Fig. 64 to compare with the measured diffusion coefficients. However, it should be noted that Lund and Fogler (1975)'s RDA experiment was done under 800 psi pressure

without additives, while our experiment was done between 1000-1300 psi and included the acidizing additives (Table 1).

In another RDA study done by Qiu et al. (2015) with 15 wt% HCl and calcite at 150°F and 1000 psi, the diffusion coefficient was found as 6.48×10^{-5} cm^2/s. Diffusion coefficient values measured by de Rozieres (1994) with RDA for 15 wt% HCl and calcite at 40°F and 84°F under 1000 psi are 1.27×10^{-6} and 2.13×10^{-5} cm^2/s respectively. These diffusion coefficient along with our measured diffusion coefficient for 15 wt% HCl were plotted for comparison (**Fig. 65**). Taylor et al. (2004)'s extrapolation was also included in this plot. Accordingly, the diffusion coefficient for 15 wt% HCl measured in this study is in close agreement with the literature.

HCl concentration (wt%)	Diffusion coefficient (cm^2/s)					
	73.4°F	100°F	122°F	150°F	185°F	200°F
0.18	3.23E-05	4.21E-05	5.02E-05	6.06E-05	7.35E-05	7.90E-05
0.36	3.21E-05	4.20E-05	5.01E-05	6.04E-05	7.33E-05	7.88E-05
0.91	3.17E-05	4.15E-05	4.96E-05	6.00E-05	7.29E-05	7.84E-05
1.81	3.09E-05	4.08E-05	4.89E-05	5.93E-05	7.22E-05	7.77E-05
3.59	2.95E-05	3.94E-05	4.75E-05	5.79E-05	7.08E-05	7.63E-05
7.07	2.70E-05	3.68E-05	4.49E-05	5.53E-05	6.82E-05	7.37E-05
15	2.21E-05	3.20E-05	4.01E-05	5.05E-05	6.34E-05	6.90E-05
16.9	2.11E-05	3.10E-05	3.91E-05	4.95E-05	6.24E-05	6.79E-05

Table 15–Taylor et al. (2004)'s diffusion coefficient data for HCl, which was extrapolated from Lund and Fogler (1975)'s data by using an increment of 6.65×10^{-7} $cm^2/s/K$

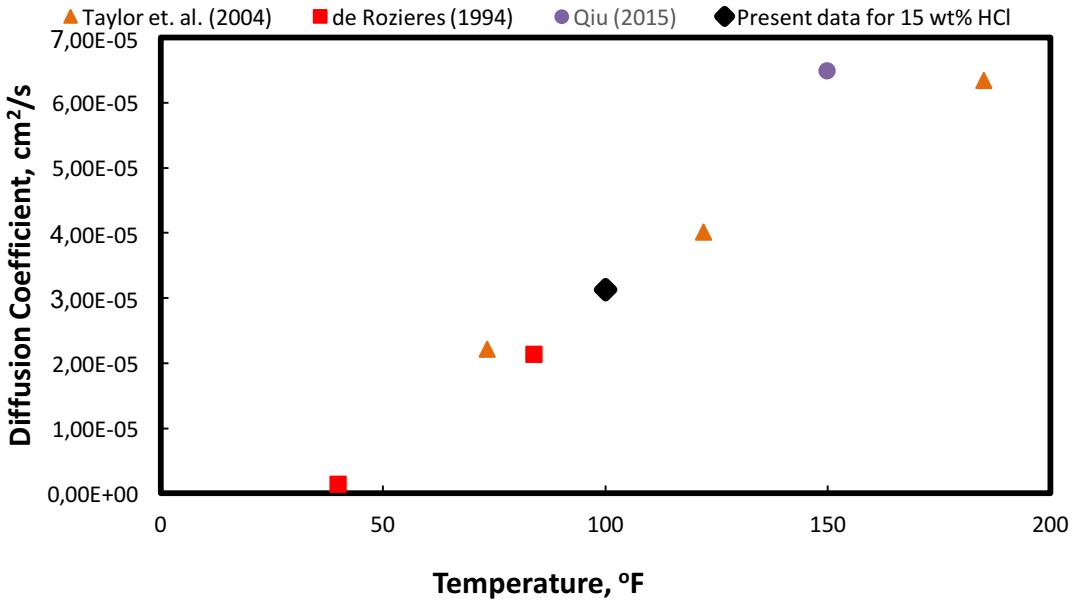

Fig. 65–Comparison of diffusion coefficient values of 15 wt% HCl with the literature

The reaction between HCl and carbonate rock is fast and it is even faster at higher temperatures (Buijse et al. 2003). Fredd and Fogler (1998a) highlighted that the matrix acid treatments require low injection rates. At low injection rates, the rapid spending of HCl prevents deep penetration of HCl, often causing face dissolution in carbonate reservoirs. In an attempt to tackle this issue, Sokhanvarian et al. (2017) presented a new in-situ generated acid, based on HCl. Their results proved that the new acid was causing less face dissolution comparing to 15 wt% HCl at the same injection rates. Diffusion coefficients of this new in-situ generated HCl were measured in this study and compared with 15 wt% HCl. According to the results given in Fig. 64, the diffusion coefficient measured for 15 wt% HCl at 100°F was around four times more than the diffusion coefficient of in-situ generated HCl at 100°F and slightly more than the diffusion

coefficient of in-situ generated HCl at 150^{o}F. These numbers show that in-situ generated HCl can stand as a good alternative of regular HCl where low acid injection rates are required.

Activation Energy

Molecules of reactant should exceed an energy barrier called activation energy to start a chemical reaction. Therefore, the higher the activation energy of a reactant, the slower the reaction starts. Activation energy (E_a) was calculated according to Arrhenius equation given in Eq. 22. Diffusion coefficients, calculated for in-situ generated HCl at 3 different temperatures (100^{o}F, 150^{o}F, and 200^{o}F), were plotted against reciprocal of absolute temperature in Kelvin on the semi-log graph (**Fig. 66**). The slope of this graph (-E_a/R) was used to calculate E_a.

The activation energy for in-situ generated HCl was calculated as 10.2 kcal/gmole (42.7 kJ/gmole) accordingly. This value is around 1.6-1.7 times higher than the activation energies of 5 wt% lactic acid with calcite (26.1 kJ/gmole, (Rabie et al. 2014)) and 0.5 M acetic acid (25.1 kJ/gmole, (Fredd and Fogler 1998b)). The activation energy of 15 wt% HCl with calcite was calculated by again using the diffusion coefficient data presented by Taylor et al. (2004) and it was 14.9 kJ/gmole, which is around three times less than in-situ generated HCl. This comparison shows that in-situ generated HCl can provide much slower reactions than organic acids and HCl.

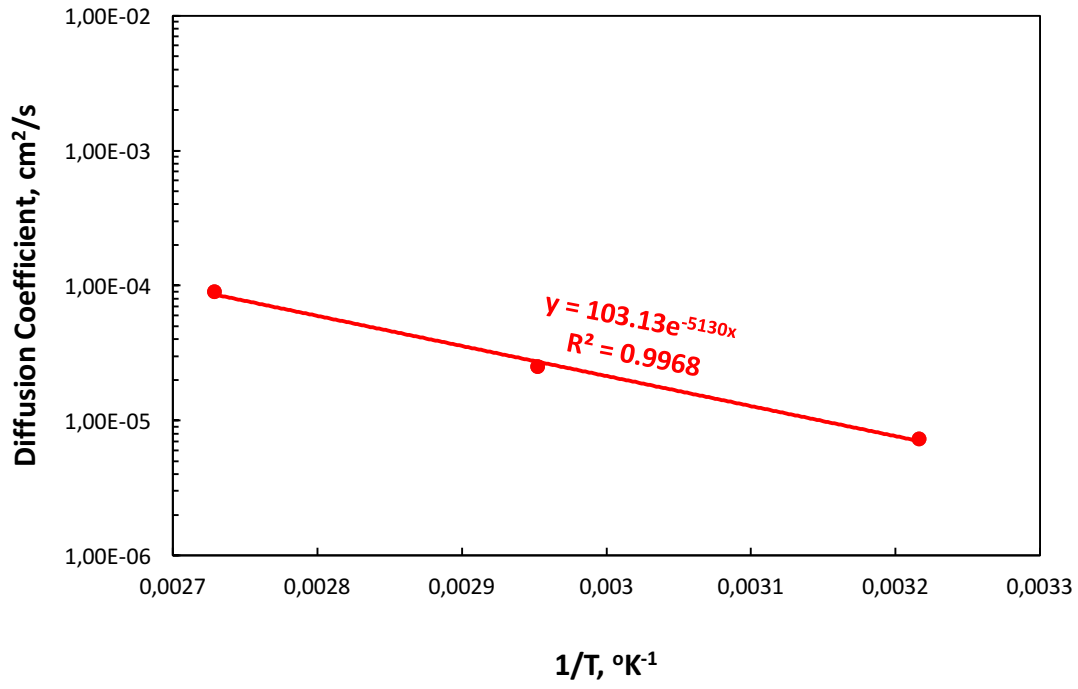

Fig. 66–Arrhenius plot obtained for in-situ generated HCl

CHAPTER IV

SUMMARY AND CONCLUSIONS

Regular HCl is known to be a very strong acid and causes problems such as corrosion to the tubular, fines migration in sandstone reservoirs, and face dissolution and shallow penetration in carbonate reservoirs, especially at high temperatures. It was shown that in-situ generated HCl provides much less corrosion than regular HCl, creates single-dominant wormholes in carbonate reservoirs, increases permeability considerably in sandstone reservoirs as pre-flush acid. The new in-situ generated HCl can replace regular HCl for dissolution of carbonate in sandstone and carbonate reservoirs at high-temperature applications with a comparable cost. In this study, low performance of in-situ generated HCl at 300^{o}F was addressed by decreasing the residence time of acid and reaction kinetics of in-situ generated acid was studied. Following conclusions were drawn from coreflood studies:

1. The injection rate of the in-situ generated HCl was increased from 1 cm^3/min to 5 cm^3/min and the injected amount was decreased from 5 PV to 1 PV for treating Grey Berea sandstone core at 300^{o}F. This modification provided a 17% increase in permeability.
2. The injection rate of the in-situ generated HCl was increased from 1 cm^3/min to 5 cm^3/min and the injected amount was decreased from 5 PV to 2 PV for treating Bandera sandstone core at 300^{o}F. This modification provided a 38% increase in permeability.

3. In-situ generated HCl performed better than 15 wt% regular HCl in both Grey Berea and Bandera sandstone at 300^{o}F.
4. In both Silurian dolomite and Indiana limestone, increasing injection rate from 1 cm^{3}/min to 2 cm^{3}/min at 300^{o}F delivered breakthrough after 3.3 PV of injection.
5. In both Silurian dolomite and Indiana limestone, in-situ generated HCl provided earlier breakthrough than 15 wt% regular HCl at 300^{o}F.
6. In-situ generated HCl caused much less face dissolution than 15 wt% regular HCl in treating carbonate cores at 300^{o}F.
7. In-situ generated HCl generated single-dominant wormholes, while 15 wt% regular HCl created branched-conical wormholes in treating carbonate cores at 300^{o}F.

Following conclusions were drawn from RDA studies:

1. The reaction between in-situ generated HCl and marble disk was mass transfer limited at 100^{o}F and 150^{o}F. The reaction became reaction rate limited above 800 rpm at 200^{o}F.
2. It was observed that an increase in rotational speed and temperature resulted in an increase in dissolution rate of calcite with in-situ generated HCl.
3. Diffusion coefficient of in-situ generated HCl was increased with increasing temperature.
4. Reaction constant of in-situ generated HCl and marble disk was found as 2.93x10^{-6}, 6.99x10^{-6}, and 1.66x10^{-5} gmole/s.cm^{2} at 100, 150, and 200^{o}F respectively.

5. Reaction constant of 15 wt% regular HCl and marble disk was found as $7.26x10^{-6}$ gmole/s.cm^2 at 100^oF, which is around 2.5 times more than in-situ generated HCl at the same temperature.
6. Diffusion coefficient for in-situ generated HCl was $7.31x10^{-6}$, $2.51x10^{-5}$, and $8.97x10^{-5}$ cm^2/s at 100, 150, and 200^oF respectively.
7. The diffusion coefficient for 15 wt% regular HCl at 100^oF was found as $3.13x10^{-5}$ cm^2/s, which was 4 times more than in-situ generated HCl.
8. Lower diffusivity and reactivity of in-situ generated HCl was quantified and confirmed the results observed in coreflood studies.
9. The activation energy of in-situ generated HCl was more than 15 wt% regular HCl which can be seen as an indication of slower reaction.

The results of using the in-situ generated HCl for carbonate dissolution was promising. Following future studies can provide a better understanding of this acid and further increase its performance:

1. Application of gelled in-situ generated HCl can provide better performance for high-temperature application by further retardation.
2. Effect of additives on reaction kinetics can be studied with more RDA tests for more accurate results.

REFERENCES

Alkhaldi, M. H., Nasr-El-Din, H. A., and Sarma, H. K. 2009. Application of Citric Acid in Acid Stimulation Treatments. Presented at the Canadian International Petroleum Conference, Calgary, Alberta**,** 16-18 June. PETSOC-2009-015. https://doi.org/10.2118/2009-015.

Boomer, D. R., McCune, C. C., and Fogler, H. S. 1972. Rotating Disk Apparatus for Reaction Rate Studies in Corrosive Liquid Environments. *Rev Sci Instrum* **43** (2): 225-229. http://dx.doi.org/210.1063/1061.1685599.

Bryant, S. L. and Buller, D. C. 1990. Formation Damage from Acid Treatments. *SPE Prod Eng* **5** (4): 455-460. SPE-17597-PA. http://dx.doi.org/17510.12118/17597-PA.

Buijse, M., de Boer, P., Breukel, B. et al. 2003. Organic Acids in Carbonate Acidizing. Presented at the SPE European Formation Damage Conference, The Hague, Netherlands, 13-14 May. SPE-82211-MS. http://dx.doi.org/10.2118/82211-MS.

Buijse, M. A. 1997. Understanding Wormholing Mechanisms Can Improve Acid Treatments in Carbonate Formations. Presented at the SPE European Formation Damage Conference, The Hague, Netherlands, 2-3 June. SPE-38166-MS. http://dx.doi.org/10.2118/38166-MS.

Bybee, K. 2002. High-Temperature Acidization Prevents Fines Migration. *J Pet Technol* **54** (3): 40. SPE-0302-0040-JPT. https://doi.org/0310.2118/0302-0040-JPT.

Chang, F. F., Nasr-El-Din, H. A., Lindvig, T. et al. 2008. Matrix Acidizing of Carbonate Reservoirs Using Organic Acids and Mixture of Hcl and Organic Acids. Presented at the SPE Annual Technical Conference and Exhibition, Denver, Colorado, USA, 21-24 September. SPE-116601-MS. http://dx.doi.org/10.2118/116601-MS.

Chatelain, J. C., Silberberg, I. H., and Schechter, R. S. 1976. Thermodynamic Limitations in Organic-Acid/Carbonate Systems. *SPE J.* **16** (4): 189-195. SPE-5647-PA. http://dx.doi.org/5610.2118/5647-PA.

Coulter Jr., A. W., Hendrickson, A. R., and Martinez, S. J. 1987. Acidizing. In *Petroleum Engineering Handbook*, ed. Bradley, H.B., Richardson, Texas: Society of Petroleum Engineers.

Crowe, C., Masmonteil, J., and Thomas, R. 1992. Trends in Matrix Acidizing. *Oilfield Review* **4** (4): 24-40.

de Rozieres, J. 1994. Measuring Diffusion Coefficients in Acid Fracturing Fluids and Their Application to Gelled and Emulsified Acids. Presented at the SPE Annual Technical Conference and Exhibition, New Orleans, Louisiana, 25-28 September. SPE-28552-MS. http://dx.doi.org/10.2118/28552-MS.

El-Monier, I. A. and Nasr-El-Din, H. A. 2013. An Al/Zr-Based Clay Stabilizer for High pH Applications. *J. Energy Resour. Technol.* **135** (2). doi: 10.1115/1.4023100

Fredd, C. N. 2000. Dynamic Model of Wormhole Formation Demonstrates Conditions for Effective Skin Reduction During Carbonate Matrix Acidizing. Presented at the SPE Permian Basin Oil and Gas Recovery Conference, Midland, Texas, 21-23 March. SPE-16887-PA. http://dx.doi.org/10.2118/16887-PA.

Fredd, C. N. and Fogler, H. S. 1998a. Alternative Stimulation Fluids and Their Impact on Carbonate Acidizing. *SPE J.* **3** (1): 34-41. SPE-31074-PA. http://dx.doi.org/31010.32118/31074-PA.

Fredd, C. N. and Fogler, H. S. 1998b. The Kinetics of Calcite Dissolution in Acetic Acid Solutions. *Chem Eng Sci* **53** (22): 3863-3874. http://dx.doi.org/3810.1016/S0009-2509(3898)00192-00194.

Frenier, W. W., Fredd, C. N., and Chang, F. 2001. Hydroxyaminocarboxylic Acids Produce Superior Formulations for Matrix Stimulation of Carbonates at High Temperatures. Presented at the SPE Annual Technical Conference and Exhibition, New Orleans, Louisiana, 30 September-3 October. SPE-71696-MS. https://doi.org/10.2118/71696-MS.

Frenier, W. W., Rainey, M., Wilson, D. et al. 2003. A Biodegradable Chelating Agent Is Developed for Stimulation of Oil and Gas Formations. Presented at the SPE/EPA/DOE Exploration and Production Environmental Conference, San Antonio, Texas, 10-12 March. SPE-80597-MS. https://doi.org/10.2118/80597-MS.

Gatewood, J. R., Hall, B. E., Roberts, L. D. et al. 1970. Predicting Results of Sandstone Acidizing. *J Pet Technol* **22** (6): 693-700. SPE-2622-PA. http://dx.doi.org/2610.2118/2622-PA.

Gdanski, R. D. 1999. Kinetics of the Secondary Reaction of Hf on Alumino-Silicates. *SPE Prod Fac* **14** (4): 260-268. SPE-59094-PA. http://dx.doi.org/59010.52118/59094-PA.

Gdanski, R. D. and Peavy, M. A. 1986. Well Return Analysis Causes Re-Evaluation of Hcl Theories. Presented at the SPE Formation Damage Control Symposium,

Lafayette, Louisiana, 26-27 February. SPE-14825-MS. http://dx.doi.org/10.2118/14825-MS.

Harris, O. E., Hendrickson, A. R., and Coulter, A. W. 1966. High-Concentration Hydrochloric Acid Aids Stimulation Results in Carbonate Formations. *J Pet Technol* **18** (10): 1291-1296. SPE-1654-PA. http://dx.doi.org/1210.2118/1654-PA.

Hartman, R. L., Lecerf, B., Freiner, W. W. et al. 2006. Acid-Sensitive Aluminosilicates: Dissolution Kinetics and Fluid Selection for Matrix-Stimulation Treatments. *SPE Prod & Oper* **21** (2): 194-204. SPE-82267-PA. http://dx.doi.org/82210.82118/82267-PA.

Hill, A. D., Lindsay, D. M., Silberberg, I. H. et al. 1981. Theoretical and Experimental Studies of Sandstone Acidizing. *SPE J.* **21** (1): 30-42. SPE-6607-PA. http://dx.doi.org/6610.2118/6607-PA.

Hoefner, M. L. and Fogler, H. S. 1989. Fluid-Velocity and Reaction-Rate Effects During Carbonate Acidizing: Application of Network Model. *SPE Prod Eng* **4** (1): 56-62. SPE-15573-PA. http://dx.doi.org/15510.12118/15573-PA.

Li, Y. H., Fambrough, J. D., and Montgomery, C. T. 1998. Mathematical Modeling of Secondary Precipitation from Sandstone Acidizing. *SPE J.* **3** (4): 393-401. SPE-53001-PA. http://dx.doi.org/53010.52118/53001-PA.

Lund, K. and Fogler, H. S. 1975. Acidization—II. The Dissolution of Calcite in Hydrochloric Acid. *Chem Eng Sci* **30** (8): 825-835. http://dx.doi.org/810.1016/0009-2509(1075)80047-80049.

Lund, K., Fogler, H. S., and McCune, C. C. 1973. Acidization—I. The Dissolution of Dolomite in Hydrochloric Acid. *Chem Eng Sci* **28** (3): 691-700. http://dx.doi.org/610.1016/0009-2509(1077)80003-80001.

Mahmoud, M. A., Mohamed, I. M., Nasr-El-Din, H. A. et al. 2011. When Should We Use Chelating Agents in Carbonate Stimulation? Presented at the SPE/DGS Saudi Arabia Section Technical Symposium and Exhibition, Al-Khobar, Saudi Arabia, 15-18 May. SPE-149127-MS. https://doi.org/10.2118/149127-MS.

Muecke, T. W. 1982. Principles of Acid Stimulation. Presented at the International Petroleum Exhibition and Technical Symposium, Beijing, China, 17-24 March. SPE-10038-MS. http://dx.doi.org/10.2118/10038-MS.

Newman, J. 1966. Schmidt Number Correction for the Rotating Disk. *Journal Phys Chem* **70** (4): 1327-1328. http://dx.doi.org/1310.1021/j100876a100509.

Qiu, X., Khalid, M. A., and Sultan, A. 2015. How to Determine True Acid Diffusion Coefficient to Optimize Formation Damage Treatment? Presented at the SPE European Formation Damage Conference and Exhibition, Budapest, Hungary, 3-5 June. SPE-174241-MS. http://dx.doi.org/10.2118/174241-MS.

Rabie, A. I., Gomaa, A. M., and Nasr-El-Din, H. A. 2010. Determination of Reaction Rate of in-Situ Gelled Acids with Calcite Using the Rotating Disk Apparatus. Presented at the SPE Production and Operations Conference and Exhibition, Tunis, Tunisia, 8-10 June. SPE-133501-MS. http://dx.doi.org/10.2118/133501-MS.

Rabie, A. I., Shedd, D. C., and Nasr-El-Din, H. A. 2014. Measuring the Reaction Rate of Lactic Acid with Calcite and Dolomite by Use of the Rotating-Disk Apparatus. *SPE J.* **19** (6): 1192-1202. SPE-140167-PA. https://doi.org/140110.142118/140167-PA.

Scribner, L. A. 2001. Corrosion by Organic Acids. Presented at the CORROSION 2001, Houston, Texas, 11-16 March. NACE-01343.

Shaughnessy, C. M. and Kline, W. E. 1983. Edta Removes Formation Damage at Prudhoe Bay. *J Pet Technol* **35** (10): 1783-1791. SPE-11188-PA. https://doi.org/11110.12118/11188-PA.

Smith, C. F. and Hendrickson, A. R. 1965. Hydrofluoric Acid Stimulation of Sandstone Reservoirs. *J Pet Technol* **17** (2): 215-222. SPE-980-PA. http://dx.doi.org/210.2118/2980-PA.

Sokhanvarian, K., Nasr-El-Din, H. A., and de Wolf, C. A. 2016. Thermal Stability of Oilfield Aminopolycarboxylic Acids/Salts. *SPE Prod & Oper* **31** (1): 12-21. SPE-157426-PA. http://dx.doi.org/157410.152118/157426-PA.

Sokhanvarian, K., Pummarapanthu, T., Arslan, E. et al. 2017. A New in-Situ Generated Acid System for Carbonate Dissolution in Sandstone and Carbonate Reservoirs. Presented at the SPE International Conference on Oilfield Chemistry, Montgomery, Texas, USA, 3-5 April. SPE-184506-MS. https://doi.org/10.2118/184506-MS.

Taylor, K. C., Al-Ghamdi, A. H., and Nasr-El-Din, H. A. 2004. Measurement of Acid Reaction Rates of a Deep Dolomitic Gas Reservoir. *J Can Pet Technol* **43** (10): 49-56. PETSOC-04-10-05. http://dx.doi.org/10.2118/2104-2110-2105.

Taylor, K. C. and Nasr-El-Din, H. A. 2009. Measurement of Acid Reaction Rates with the Rotating Disk Apparatus. *J Can Pet Technol* **48** (6): 66-70. PETSOC-09-06-66. http://dx.doi.org/10.2118/2109-2106-2166.

Wilson, A. 2015. Sodium Gluconate as a New Environmentally Friendly Iron-Control Agent for Acidizing. *J Pet Technol* **67** (9): 158-159. SPE-0915-0158-JPT. https://doi.org/0910.2118/0915-0158-JPT.

Ziauddin, M., Berndt, O., and Robert, J. 1999. An Improved Sandstone Acidizing Model: The Importance of Secondary and Tertiary Reactions. Presented at the SPE European Formation Damage Conference, The Hague, Netherlands, 31 May-1 June. SPE-54728-MS. http://dx.doi.org/10.2118/54728-MS.